universität wien

DISSERTATION / DOCTORAL THESIS

Titel der Dissertation /Title of the Doctoral Thesis

„Genetic interactions between specific chromosome copy number alterations dictate complex aneuploidy patterns“

verfasst von / submitted by

Madhwesh Coimbatore Ravichandran

angestrebter akademischer Grad / in partial fulfilment of the requirements for the degree of

Doctor of Philosophy (PhD)

Wien, 2019 / Vienna 2019

Studienkennzahl lt. Studienblatt / Degree programme code:	UA 794 685 490
Dissertationsgebiet lt. Studienblatt / Field of study:	Molekulare Biologie
Betreut von / Supervisor:	Ass. Prof. Christopher Campbell, PhD

This thesis is dedicated to my fiancé and my parents.

Acknowledgements

I would like to thank many important people and without them this thesis would not have been possible.

First of all, my sincere acknowledgements go to my advisor, Dr. Christopher Campbell, for giving me an opportunity to work with this exciting research project. His scientific guidance, patience and dedication has inspired me to become an independent and critical scientist. His enthusiasm and trust was my biggest source of motivation throughout the whole time. Moving away from India to a landlocked country in the heart of Europe was tough, but Chris made this much easier by not just being a mentor but also a reliable friend. He has always been there for me through many moments of crisis and always knew how to diffuse them.

I would like to make a special mention of my Fiancé, Sarah Fink who was the strongest pillar of support, confidence and inspiration in the lab. Every day in the lab I lived in awe looking at her efficiency and experimental throughput. I have never seen such a plethora of skills in any other person in my life and am very lucky to have her in my life. I have learnt many skills from her and will continue to do so.

Another star that never failed to shed light on my self-esteem was Dr Manish Grover. His charm, enthusiasm, melodrama and never ending stream of happiness is what got me into science and has kept me going. Regardless of the distance between us he has maintained his positive influence on me and has single-handedly pulled me out of my “lows” which kept me going.

My entire lab consisting of Matthew, Manuel, Poornima, Theo, Sophie, Tamara, Claudia, Chiara have travelled along with me through my entire PhD and I couldn't ask for a more entertaining group. A special mention of Theo and Matthew who were a constantly there for me whenever I needed support.

A special thanks to Dr Alexander Dammerman and his entire lab for all the intellectual critique at the joint lab meetings. His raw critique was almost indispensable for my PhD and helped me gain many alternative perspectives of my work. The entire team of the DK chromosome dynamics including students and faculty. I would like to extend my gratitude to Tesi and Gerlinde for assisting me with all my queries and their support helped me glide through my graduate life. Moreover, I am grateful for being given the opportunity to advise some enthusiastic students, Laura Brandt and Aniruddh Yadav.

Lastly, I would also like to thank my parents and my brother for their endless love, trust and motivation. They have constantly inspired me to aim higher and fight harder to achieve my goals.

Table of Contents

Abstract (English) 9

Abstract (Deutsch) 10

Chapter 1: Introduction 11

1. Aneuploidy and its origin 13

1.1 Mitotic spindle defects 15

1.2 Spindle assembly checkpoint defects 17

1.3 Cohesin Defects 18

2. Living with aneuploidy 19

2.1 Aneuploidy is detrimental to cellular fitness 21

2.2 Why does aneuploidy impair cellular fitness? 23

2.1.1 Effects on the transcriptome 24

2.1.2 Effect on the Proteome 26

2.1.3 Repercussions of Aneuploidy-associated imbalances 27

- **General stress response** 28
- **Proteotoxic stress** 29
- **Replication stress and genomic instability** 31
- **Diverse stresses associated with aneuploidy** 32

2.3 Beneficial aneuploidies drive adaptation against stress 35

3. Aneuploidy, CIN and cancer 37

3.1 Patterns across cancer karyotypes 39

3.2 Effect of aneuploidy in tumorigenesis depends on the context 41

4. Genetic interactions within cancer karyotypes 44

5. Need for a model to study complex aneuploid karyotypes 47

Chapter 2: Results 48

1. Yeast cells with Survivin/*BIR1* deletion adapt by accumulating a high degree of aneuploidy 48

2. Adaptation to high rates of CIN occurs through many different disomic chromosomes in *bir1Δ-ad* strains..... 53

3. Chromosome copy number alterations in bir1Δ-ad strains share positive and negative correlations..... 59

4. Correlations between chromosomal copy number alterations are a result of genetic interactions among aneuploid chromosomes 62

5. Degree of aneuploidy is proportional to the degree of CIN induced..... 69

6. Correlations between chromosomal copy number alterations are affected by the ploidy of the cell..... 71

7. Aneuploid cancer karyotypes also display chromosome copy number correlations..... 75

8. The adapted strains converge on an optimal karyotype after an extended period of competitive adaptation..... 77

***Chapter 3: Discussion*.....83**

***Chapter 4: Materials & Methods*.....94**

***Tables*..... 104**

***References*..... 114**

Abstract (English)

Cells that contain an abnormal number of chromosomes are called aneuploid. High rates of aneuploidy in cancer are correlated with an increased frequency of chromosome missegregation, termed chromosomal instability (CIN). High levels of aneuploidy and CIN are both associated with cancers that are resistant to treatment. Although aneuploidy and CIN are typically detrimental to cell growth, they can aid in adaptation to selective pressures. Here, we induced extremely high rates of chromosome missegregation in yeast to determine how cells adapt to CIN over time. We find that adaptation to CIN initially occurs through many different individual chromosomal aneuploidies. Interestingly, the adapted yeast strains acquire complex karyotypes with specific subsets of the beneficial aneuploid chromosomes. These complex aneuploidy patterns are governed by synthetic genetic interactions between individual chromosomal abnormalities, which we refer to as chromosome copy number interactions (CCNIs). Given enough time, distinct karyotypic patterns in separate yeast populations converge on a refined complex aneuploid state. Surprisingly, some chromosomal aneuploidies that provided an advantage early on in adaptation are eventually lost due to negative CCNIs with even more beneficial aneuploid chromosome combinations. Together, our results show how cells adapt by obtaining specific complex aneuploid karyotypes in the presence of CIN.

Abstract (Deutsch)

Zellen mit einer abnormalen Anzahl an Chromosomen werden als Aneuploide bezeichnet. Hohe Aneuploidieraten in Krebs korrelieren mit einer erhöhten Chromosomenfehlverteilung, der so genannten chromosomalen Instabilität (CIN). Ein hoher Grad an Aneuploidie und CIN ist mit Krebserkrankungen assoziert, welche gegen Behandlungen resistent sind. Obwohl Aneuploidie und CIN typischerweise das Zellwachstum beeinträchtigen, können sie bei Anpassung an selektiven Druck helfen. In dieser Arbeit haben wir sehr hohe Chromosomenmissegregationsraten in Hefe induziert, um zu bestimmen, wie sich die Zellen im Laufe der Zeit an CIN anpassen. Wir haben festgestellt, dass die Anpassung zunächst durch viele verschiedene individuelle chromosomale Aneuploidien erfolgt. Interessanterweise erwerben die angepassten Hefestämme komplexe Karyotypen mit spezifischen Teilmengen der vorteilhaften aneuploiden Chromosomen. Diese komplexen Aneuploidiemuster werden durch synthetische genetische Wechselwirkungen zwischen einzelnen Chromosomenanomalien gesteuert, die wir als Chromosomenkopienzahlinteraktionen (CCNIs) bezeichnen. Mit genügend Zeit konvergieren unterschiedliche karyotypische Muster in verschiedenen Hefepopulationen zu einem komplexen aneuploiden Zustand. Überraschenderweise gehen einige zunächst vorteilhafte chromosomale Aneuploidien schließlich durch negative CCNIs mit noch vorteilhafteren Kombinationen verloren. Zusammen zeigen unsere Ergebnisse, wie sich Zellen anpassen, indem sie spezifische komplexe aneuploide Karyotypen in Gegenwart von CIN erhalten.

Chapter 1: Introduction

Aneuploidy, an imbalance in the chromosome complement, was identified as a distinct feature of cancer cells (Fig. 1) several decades before genomic alterations in the DNA sequence were known to drive tumorigenesis (Boveri T, 1914). Aneuploidy is well tolerated in cancer cells, with over 90% of aneuploid solid tumors, ranging from 26% across some cancer types to nearly 99% in others (Taylor AM et al., 2018). Typically in a solid tumor, about a quarter of the genome is affected by copy number changes with a median of five losses and three gains of chromosomal arms per tumor (Beroukhim R et al., 2010; Zack TI et al., 2012). No other genomic alteration in the cancer genome has been observed at such high frequencies, making aneuploidy the most prevalent genomic alteration in cancers. Chromosome instability (CIN), the source of such numerical chromosomal imbalances has been the primary focus of many studies, leading to various therapies that target cancer cells with high rates of CIN. However, there has been limited progress in understanding the role of aneuploidy in tumor progression. Moreover, aneuploidy has not yet been effectively exploited for cancer therapeutics.

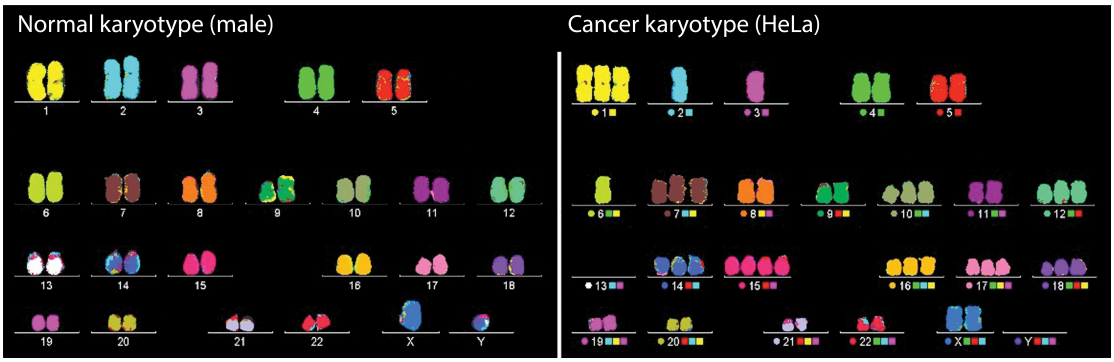

Figure 1: Comparison of a normal karyotype of a euploid human cell and a cancer cell karyotype of HeLa cells.
Source: http://berkeleysciencereview.com/article/good-bad-hela/

There are multiple challenges to understanding the significance of aneuploidy in cancer and its exploitation for therapeutic interventions of the disease. One originates from the aneuploidy paradox, wherein aneuploidy under most circumstances cause a severely detrimental effect to the fitness of a cell. However, cancerous cells have a high tolerance to the presence of aneuploid chromosomes. Furthermore, whole chromosome copy number changes affect the expression of hundreds of genes, all at once. This makes it strenuous to identify genes that drive the repeated selection of specific chromosomal aneuploidies in cancers.

Additionally, the cellular context also heavily influences the role of aneuploidy in cancers, often leading to opposing conclusions in different contexts. Engineering aneuploid chromosomes in human cells is laborious, despite a variety of tools such as micronuclei mediated chromosome transfer (where extra chromosomes were isolated in structures called micronuclei and then transferred to acceptor strains) (Fournier RE et al., 1977), loss of a chromosome assisted by CRISPR-Cas9 (Adikusuma F et al., 2017; Zuo E et al., 2017), and Cre-Lox based techniques (Thomas R et al., 2018). Therefore we are often unable to systematically characterize the consequences of gaining or losing each chromosome across an aneuploid karyotype. Finally, an additional hurdle to study the aneuploidy arises from the difficulty to disentangle the cellular consequences of an abnormal cancer karyotype, from CIN, the process that generated the aneuploid karyotype. Although there is a good correlation between CIN and the degree of aneuploidy (Nicholson JM and

Cimini D, 2013), there are some cancers that are highly aneuploid but lack any measurable level of CIN. Despite the pervasiveness of high levels of CIN, its role in tumor evolution and cancer progression is a paradox (Birkbak NJ et al., 2011). Nevertheless, a decade of research in the field of aneuploidy has paved the way to tackle many of these obstacles in the laboratory and have contributed to development of various cancer therapies.

1. Aneuploidy and its origin

Cell division, a process that forms the basis of many eukaryotic organisms, involves the proper duplication and segregation of the genetic material of the cell. Mitosis involves many discreet stages wherein chromosomes align in the middle of the cells and attach to the opposite poles of the cell by microtubules. Microtubules attach to the chromosomes via specialized structures called kinetochores and pull the chromosomes to opposite ends of the cells. Here the chromosomes de-condense and form two identical nuclei in separate daughter cells.

While budding yeast strains can have both single and double the complement of chromosomes (known as haploid cells, n = 16 and diploid cells, 2n = 32), most eukaryotic organisms have a diploid genome. However, cells that are aneuploid, display an abnormal complement of chromosomes with either a loss or gain of whole chromosomes. A gain of a single extra copy of a chromosome over either the haploid or the diploid set of chromosomes are respectively known as disomy (n+1) or trisomy (2n+1) (Fig. 2). While chromosomal gains

are tolerated, the loss of a chromosome copy or monosomy, leads to loss of expression of the genes on it, often resulting in lethality (Beach RR et al., 2017). Aneuploidies such as chromosomal gains are known to cause specific human pathologies like the Down syndrome (trisomy 21), Patau syndrome (trisomy 13), and Edwards syndrome (trisomy 18) that cause severe developmental defects (Edwards JH et al., 1960; Patau K et al., 1960; Nagaoka SI et al., 2012,). Aneuploidy of the sex chromosomes such as monosomy of the X chromosome, known as Tuner syndrome, and gain of an extra copy of the X chromosome, as seen in Klinefelter's (XXY) and Triple X (XXX) syndrome, are also associated with developmental irregularities. These aneuploid chromosomes commonly arise from unfaithful meiotic chromosome segregation in the germline, which upon fertilization and development results in aneuploid cells across all tissues of an individual.

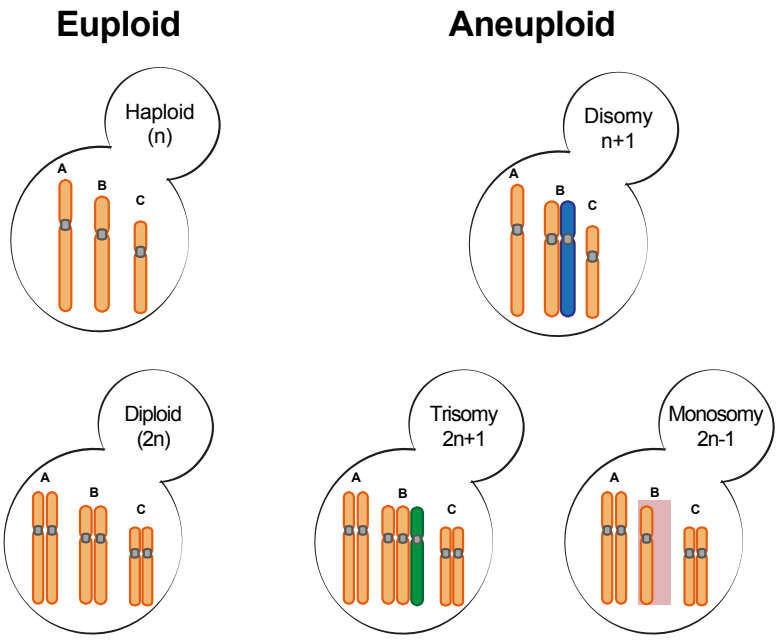

Figure 2: Different states of aneuploidy.
Euploid and aneuploid yeast cells. The picture depicts the chromosomes in orange and the aneuploid chromosomes are displays in blue (Disomy), in green (Trisomy), and in red for the loss of a chromosome copy.

Errors that lead to chromosome missegregation occurs once every 10^4 or 10^5 cell divisions in human cells or once every 5 x 10^4 in microorganisms like budding yeast, *Saccharomyces cerevisiae* (Hatwell LH et al., 1982; Rosenstraus MJ and Chasin LA, 1978). In humans, aneuploidy is also present at the tissue level of an individual, a phenomenon known as mosaic aneuploidy. For example, most humans acquire mosaic aneuploidy in the liver, as this tissue accumulates aneuploidy due to low levels of CIN (Duncan AW et al., 2010; Knouse KA et al., 2014). Accumulation of aneuploid cells due to mitotic errors is speculated to also occur during embryo development (Delhanty JD et al., 1993; van Echten-Arends J et al., 2011). Such aneuploid populations are often eliminated either by competition from better proliferating euploid cells or via activation of senescence or apoptotic pathways in aneuploid cells (Bazrgar M et al., 2013; Bolton H et., 2016). Taken together, aneuploidy across an entire organism or in specific tissues have a detrimental impact. Since aneuploidy commonly arises due to CIN, it is essential to understand which cellular machineries accumulate defects, in order to detect and prevent various pathologies associated with aneuploidy.

1.1 Mitotic spindle defects

During cell division chromosomes must align at the center of the cell in order to correctly connect the kinetochores of the duplicated chromosomes to the opposite poles of the mitotic spindle. This process, termed bi-orientation of chromosomes, is a pre-requisite for faithful chromosome segregation and is mainly controlled by the chromosomal passenger complex (CPC). The CPC

comprises of 4 subunits, an enzymatic core, Aurora B kinase (Ipl1 in yeast) that is assisted by INCENP (Sli15), Survivin (Bir1) & Borealin (Nbl1) (Carmena M et al., 2012; Dephoure N et al. 2008; Hegemann B et al., 2011) (Fig. 3). The CPC destabilizes improper microtubule-kinetochore connections via phosphorylation of kinetochore proteins (Cimini D et al., 2006) (Fig. 3) This phosphorylation allows the turnover of improper connections between the kinetochore and the mitotic spindle until chromosomes achieve a bioriented attachment state. As observed in some cancers, perturbation of the CPC-mediated error-correcting mechanism leads to incorrect microtubule attachments that can promote CIN (Abe Y et al., 2016). Aberrant microtubule-kinetochore attachments are a significant source of chromosome missegregation and aneuploidy.

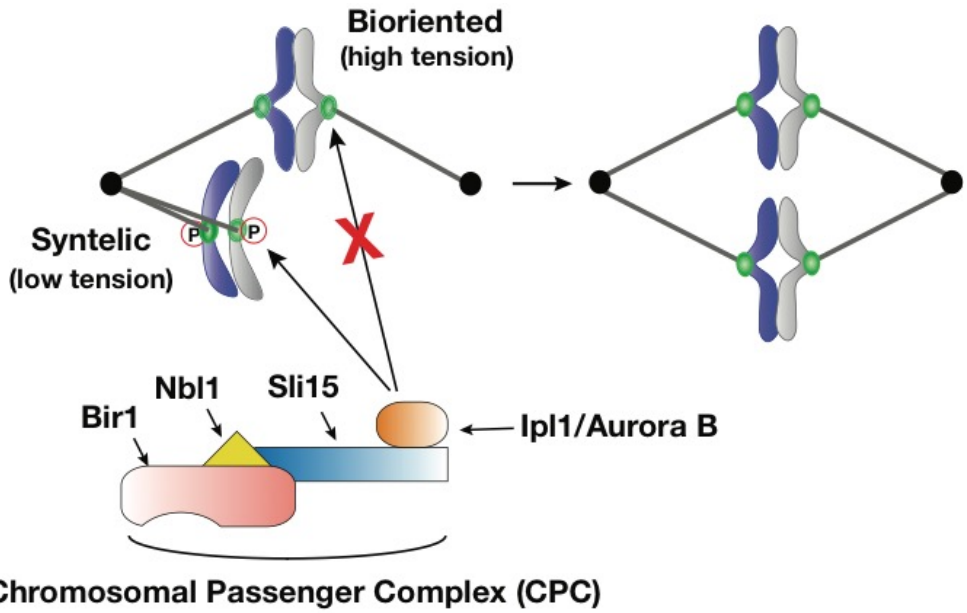

Figure 3: Ipl1/Aurora B promotes chromosome biorientation by specifically phosphorylating misattached kinetochores.

Mis-attached states like merotely where a single kinetochore can form attachments with microtubules emanating from both the spindle poles, is a frequent occurrence in many cancer cells (Cimini D et al., 2001; Bakhoum SF

et al., 2009; Thompson SL and Compton DA, 2008). If these missattached states persist, the chromosomes lag in the center of the mitotic spindle during anaphase and are likely to missegregate to the wrong daughter cell. From the cell's perspective it can be challenging to detect merotely as subtle differences in tension across misattached kinetochores need to be recognized and fixed by the error checking mechanisms. While merotely in normal mitotic cells are corrected, it is often error-prone in cancer cells likely due to the lack of robust error correcting mechanisms and contexts like supernumerary centrosomes that enhance the frequency (Gregan J et al., 2011). In many organisms, centrosomes are the microtubule organizing centers that serve as the point of origin of microtubules during mitosis. There are multiple paths that lead to excess centrosomes such as loss of regulation of centrosome duplication, cell fusion, failed cell division, or mitotic slippage etc. Supernumerary centrosomes form multipolar spindles in various cancers that are known to increase the chance of merotelic attachments. (Ganem NJ et al., 2009). A recent study overexpressed Plk4, a regulator of centrosome duplication in mice to show that excess centrosomes are sufficient to cause CIN and drive tumorigenesis is various murine tissues (Levine MS et al., 2017). These spontaneous tumors displayed high CIN and aneuploidy primarily due to enhanced frequency of merotelic attachments.

1.2 Spindle assembly checkpoint defects

High levels of CIN and aneuploidy are also prevalent consequences of a compromised spindle assembly checkpoint (SAC), which functions in

metaphase as a gatekeeper to subsequent stages of chromosome segregation. In metaphase the SAC keeps track of stably bound kinetochores. If the kinetochore attachments to the mitotic spindle are incorrect or absent, MPS1 and CENP-E proteins, along with proteins of the BUB and MAD family, form a sophisticated machinery that causes a cell cycle delay until the spindle is correctly attached to all chromosomes. The SAC causes this delay by preventing the cell cycle progression to the next stage, anaphase, by inhibiting the anaphase promoting complex (APC/C) (Musacchio A & Salmon ED, 2007). Turning off the gatekeeping function of the SAC would be an obvious mechanism to generate CIN and aneuploid cells. However, cancers that are highly aneuploid rarely have mutations in the SAC genes (Simonetti G et al., 2019). Nevertheless, the SAC is compromised in certain cancer cells due to deregulation at the protein or mRNA level, which leads to unsupervised chromosome segregation and results in aneuploid populations.

1.3 Cohesin Defects

Once the SAC permits cell cycle progression the APC/C promotes anaphase by degrading Securin, an inhibitor of Separase, which releases the enzyme and facilitates the removal of cohesin molecules that bind the sister chromatids together. Once released, the sister chromatids can be pulled to the opposite poles where they form two daughter nuclei. Cohesion defects are an important source of CIN, primarily causing a premature loss of sister chromosome cohesion. This premature release of sister chromosomes virtually leads to random chromosome segregation as these chromosomes are pulled to the

opposite spindle poles immediately following microtubule attachment (Nasmyth K and Haering CH, 2009). Inactivating mutations in STAG2, a subunit of the human cohesin complex, were identified in human colorectal tumors as one of the sources of CIN that generates a high degree of aneuploidy (Solomon DA et al., 2011). However, it is essential to note that cohesins also control other processes of the cell, such as transcription (Dorsett D, 2011). Hence, conclusions from such bottom-up studies may have some caveats. Many such integral experiments have exploited the numerous routes to aneuploidy mentioned above and to understand the direct consequences of CIN and aneuploidy. These investigations have been instrumental in identifying the impact of aneuploidy across an entire organism and its cellular consequences.

2. Living with aneuploidy

Aneuploidy across all tissues in humans are rare and severely impair development. A high number of miscarriages and cases of mental retardations are caused due to whole organismal aneuploidy (Hassold T et al., 1996; Brown S, 2008). In humans, only 4 of the 23 trisomies can lead to live births, while the rest, along with all monosomies are embryonic lethal. Of the three autosomal trisomies that lead to live births, individuals with trisomy of Chr 21 are the only ones that can make it to adulthood (Pai GS et al., 2002). The gain of an extra copy of chromosome 21 accounts for approximately one in 800 live births (de Graaf G et al., 2015). These affected individuals have a spectrum of physical and mental disabilities (Roizen NJ and Patterson D, 2003) and often have a diminished life expectancy (Carfi A et al., 2014; Roper RJ and Reeves RH,

2006). Similarly, in mice, all forms of aneuploidy are embryonic lethal except Trisomy 19 that can survive for a few weeks after birth (Lorke DE, 1994). Analogous to humans, these mice display a variety of developmental disorders like craniofacial abnormalities, hypoplasia, and nuchal edema (Krushinskii LV et al., 1986; Gropp A et al., 1975). The detrimental effects of whole-organism aneuploidy are evident in other organisms as well including maize (McClintock B, 1929), flies (Lindsley DL, 1972), and nematodes (Hodgkin J, 1983; Hodgkin J et al., 1979; Sigurdson DC et al., 1986). Thus, multiple studies have concluded that whole organism aneuploidy clearly generates a barrier to healthy development.

Mosaic aneuploidies on the other hand are well tolerated in individuals with a rare genetic disorder called Mosaic Variegated Aneuploidy (MVA) (Callier P et al., 2005; Garcia-Castillo H et al., 2008) and just 50 cases of MVA are known in medical literature (Hank S et al., 2012). MVA is generally caused by mutations in either the CEP57 gene (Snape et al., 2011), a centrosomal protein that is responsible for proper chromosome segregation or in the BUB1B gene (Hanks S et al., 2004), which has a primary function in the SAC. MVA consequently leads to approximately 25% of aneuploid cells across the organism. Mouse models of MVA with mutations in the BUB1B gene display phenotypes associated with progeria and increased infertility (Baker et al., 2004). Overall, aneuploidy across the entire organism causes many irregularities and impairs the life of the organism.

2.1 Aneuploidy is detrimental to cellular fitness

Identifying the consequences of aneuploidy at the level of individual cells is the first step towards understanding the negative impact of aneuploidy at the whole organismal level. Several reports have shown that aneuploidy slows down the rate cellular proliferation likely an amalgamation of several aneuploidy-associated imbalances (Dephoure N et al., 2014; Sheltzer JM et al., 2011; Torres EM et al., 2007; 2010). The earliest studies were performed in primary fibroblasts collected from patients with Down syndrome, which grew much slower than age-matched euploid cells (Segal DJ et al., 1974). More recently, studies have acutely induced aneuploidy by mutating pathways such as inhibiting proteins that maintain the accuracy of chromosome segregation (Santaguida S et al., 2017; Michel LS et al., 2001; Sotillo R et al., 2007). This method induces high levels of CIN and heterogenous aneuploid populations that display various aneuploidy-associated cellular stresses. Interestingly the Compton lab pioneered an alternate approach by inducing random aneuploidy in near diploid human cells using a spindle poison, Monastrol. Consistent with other models of aneuploidy, these chemically induced aneuploid cells have displayed impairment in their fitness relative to euploid cells (Thompson SL and Compton DA, 2008; 2010).

To understand the impact of aneuploid chromosomes on cellular physiology, the Amon lab took a systematic approach and generated 17 haploid stains, each engineered with one or few disomic chromosomes in the budding yeast *Saccharomyces cerevisiae* (Torres EM et al., 2007; 2010). The proliferation of

all of the engineered strains had a heterogenous distribution and was on average slower than their isogenic euploid counterparts (Fig. 4; Beach RR et al., 2017). Similarly, all aneuploid cells derived by meiosis of triploid and pentaploid yeast cells exhibited impaired cellular fitness in normal growth conditions (Niwa O et al., 1985; 2006).

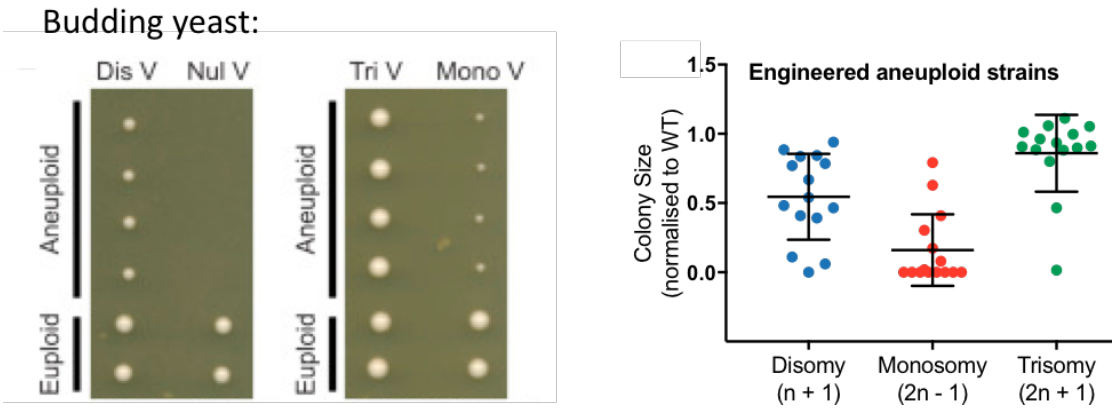

Figure 4: All aneuploid states lead to a decrease of proliferation rate.
Yeast strains engineered with disomic, monosomic and trisomic chromosomes cause a decrease in proliferation rate relative to isogenic euploid strains. On the left is an example of a typical budding yeast growth assay where the colony size of each engineered aneuploid strains is smaller than the euploid counterparts. Adapted from Beach RR et al., 2017.

Additionally, sibling matched trisomic and euploid embryos were generated using a unique mating scheme and naturally occurring Robertsonian translocations in mouse models. After harvesting the fibroblasts from such embryos, analysis of their growth revealed that the trisomic fibroblasts grew significantly slower than their euploid counterparts (Williams BR et al., 2008). Lastly, the Storchova lab also observed growth defects in aneuploid human cells made by utilizing microcell-mediated chromosome transfer (MMCT) to stably transfer extra chromosomes into euploid RPE1 or HCT116 cell lines (Stingele S et al., 2012). Taken together many independent methods to generate aneuploid cells have revealed that aneuploidy causes a general growth impairment. While the exact basis of these growth impairments remains

elusive, the evidence in yeast and human cells indicate that it could be a consequence of the transcriptomic and proteomic imbalances caused by aneuploid chromosomes (Stingele S et al., 2012; Thorburn RR et al., 2013).

2.2 Why does aneuploidy impair cellular fitness?

There are several hypotheses regarding why aneuploidy lowers the cellular growth rate. By definition, cells that contain aneuploid chromosomes have both the extra quantities of DNA relative to euploid cells and an increase in gene dosage due to the excess genes on the aneuploid chromosomes. However, evidence in yeast shows that this extra DNA is likely not the cause of the aneuploidy-associated fitness impairment. Yeast strains engineered to contain artificial chromosomes that encode almost no genes that are expressed in yeast have no proliferative defects. (Torres EM et al., 2007). Some studies have shown that an excessive amount of specific DNA sequences such as centromere sequences, does stall chromosome segregation at metaphase and increases the loss of chromosomes (Futcher B and Carbon J, 1986; Runge KW and Zakian VA, 1989). However, these effects were only observed when cells carried more than 10 extra centromeres, while the toxicity was reduced with fewer extra centromeres.

Clear evidence in human cells linking the fitness impairment with the increased gene dosage by aneuploidy was provided by Jiang et al. (2013). Here, the Xist non-coding RNA was introduced on the trisomic chromosome 21 in cells derived from patients with Down syndrome. These cells displayed an enhanced

proliferation rate after the extra copy of chromosome 21 was silenced by Xist induction. Hence a low degree of excess DNA remains benign in aneuploid cells, and aneuploidy induced growth impairment is likely a consequence of imbalances of the cellular transcriptome and proteome.

2.1.1 Effects on the transcriptome

On a fundamental level, aneuploidy of a chromosome effectively changes the dosage of a large proportion of genes present on the chromosome. In aneuploid yeast strains, this increase in gene dosage proportionally alters the gene products, at both the RNA and protein level (Torres EM et al., 2007; Pavelka N et al., 2010). The scaling of RNA expression with the dosage of genes on the gained chromosome was also identified in aneuploid mouse embryonic fibroblasts (Williams BR et al., 2008). A more recent, single-celled RNA sequencing study revealed the same for loss of the human chromosome 7 (Zhao X et al., 2017). Similar studies in engineered murine and human cell lines (Upender MB et al., 2004; Stingele S et al., 2012), Arabidopsis thaliana (Huettel B et al., 2008), and patient-derived cells or tissues (Mao R et al., 2008; Lockstone HE et al., 2007; Halevy T et al., 2016; Aziz NM et al., 2018) have reaffirmed the scaling of mRNA abundance with gene dosage.

However, not all genes present on an aneuploid chromosome are expressed at levels proportional to their gene copy number. Some genes can be regulated to bring the expression levels back to the euploid state, a phenomenon known as dosage compensation. The best example of an entire aneuploid

chromosome being transcriptionally silenced is observed in the triple X syndrome, where a female has three copies of the X chromosome. Unlike other aneuploidy associated syndromes, women with triple X syndrome are nearly indistinguishable from euploid women (Tartaglia NR et al., 2010). This is due to the silencing of the extra X chromosome by a specific dosage compensatory mechanism called X chromosome inactivation or XCI (Payer and Lee, 2008). In some species of maize and wheat, aneuploidies of autosomal chromosomes also show dosage compensation (Makarevitch et al., 2008; Zhang et al., 2010; Zhang et al., 2017). The exact mechanism of dosage compensation of specific genes on aneuploid chromosomes remains elusive (Torres EM et al., 2016; Gasch AP et al., 2016; Hose J et al., 2015).

Analogous to direct gene dosage effects of aneuploidy, reports using yeast as a model have shown that supernumerary chromosomes also affect the expression of genes located on other euploid chromosomes (Pavelka N et al., 2010; Rancati G et al., 2008). Transcription factors expressed from the aneuploid chromosome act on their downstream targets and proportionately increased their expressions. Primary cells from monozygotic twins with Down syndrome (Trisomy 21) showed differential expression of 182 genes, but surprisingly only 6 of those were present on chromosome 21, thus confirming the indirect effects of aneuploidy on the human transcriptome (Letourneau et al., 2014). Additionally, more dramatic effects of aneuploidy on gene expression were highlighted by a study that showed disruption of the assembly of heterochromatin at specific loci in aneuploid strains (Mulla et al., 2017). The

study specifically showed that the gain of chromosome 10 in yeast perturbed the gene silencing at the mating loci by altering the localization of specific chromatin remodelers.

2.1.2 Effect on the Proteome

The previous section, discussed various studies that linked aneuploidy-associated gene dosage changes to a proportional change in mRNA levels, but does this change at the RNA level translate to the level of proteins? Two studies in budding yeast concluded that aneuploidy associated copy number changes of genes indeed proportionately translate into increased protein abundance. Further studies performed on the human cancer cell line HCT116, showed that a tetrasomic gain of chromosome 5 leads to a 1.6 fold increase in protein levels (Stingele S et al., 2012). In a near-haploid leukemia cell line, similar results were observed where the cells gained an extra copy of chromosome 8 (Burckstummer T et al., 2013). This suggests that some proportion of the gene dosage imbalance is not efficiently translated to the protein level. Elegant studies in budding yeast show that these genes either undergo dosage compensation at the RNA level or are degraded in order to maintain protein stoichiometry of multi-subunit complexes (Dephoure N et al., 2014; Brennan CM et al., 2019).

2.1.3 Repercussions of Aneuploidy-associated imbalances

Both transcriptomic and the proteomic changes disturb cellular homeostasis likely due to the imbalances generated by aneuploidy associated gene dosage changes. There have been multiple bottom-up efforts to illustrate how proteome imbalances induced by aneuploidy push various cell processes out of balance (Stingele S et al., 2012; Torres EM et al., 2007; Beach RR et al., 2017; Segal DJ et al., 1974; Thorburn RR et al., 2013; Ariyoshi K et al., 2016). Nearly all the studies with aneuploid cells have found substantial defects with cellular proliferation, as the cell cycle frequently develops a delay in G1 and S phases in most aneuploid cells, likely due to the stoichiometric imbalances of cell cycle regulators such as cyclins (Stingele S et al., 2012; Torres EM et al., 2007). Another study showed that the only embryonic human trisomies that survived the gestation period were those chromosomes that had the fewest genes on them (Torres EM et al., 2008). This indicates that there is a proportional relationship between gene dosage imbalances induced by aneuploidy and the fitness of aneuploid organisms. Additionally, in utero survival rate of mouse embryos highly correlate with the number of genes on the additional chromosome (Sheltzer JM and Amon A, 2012). Likewise, in budding yeast, the fitness impairment positively correlates with the number of extra genes on the aneuploid chromosomes (Torres EM et al., 2007; Sheltzer JM and Amon A, 2012), while some exceptions exist with disproportionate effects of specific toxic genes (like ß-tubulin) present on small chromosomes (Katz W et al., 1990; Anders KR et al., 2009). Given that aneuploidy associated imbalances are caused by expression changes of a large number of genes the end result of

such imbalances are dysregulation of several cellular pathways. This failure to carefully orchestrate several cellular pathways lead to various stress states, which are highlighted below.

- **General stress response**

Since aneuploid cells show a weakened fitness when compared to euploid cells within an organism, it was hypothesized that the aneuploidy-associated imbalance might cause a specific general stress response. To uncover the existence of a general stress response the Amon lab identified gene expression changes of disomic yeast strains and compared them to known stress response expression signatures. In budding yeast, stable chromosome gains were created, and disomies of chromosome 4, 8, 15, and 16 notably displayed an expression signature that resembled the yeast environmental stress response (ESR) commonly seen in yeast (Torres EM et al., 2007). The ESR gene expression signature is commonly observed in yeast in response to multiple stress conditions like heat shock and oxidative stress (Gasch AP et al., 2000).

Other studies in human cell lines with many gains or losses of chromosomes looked into the transcriptional profile and also found upregulation of genes in stress response (Sheltzer JM et al., 2012; Durrbaum M et al., 2014). These genes were involved in metabolic pathways or protein stability and degradation at the Endoplasmic reticulum (ER), Golgi, and lysosome. One finding indicates that the aneuploidy-associated ESR-like signatures is partly a byproduct of cell cycle delays in yeast (O'Duibhir E et al., 2014). Nevertheless, further elucidation

is required to ascertain the generality of this stress response as it could depend on the genome composition, ploidy, cell, or tissue type.

- **Proteotoxic stress**

Since alterations in chromosome stoichiometries lead to excess protein production from the genes encoded on the supernumerary chromosomes, it is expected that the protein folding machinery is overworked. This further adds to the stress as proper protein folding is impaired (Donnelly N et al., 2014). Such excess proteins that are misfolded accumulate into aggregates and activate the protein degradation pathways. This state of overburdened protein degradation systems is called proteotoxic stress (Stingele S et al., 2012; Ariyoshi K et al., 2016; Tang YC et al., 2011; Oromendia AB et al., 2012). For example, a state of proteotoxic stress is evidenced by the presence of protein aggregates in aneuploid cells likely due to a reduced Hsp90 mediated folding capacity (Donnelly N et al., 2014; Oromendia AB et al., 2012). Not surprisingly, aneuploid yeast, murine and human cells are sensitive to Hsp90 inhibitors (Torres EM et al., 2007; Tang YC et al., 2011; Donnelly N et al., 2014). This sensitivity can be rescued by the overexpression of *HSF1*, a transcription factor that regulates the expression of many chaperones (Donnelly N et al., 2014).

Since failure to clear misfolded protein aggregates reduces the cellular viability (Stefani M and Dobson CM, 2003), the cell heavily relies on its proteasomal degradation machinery to degrade them. Proteins in the nucleus or the cytoplasm can typically be degraded by 26S proteasome (Goldberg AL, 2003;

Wójcik C and DeMartino GN, 2003), or by acid hydrolases in a cellular compartment called the lysosome (Nakatogawa H et al., 2009). Proteasomal inhibitors like MG132, severely impair cellular viability in aneuploid cells as they hinge on its ability to degrade the excess protein and rebalance the protein stoichiometries (Ohashi A et al., 2015; Torres EM et al., 2007). Similarly, *UBP6*, an enzyme that removes the ubiquitin from degradation targets, allowing these proteins to escape proteasomal degradation (Hanna J et al., 2006), is often found mutated in specific aneuploid strains (Torres EM et al., 2007). Hence, the UBP6 mutation was found to increase cellular fitness of aneuploid cells by facilitating tolerance to specific aneuploidies. Together, these studies highlight the dependence of aneuploid cells on the proteasomal degradation machinery such that stoichiometric imbalances are corrected and restore protein homeostasis.

Proteins that function as a part of multimeric complexes do so while maintaining well-defined stoichiometries of each subunit (Li G-W et al., 2014). Transient gene copy number changes due to aneuploidy can lead to the production of complex subunits that are unbound. These complex subunits are orphaned and hence, either misfold or aggregate, which contributes to proteotoxic stress (Brennan CM et al., 2019). Misfolded proteins and aggregates that need to be degraded or require assistance by various protein quality machineries, are a frequent occurrence in aneuploid cells (Oromendia AB et al., 2012). Persistent assistance of misfolded proteins by chaperones in aneuploid cells, sequesters the chaperones from guiding the folding of essential proteins (Hartl FU et al.,

2011), which is likely the cause of the proliferative defects. Among proteins that function as part of complexes, 73% of them are either degraded or aggregated when present in excess (Brennan CM et al., 2019). In sum, protein homeostasis is disturbed by aneuploid chromosomes due to the production of excess unbound proteins that contribute to proteotoxic stress and severely taxes the protein quality control pathways.

- **Replication stress and genomic instability**

Replication stress is a prominent feature of aneuploid cells (Santaguida S et al., 2017; Sheltzer JM et al. 2015; Passerini V et al., 2016). Disruptions of ongoing DNA replication by these stoichiometric imbalances in aneuploid cells were mainly due to the loss of function of several protein complexes that are essential for the process of DNA replication (Passerini V et al., 2016). As an example, a study in human cells induced acute aneuploidy in an untransformed but immortalized RPE-1 cell line, which increased the incidence of replication fork stalling and slowed down the fork progression (Santaguida S et al., 2017). These defects were seen in part due to imbalances of six subunits that form the MCM2-7 helicase complex (Santaguida S et al., 2017; Passerini V et al., 2016). The rate of spontaneous mutagenesis across the genome also increased due to the aneuploid chromosomes (Sheltzer JM et al. 2015). Analogously, aneuploid yeast and human cells show aberrant mitosis and accumulate high levels of DNA damage (Ariyoshi K et al., 2016; Nicholson JM et al., 2015; Blank HM et al., 2015; Passerini V et al., 2016). Accumulation of DNA damage occurs mainly due to the pressure exerted on DNA replication by aneuploidy-

associated imbalances. A high frequency of DNA damage at the telomeres and activation of senescence via the p53 gene were the main cellular consequences of inducing acute aneuploidy. However, increasing the expression of telomerase, an enzyme that maintains the telomere region, abrogated such consequences (Meena JK et al., 2015).

Additionally, the proteome imbalances due to aneuploidy can impair the protein stoichiometry of major DNA repair complexes, which impairs their function. Such faulty repair mechanisms can give rise to chromosomal rearrangements, thus adding to the genomic instability induced by aneuploid chromosomes and contribute to the progression of diseases like cancer (Passerini V et al., 2016). Further mechanistic insights need to be worked out to fully understand if replication stress is a typical phenotype associated with extra copies of random chromosomes and its role in cancer progression.

- **Diverse stresses associated with aneuploidy**

While many studies have utilized various genetic perturbations to identify aneuploidy-associated stresses, both transcriptomic and phenotypic profiles acquired from these studies have revealed that certain stresses are associated only with a few combinations of aneuploid chromosomes. One recent study overcame this by intermixing several aneuploid populations that effectively canceled out the specific responses that arise from dosage imbalances of specific combinations of aneuploid chromosomes (Tsai H-J et al., 2019). They identified a common aneuploid gene expression (CAGE) pattern that positively

correlated with hypo-osmotic shock gene expression signature. Since changes in chromosome copy number lead to proteome imbalance with many of orphaned proteins, they concluded that the solute concentration within the cell would naturally increase. Increases in solute concentration would create a cytoplasm with high osmolarity, which induces a state of osmotic shock (Tsai H-J et al., 2019).

Similarly, while screening for the dependencies of specific aneuploid yeast strains, a study revealed that aneuploid cells were highly sensitive to the deletion of genes that function in protein trafficking involving localization to the cell membrane or other membranous structures like Vacuole and Golgi bodies (Dodgson SE et al., 2016). Cells with specific chromosomal gains were also sensitive to the loss of cell wall integrity, which in turn heavily depends on the pathways that mediate protein trafficking. Perturbation of the protein secretory or endocytic pathways significantly slowed down the growth of aneuploid strains suggesting that engineered aneuploid cells display membrane stress (Dodgson SE et al., 2016).

From the growing list of stresses associated with aneuploidy, one other stress worth highlighting is the disturbance of metabolic homeostasis or metabolic stress. Aneuploidy driven metabolic alterations include changes in nucleotide and carbohydrate metabolism, rate of glucose uptake, glutamine usage (Torres EM et al., 2007; Williams BR et al., 2008), elevated levels of tricarboxylic acid cycle intermediates (Thorburn RR et al., 2013), downregulation of DNA/RNA

metabolism, and changes in mitochondrial metabolism (Stingele S et al., 2012). Aneuploid strains were found to be not just highly dependent on sphingolipid production, but during its synthesis aneuploid cells also need to limit the production of an intermediate called ceramide that hinder cellular fitness (Hwang S et al., 2017). Further elevation of ceramide levels in aneuploid cells either by using drugs or genetic perturbations lead to severe proliferative defects.

Overall, at the cellular level, a numeric deviation from the euploid complement of chromosomes is associated with various stresses that could collectively have a detrimental effect on the physiology of an organism. Attempts to identify genes responsible for these fitness defects are almost always unsuccessful. For example, a candidate-based approach in yeast with a focus on dosage sensitive genes was neither able to entirely recapitulate or suppress the defects caused by aneuploid chromosomes (Bonney ME et al., 2015). Correspondingly, more than a century after Down syndrome was first described, attempts to find a specific gene on chromosome 21 responsible for the developmental and cognitive defects seen in patients with Down syndrome were unsuccessful (Lana-Elola E et al., 2011; Korbel JO et al., 2009). Aside from one notable example (Anders KR et al., 2009), these studies were unable to single out particular genes that are responsible for the defects caused by aneuploidy. Perhaps this inability stems from the complexity and variance of the proteome imbalance caused by different aneuploidies. Since aneuploidy has been described to cause a variety of stresses, it becomes clear that a combination of

several regulatory pathways are disturbed by the proteome imbalance. However, if aneuploidy causes a fitness deficit, why is aneuploidy a prominent feature of diseased states such as cancer? Since cancers harbor more than one aneuploid chromosome, have these cells been able to adapt to the proteome imbalances caused by such complex aneuploidies?

2.3 Beneficial aneuploidies drive adaptation against stress

While many evidences portray the load of aneuploidy and its detrimental effects on cellular fitness, in specific cases under strong selective forces, aneuploidy can provide a competitive edge. Aneuploidy has been shown to enhance cell proliferation in stem cells, either derived from mouse embryos or human pluripotent tissues (Liu X et al., 1997; Ben-David U et al., 2014; Zhang M et al., 2016). Aneuploidy also confers a proliferative enhancement to human cells with chromosome gains (Rutledge SD et al., 2016) and various species of fungi that experience diverse stress environments (Selmecki A et al., 2006; 2008 & 2010; Yona AH et al., 2012). Euploid and aneuploid cells derived from near diploid colorectal cancer cells show that although aneuploidy is detrimental to normal growth conditions, under conditions of stresses like starvation, hypoxia, and chemotherapeutic drugs, aneuploid cells display an enhanced proliferative rate (Fig. 5; Rutledge SD et al., 2016). For example, in order to survive treatment with the antimycotic drug fluconazole the human pathogen Candida albicans gained an additional copy of chromosome 5, which provided resistance against the drug (Selmecki A et al., 2006). In this scenario, the extra copy of chromosome 5 led to the increase in dosage of *ERG11* (a target of fluconazole) and *TAC1* proteins (which is a transcriptional factor for genes that encode drug efflux pumps).

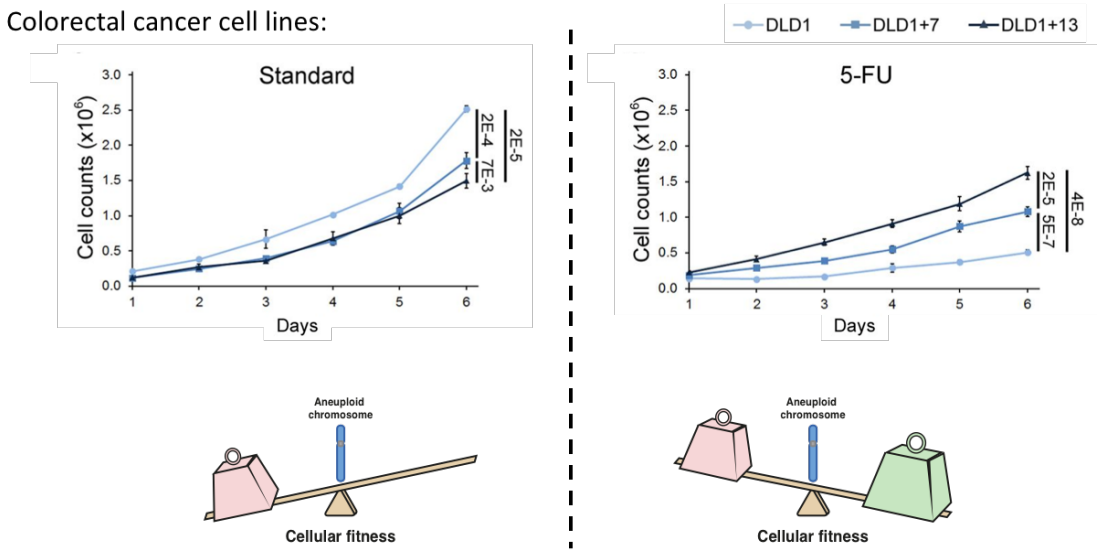

Figure 5: Aneuploidy generally decreases fitness but under specific conditions it can be beneficial.
Euploid and aneuploid (Chr. 7 or 13) DLD1 colorectal cancer cell lines were subjected to a proliferation assay in normal (Standard medium) or stressful (medium containing 10μM 5-Fluorouracil or 5-FU) conditions. Adapted from Rutledge SD et al., 2016.

By increasing the abundance of Erg11 and Tac1, the effect of the drug on the cell diminished (Coste A et al., 2007; Selmecki A et al., 2006; 2008).

Under laboratory conditions, budding yeast cells spontaneously acquire aneuploidy to cope with starvation by upregulating the number of nutrient transporters on the cell membrane, which in turn help them survive under nutrient limiting conditions (Dunham MJ et al., 2002; Gresham D et al., 2008). Specific genomic lesions could also be suppressed by aneuploidy to enhance cellular viability (Rancati G et al., 2008; Ryu H-Y et al., 2016). These studies collectively indicate that the selective advantage is often attributed to the change in expression of one or two genes, although aneuploidy alters the protein abundance of many genes (Hughes TR et al., 2000; Rancati G et al., 2008; Pavelka N et al., 2010; Ryu H-Y et al., 2016). Intriguingly one study (Yona AH et al., 2012) extended the laboratory evolution experiments to a time point

beyond the initial selective advantage. They observed that specific chromosome duplications were the first responses to a heat shock, but given enough time under the persistent stress, more favorable genomic alterations at the gene level replaced the beneficial effect conferred by the aneuploid state. These results suggest that although aneuploidy may confer fitness advantages to a cell under specific contexts, but aneuploidy-based solutions are temporary and other genomic alterations substitute the beneficial effects of aneuploidy. However, in a general context, the burden caused by the proteome imbalance deters cell populations from maintaining them as permanent solutions. Hence, similar to mutations, aneuploidy is typically detrimental but can be beneficial to cellular fitness in specific cases.

3. Aneuploidy, CIN and cancer

Cancer is a disease characterized by fast and uncontrolled cycles of cell division. Healthy human cells transform into cancerous cells when they acquire various genomic alterations, some of which confer a proliferative advantage that enables continuous and rapid proliferation. These genomic alterations range from base-pair substitutions, indels (insertions or deletions of new sequences), and whole chromosome or structural aneuploidies. Aneuploidy is the most common genomic alteration in human cancers as more than 90% of solid tumors, and 70% of hematopoietic malignancies are aneuploid (Weaver BA and Cleveland DW, 2006; Garraway LA and Lander ES, 2013; Beroukhim R et al., 2010). However, the role of aneuploidy in tumorigenesis and cancer

progression remains unclear (Hardy PA et al., 2005; Taylor AM et al., 2018; Knouse KA et al., 2017).

Across tumor types, early-stage cancers have an unstable karyotype caused by an enhanced rate of chromosome missegregation or CIN (Knouse KA et al., 2017). However, there are no clear mechanistic explanations for the source of CIN in cancer. Studies probing the cause of CIN in cancers have found the presence of multiple centrosomes (Silkworth WT et al., 2009), loss of sister chromatid cohesion (Barber TD et al., 2008), telomere attrition and DNA-damage (Burrell RA et al., 2013) as some of the many alterations that correlate with high CIN. Although there are a variety of known sources of CIN in cancer cells, it is essential to note that many such conclusions come from in-vitro experiments that utilize cancer cell lines, and the exact cause of CIN among cancer cells in-vivo remains unknown. Nevertheless, these genetic perturbations have been used by various studies to induce a high degree of CIN and aneuploidy in healthy cells to study the role of aneuploidy in tumorigenesis. Findings in cancer cell lines reveal that rates of CIN often correlate with the complexity of the karyotype. Karyotyping patient samples across various cancer types have helped to study complex karyotypes in detail, identify common aneuploidies among them and determine the patterns that emerge within complex aneuploid karyotypes.

3.1 Patterns across cancer karyotypes

In the past decade a massive collaborative effort by the cancer genome atlas (TCGA) has made it possible to identify and document whole chromosome aneuploidies across different cancer types from patient biopsies. A review study analyzed a subset of the TCGA database comprising of tumor samples from 10,249 individuals to detailed insights into the patterns that emerge within complex aneuploid karyotypes across cancers (Knouse KA et al., 2017). 77% of the samples had at least one whole chromosome aneuploidy, and in agreement with previous pan-cancer studies, chromosome losses were seen to be more likely than chromosome gains (Carter SL et al., 2012; Taylor AM et al., 2018). Although currently, no mechanism explains a bias in the missegregation of specific chromosomes, they reported that individual chromosomes like 7 and 20 were more likely to be gained, and others like chromosomes 13 and 22 were more likely to be lost. A probable explanation for these biases could be the selection pressure created by the proteome imbalance associated with each aneuploidy and its impact on cellular fitness. This explanation stems from a correlation between the frequency of specific chromosome losses in cancers and the number of genes on them.

Many pan-cancer analyses importantly conclude that there is no one single aneuploid signature across various cancers (Knouse KA et al., 2017; Taylor AM et al., 2018). Much like how different cancers carry a variety of mutational signatures, they drastically differ in their aneuploid karyotypes. For example, glioblastomas have low amounts of aneuploidy, but a large proportion of them

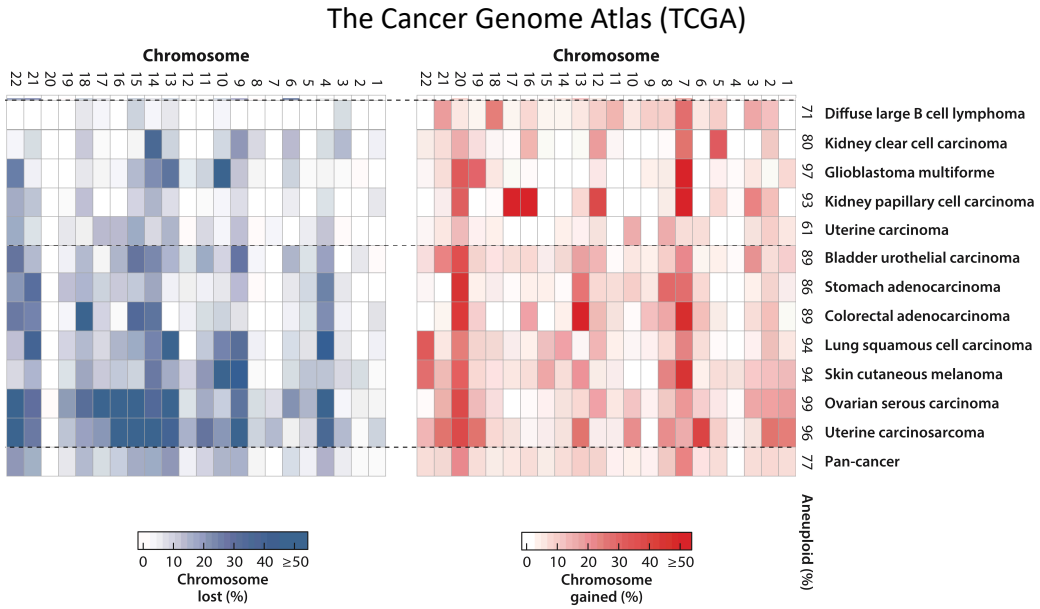

Figure 6: Patterns among aneuploid cancer karyotypes
Aneuploidy patterns across 12 different cancers analyzed from the TCGA database and their karyotypes are depicted either individually (first 12 rows) or together (Last row). The heat maps show the percentage of tumors of each cancer type that show a loss (blue) or gain (red) of a particular chromosome. Adapted from Knouse KA et al., 2017

gain an extra copy of chromosome 7 along with the loss of chromosome 10 (Fig. 6). Colorectal cancers and melanomas display a high degree of aneuploidy with aneuploidies of 6 different chromosomes and very often harbor gains of chromosome 13 and losses of chromosome 18. However, recurrent patterns in aneuploid cancers are not homogenous across every tumor type. Many cancers harbor a complex aneuploid karyotype with a high degree of karyotypic heterogeneity within a tumor. These observations argue that recurrent aneuploidies as in glioblastoma, melanoma or colorectal carcinomas could in-part drive tumorigenesis. While in several other cancers like breast carcinoma or lung adenocarcinoma, the aneuploidies are either passengers that arise as a consequence of high levels of chromosome missegregation or provide minimal benefits during adaptation to stressful environments . It is still unclear why the effect of aneuploid chromosomes is dependent on the cellular

context, and further bottom-up experiments are needed to ascertain whether aneuploidy plays a role in tumorigenesis.

3.2 Effect of aneuploidy in tumorigenesis depends on the context

Much like mutagenesis, chromosome instability aids tumorigenesis by providing the genetic diversity to fuel tumor evolution (Sansregret L and Swanton C, 2017). Several findings indicate that aneuploidy, a product of CIN, can both promote and suppress tumor formation in a context-dependent manner. As discussed in the previous sections, aneuploidy is generally associated with the impairment of cellular fitness, mainly due to gene dosage imbalances and the resulting aneuploidy-associated stresses. Furthermore, cells transformed with an oncogene display a lower tumorigenicity in the presence of an aneuploid chromosome (Sheltzer JM et al., 2017). Across cancers, the frequency of gains and losses of whole chromosomes or whole chromosomal arms correlate with the number of genes on the aneuploid chromosomes (Beroukhim R et al., 2010; Duijf PH et al., 2013). This correlation indicates that aneuploid chromosomes generally present a fitness penalty, and such aneuploidies would inhibit tumor formation rather than promoting it.

On the other hand, multiple reports analyzed clinical tumor samples and observed positive correlations between the extent of aneuploidy and transcriptional signatures generally associated with promoting tumor formation (Taylor AM et al., 2018; Buccitelli C et al., 2017; Davoli T et al., 2017). Patients with mosaic variegated aneuploidy (MVA) display an increased risk of childhood

cancers (Hanks S et al., 2004). Mouse and human embryonic stem cells spontaneously acquire beneficial aneuploidies that enhance tumorigenicity (Ben-David U et al., 2014; Zhang M et al., 2016).

Patients with Down syndrome are the best example that reveals the paradoxical role of aneuploidy in tumorigenesis. The presence of an extra copy of chromosome 21 across all cells in a human and a mouse model for Down syndrome display a lowered incidence of solid tumors (Hasle H et al., 2000; Sussan TE et al., 2008; Yang Q et al., 2002). However, they have a heightened risk for leukemia. Interestingly, across leukemias, a gain of an extra copy of chromosome 21 is a prominent feature and hence the trisomic cell of Down syndrome patients could predispose them to cancers that frequently gain chromosome 21 while deterring cancers that infrequently gain chromosome 21 (Hasle H et al., 2000; Yang Q et al., 2002).

Such puzzling observations featuring aneuploidy as both promoting and suppressing tumors closely resemble the paradoxical role of CIN in tumorigenesis (Weaver BA et al., 2007). Multiple reports that enhanced CIN either by mutating a SAC protein Bub1, or overexpressing another SAC protein Mad2 concluded that the induced CIN and its resultant aneuploidy increases spontaneous tumorigenesis in mice (Jeganathan K et al., 2007; Li M et al., 2009; Sotillo R et al., 2007). While reduced protein levels of CENP-E, a mitotic motor essential for the movement of chromosomes, lead to an elevated frequency of lymphomas and lung cancers. The same perturbation reduces spontaneous tumor formation in the liver and tumors that are induced by known

carcinogens or genetic manipulation (Weaver BA et al., 2007). These studies suggest a combination of increased CIN and the resultant aneuploidy appear to facilitate tumorigenesis, but this is not an obligatory outcome and is influenced by tissue context or the degree of CIN induced. Taken together, these paradoxical observations indicate that cellular context can determine the circumstances under which aneuploidy confers a fitness advantage and promotes tumor formation.

Two key reports analyzed the gene composition of recurrent chromosomal gains and losses to determine how aneuploidy exerts its influence during tumor formation. The analysis demonstrated that altered gene expression changes of a subset of genes on the aneuploid chromosome might explain the pro- or anti-tumorigenic effect of aneuploidy. One found that frequently recurring deletions of large DNA fragments were enriched in STOP genes that negatively regulated cellular proliferation and had a low density of GO genes that positively impacted cellular proliferation (Solimini NL et al., 2012). Correspondingly, the second report revealed that across tumor types, the frequency of aneuploidy, amplifications, or deletions of large genomic regions correlate with the density and potency of STOP and GO genes on them (Davoli T et al., 2013).

The role of the aneuploid state in aiding tumor evolution during tumor progression is prevalent despite its description as a double-edged sword. Since most numerical chromosome aberrations are associated with various stressors like proteotoxic stress, genotoxic stress, and hypo-osmotic stress, cancer cells

need to first evade the deficits of the aneuploid state before exploring the benefits of altered gene expression associated with aneuploidy. Indeed, there are several aneuploidy-tolerating mutations that the cells acquire to help ease the unfavorable consequences of aneuploidy, such as proteotoxic stress (Torres EM et al., 2010). In conclusion, recurrent aneuploidies across clones of select cancers suggest that specific karyotypes are purposefully selected to facilitate tumorigenesis.

4. Genetic interactions within cancer karyotypes

Genetic interactions characterize unexpected deviations from the anticipated phenotype of a double mutant which is calculated as the product of the single mutant phenotypes. Genetic investigations in fruitflies were the earliest to demonstrate that genetic interactions arise from the redundancies in several cellular pathways. These studies showed that a double mutant was inviable, although each of the single mutants were able to survive (Fisher RA, 1918), a phenomenon known as synthetic lethality. Synthetic lethality is a more dramatic example of genetic interaction where cell death is the unexpected phenotype of a double mutant. Genetic interactions stem from multiple redundancies in cellular pathways that have been evolved to buffer genetic variation and prevent the loss of essential functions. For example, in budding yeast, only about 20% of the genes are essential for viability under standard conditions, and the rest are dispensable when deleted in haploid yeast (Giaever G et al., 2002; Winzeler EA et al., 1999). Since various large-scale whole-genome analysis across the human genome have revealed that a large proportion of genes are dispensable,

it is expected that genetic interactions are also very prevalent across the human genome. For example, a group of yeast geneticists have generated a complete map of genetic interactions in budding yeast which comparatively has only a third of the number of genes in the human genome. However, approximately 900,000 genetic interactions were mapped across all genes in the relatively small yeast genome (Costanzo M et al., 2019).

Genetic interactions can be positive when the observed phenotype is above the expected phenotype, and vis-a-versa it can be negative when the observed phenotype is below the expected outcome (Mani R et al., 2008). Since synthetically lethal interactions between a pair of genes are also common in the human genome, they have been utilized to develop successful therapies to combat diseased states like cancers. Several cancers are driven by a variety of mutations in vital cellular processes. In many cases these cellular processes are performed by two redundant pathways and therapeutic inhibition of the second redundant pathway is selectively lethal for cancerous cells while the normal cells are unaffected. One prominent example is the development of the drug Olaparib, a poly(ADP-ribose) polymerase (PARP) inhibitor (Beijersbergen RL et al., 2017). This DNA repair enzyme negatively interacts with the BRCA family of enzymes as they perform redundant DNA repair functions (Bryant HE et al., 2005; Farmer H et al., 2005). Since several breast and ovarian cancers harbor mutations in the BRCA genes (Venkitaraman AR, 2002), inhibiting PARP would selectively result in the elimination of these cancer cells while normal cells are unaffected due to the functional BRCA gene .

Correspondingly, aneuploid chromosomes, also share synthetically lethal interactions with other genes or chemical compounds that inhibit specific protein function (Tang YC et al., 2011; 2017; Dodgson SE et al., 2016). Hence, one could hypothesize that genetic interactions between aneuploid chromosomes can help explain the high frequencies of recurring aneuploid chromosomes in cancer karyotypes. Partial evidence for the role of genetic interactions as the basis of an aneuploidy pattern came from the aneuploidies of chromosome 6 and 13. This aneuploidy pair coexists in budding yeast due to strong positive genetic interactions between the constitutively expressed tubulin genes (Katz W et al., 1990; Anders KR et al., 2009). Now hypothetically if an external stress exerts strong positive selection on chromosome 6 aneuploidy, due to the strong positive genetic interaction with aneuploidy of chromosome 13, all yeast strains that adapt against the stress would display a karyotype where aneuploidies of chromosome 6 and 13 co-occur. However, very little is known about genetic interactions between aneuploid chromosomes and how they shape complex aneuploid karyotypes. Nevertheless, regardless of whether genetic interactions exist across many aneuploid chromosomes, we

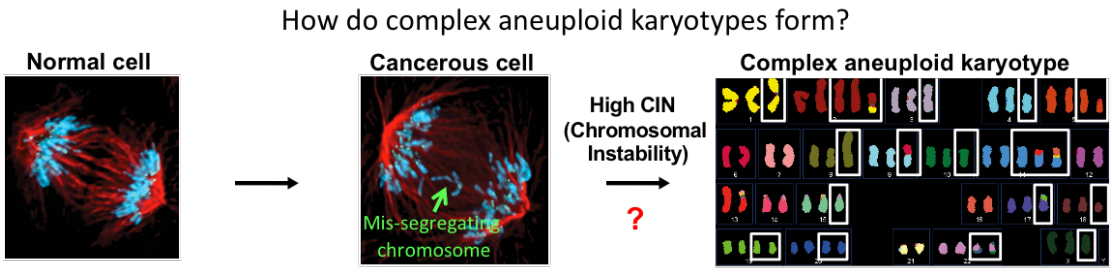

Figure 7: How do complex karyotypes form under the context of persistent CIN.
High frequencies of chromosomal instability is frequently seen in cancers and it gives rise to complex aneuploid karyotypes that correlate with poor prognosis of cancer patients. However we lack a basic understanding of how such complex aneuploid karyotypes are formed from persistent CIN. Adapted from Cover photo of *Clin. Cancer Res.* 2011 and Abdel-Rahman et al. PNAS. 2001.

also lack a general understanding of the formation of complex aneuploid karyotypes. While many top-down approaches have attempted to understand the role of aneuploidy patterns in tumorigenesis, first understanding how aneuploidy patterns among complex aneuploid karyotypes are formed and evolve during adaption is of utmost importance (Fig. 7).

5. Need for a model to study complex aneuploid karyotypes

Cancer karyotypes are frequently aneuploid, often with many gains and losses of whole chromosomes (Knouse KA et al., 2017). Further, highly complex aneuploid karyotypes correlate with the ability of cancer cells to evade the immune response (Taylor AM et al., 2018; Davoli T et al., 2017) and, therefore, the degree of aneuploidy is a predictor of the efficacy of immunotherapy in cancer patients. The higher complexity of aneuploid karyotypes often leads to a lowered chance of patient survival (Smith JC et al., 2018). Owing to the complexity of cancer karyotypes, it becomes challenging to follow the evolution of aneuploid karyotype through time and space in cancerous tissue and piece together the formative steps of a complex cancer karyotype. Currently, a simplified model to better understand the formation of complex karyotypes is of utmost importance as it can shed light on the evolution of complex karyotypes and its optimization over time to maximize the cellular fitness under stressful conditions. In the next chapter, we describe and characterize a novel method in *S. cerevisiae* to create complex karyotypes and understand their impact on cellular physiology.

Chapter 2: Results

1. Yeast cells with Survivin/*BIR1* deletion adapt by accumulating a high degree of aneuploidy

Deletion of *BIR1*, a critical subunit of the CPC in haploid budding yeast, perturbs chromosome bi-orientation and induces high rates of chromosomal instability. Tetrads of diploid yeast strains with a heterozygous deletion of *BIR1* were dissected to select for haploid strains with the *BIR1* deletion. This deletion was found to be often lethal as only 10% of the mutant spores survived. Live fluorescence microscopy of the *bir1Δ* strains revealed high levels of CIN ranging from 2.8% to as high as 7.7% per chromosome per cell division (Fig. 8A), which are consistent with the high degree of lethality previously associated with *BIR1* deletion (Sandall S et al., 2006).

For further analysis, 102 strains derived from 19 different *BIR1*-deleted spores were subjected to 10 clonal expansions. Propagating a single colony every other day to a fresh plate allowed the *BIR1* deleted strains to adapt to high levels of CIN and acquire faster growth rates than those prior to the clonal expansions. These strains, referred to as *bir1Δ-ad* strains, displayed enhanced cellular fitness when compared to the unadapted *bir1Δ* strains. However, they still grew poorly relative to wildtype strains (Figs. 8A, B). To measure the rate of chromosome missegregation directly in the *bir1Δ-ad* strains we tracked LacI-GFP foci on chromosome 4 tagged with a LacO array. As cells progressed through the cell cycle, they missegregated at a rate of 0.5% to 4.2% per chromosome per cell division. On comparison of the ongoing CIN measured

prior to the clonal adaptations, the adapted strains had a significantly lower CIN rate (P = 0.0013).

As a secondary measure of CIN, cells were then grown on plates with moderate amount of a drug that depolymerizes microtubules (Benomyl; 10 μg/mL). All the *bir1Δ* strains maintained their sensitivity to the drug after adaptation, indicating

Ravichandran et al. 2018 Figure 1

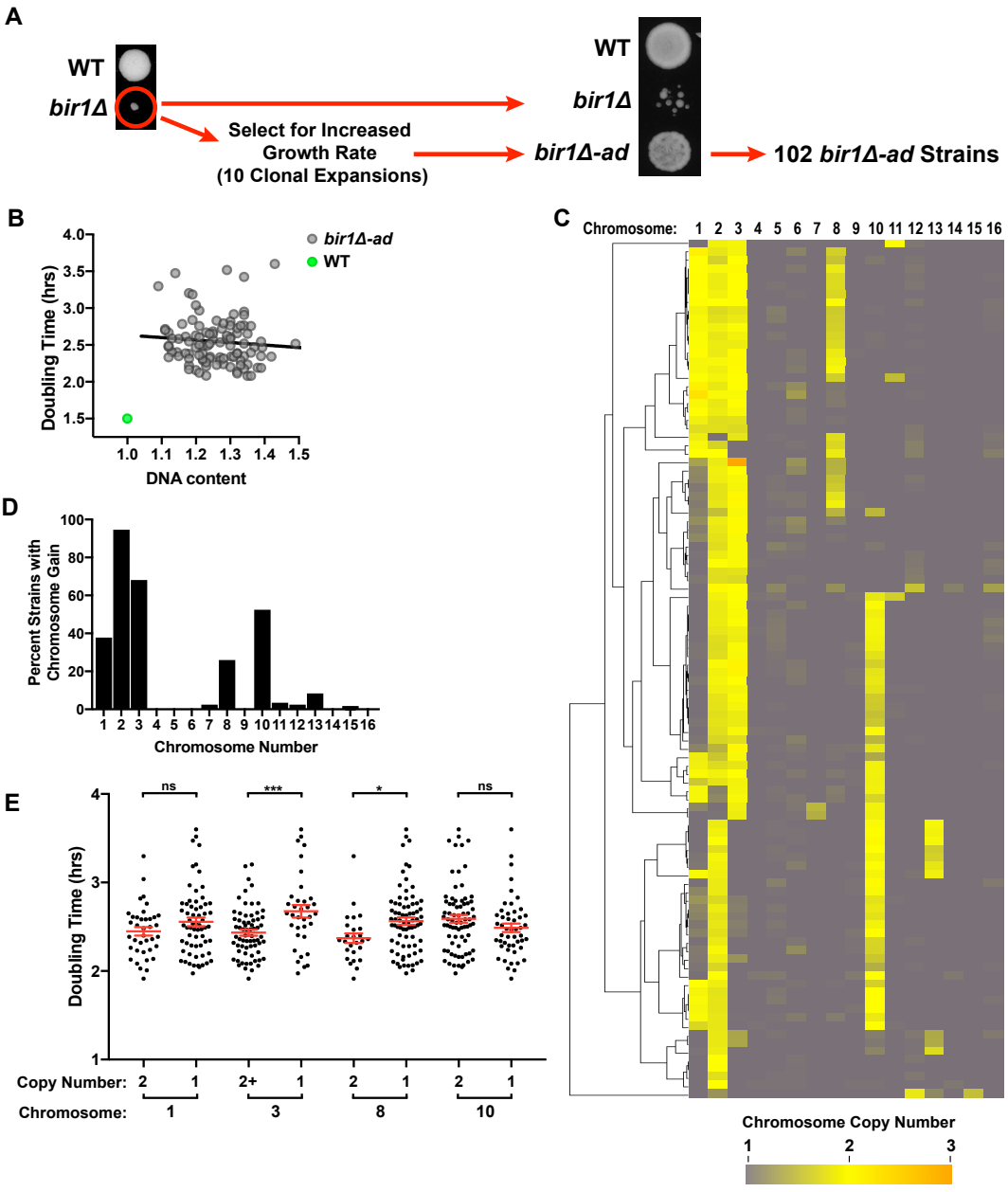

Figure 8: Complex aneuploid karyotypes arise from adaptation to BIR1 deletion.
A) Graphical representation of the steps taken to generate approximately 102 bir1Δ-ad (BIR1 deletion) strains. A tetrad dissection of the BIR1/ bir1Δ diploid strain depicting a wildtype (WT) and BIR1 deleted spores (bir1Δ) after four days of growth are shown on the left. Subsequently 10 clonal selections were performed to allow the bir1Δ strains to adapt (~200 generations). Equal optical densities (OD600) were spotted on rich medium (YPAD), to depict the cellular fitness of the bir1Δ and the corresponding bir1Δ-ad strain.
B) Absence of a correlation between the growth rates of all 102 bir1Δ-ad strains and the excess DNA accumulated by them during adaptaion. DNA content as measured by flow cytometry was plotted against doubling time in rich liquid medium (YPAD) calculated using optical density measurements of cultures in the exponential phase of growth. Two-tailed p-value = 0.38. Pearson's correlation coefficient = -0.09.
C) Visualization of the karyotypes using heat-map depicting the chromosome copy number data of each of the 102 bir1Δ-ad strains which was measured by the density of read counts from next generation sequencing of the whole genome. Each row represents the karyotype of one of the bir1Δ-ad strains and the chromosome copy number data is clustered to depict karyotype patterns.
D) Frequency of each aneuploidy chromosome in the adapted bir1Δ strains after binarization of the karyotypes in C.
E) Growthrate comparisons of the haploid bir1Δ strains with and without aneuploidy of chromosomes 1, 3, 8 and 10. Mean doubling time along with their standard errors are shown. *p ≤ 0.01, ***p ≤ 0.0001, ns = not significant (from unpaired t test).
Taken from Ravichandran MC et al., 2018

that all the adapted *bir1Δ* strains continue to missegregate their chromosomes (Figs. 9B, C). Taken together the *bir1Δ-ad* strains have adapted by partially reducing their levels of CIN while they do not fully abrogate the strong CIN phenotype.

To ascertain if the high levels of CIN translate to an elevation in the amount of DNA, we measured the DNA content of the *bir1Δ-ad* strains by flow cytometry. All 102 *bir1Δ-ad* strains had a high degree of aneuploidy with 10 to 40 percent elevation in DNA content relative to euploid controls. Even though the adapted strains displayed remarkable heterogeneity in both cellular fitness and degree of aneuploidy, the two did not share any correlative relationships (Fig. 8B). This lack of a clear correlation between the elevated DNA content and cellular fitness may be indicative of the absence of a direct relationship between gaining extra chromosomes and the adaptation to CIN.

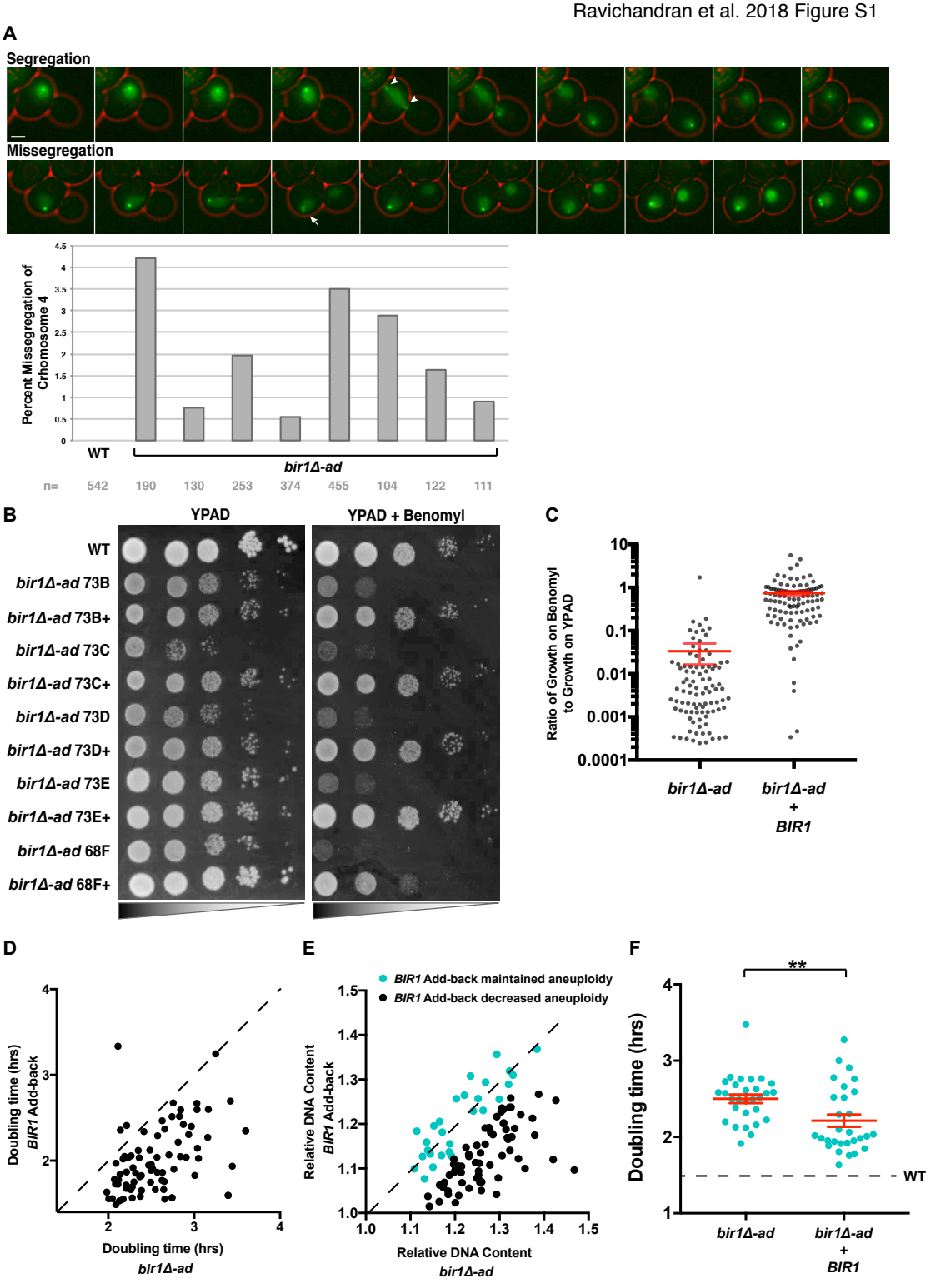

On average the adapted *bir1Δ* strains doubled every two and a half hours, approximately 60% slower than the wildtype strain (Fig. 8B) and these severe growth defects could either be a result of the ongoing CIN (induced by the

Figure 9: BIR1 gene addback to the bir1Δ-ad strains. Associated with Figure 8.
A) Rates of missegregation for bir1Δ-ad strains measured by tracking GFP-labeled chromosome IV. The images show examples of a time lapse of a properly segregated (white arrowheads) and missegregated (white arrow) chromosome IV. The time interval is 6 minutes between images and the length of the scale bar is 2 μm. The graph plotted below depicts the quantification of the rate of missegregation per chromosome in the wild-type (WT) and several different bir1Δ-ad strains. WT strains showed no missegregation events and the number of chromosome segregation events counted (n) are displayed below the graph for each strain.
B) Benomyl sensitivity test as a secondary measure of missegregation rates in bir1Δ-ad and *bir1Δ-ad* + *BIR1* add-back strains. Moderate (10 μg/ml) amount of the microtubule-depolymerizing drug Benomyl were added to the media in which the *bir1Δ-ad* and *bir1Δ-ad* + *BIR1* add-back strains were grown for two days. Dilution spotting (10-fold) were performed with wildtype, multiple *bir1Δ-ad* and their respective *BIR1* add-back strains on rich medium (YPAD) plates supplemented with or without Benomyl.
C) Quantification of the Benomyl sensitivity test of the *bir1Δ-ad* and *bir1Δ-ad* + *BIR1* add-back strains. The y-axis represents the ratio of growth with vs. without Benomyl for all 102 bir1Δ-ad and *bir1Δ-ad* + *BIR1*. The standard errors and mean values the are shown in red.
D) A graphical plot of the fitness (represented as doubling times) of bir1Δ-ad strains vs. bir1Δ-ad + *BIR1* add-back strains.
E) A graphical plot of the measured DNA content (by flow cytometry) for bir1Δ-ad strains and bir1Δ-ad + *BIR1* add-back strains. The strains that displayed similar levels of aneuploidy before and after the add-back of *BIR1* are indicated as blue dots indicate .
F) Cellular fitness of the *bir1Δ-ad* and *bir1Δ-ad* + *BIR1* add-back strains for all strains that displayed similar levels of aneuploidy before and after the add-back of *BIR1* (blue dots from D). Optical density measurements were used to calculate the doubling times. The standard errors and mean values the are shown in red. ** $p < 0.001$.
Taken from Ravichandran MC et al., 2018

continued lack of Bir1) or the aneuploidy generated by the CIN. To differentiate between the growth defects caused by CIN and aneuploidy, a single copy insertion of the *BIR1* gene was added back into the *bir1Δ-ad* strains. For nearly all the strains, the reintroduction of the *BIR1* gene completely rescued the sensitivity towards the drug Benomyl demonstrating the elimination of ongoing CIN (Figs. 9B, C). Despite the abrogation of CIN, the growth rates of the add-back strains were only partially rescued, indicating that the persistent aneuploidy also contributes to the fitness defects of the *bir1Δ-ad* strains (Fig. 9D). Further, most of the add-back strains lost the aneuploidy as soon as *BIR1* was added back, suggesting that the deletion of *BIR1* was a source of ongoing selection for the observed elevation in DNA content (Fig. 9E). By specifically focusing on the cellular fitness of those *BIR1*-addback strains that maintained

their DNA content after reintroduction of *BIR1*, we observed only a partial (~50% median) rescue of the growth phenotype (Fig. 9F). Hence, these results show that the growth defects of the *bir1Δ-ad* strains are a sum of the effects of both the ongoing CIN and the resultant aneuploidy. Taken together these results suggest that the adaptive traits acquired by the *bir1Δ-ad* strains aim to lower the rates of chromosome missegregation likely by gaining aneuploid chromosomes.

2. Adaptation to high rates of CIN occurs through many different disomic chromosomes in *bir1Δ-ad* strains

In order to examine the heterogeneous aneuploidies acquired in the adapted *bir1Δ* strains, we used next generation sequencing to sequence the genomes of 102 adapted strains. We used a custom python script that utilized the read counts from the sequencing data to identify the relative copy numbers of specific aneuploidies commonly gained by the adapted strains. Frequent gains of extra copies of chromosomes 1, 2, 3, 8, and 10 were observed with each aneuploidy seen in over a quarter of the *bir1Δ-ad strains* (Figs. 8C, D). Chromosomal rearrangements or any large indels were absent across all the strains. On average, the strains acquired two mutations in their genomes, however the non-synonymous mutations within coding regions were not significantly enriched for the 'CIN' gene ontology (GO) term (P = 0.53). Among the 190 genes mutated in the *bir1Δ-ad* strains, only 15.8% (30 of 190 mutated genes) were CIN genes, which is similar to the overall proportion of CIN genes in the entire yeast genome (14.5%, 874 of 6000 genes). Along the same lines,

collectively across all 190 mutated genes, there were no other statistically significant GO term enrichment in the *bir1Δ-ad* strains (False discovery rate [FDR] < 0.05). Additionally, 41 heterozygous mutations identified on disomic chromosomes (Table 4) did not correlate with any common cellular pathway suggesting that they do not contribute to the adaptation to CIN. A few candidate mutations were further reintroduced into the yeast strains prior to the *BIR1* gene deletion but they did not correlate with better fitness (data not shown), indicating that these mutations were merely a consequence of the genome instability caused by *BIR1* deletion. The above results suggest that the mutations acquired during the adaptation against high levels of CIN did not contribute to the improved growth of the *bir1Δ-ad* strains.

So far, all the results point at aneuploidy as the most substantial genomic alteration in the *bir1Δ-ad* strains. To determine the extent to which each aneuploidy contributes to the improved cellular fitness of the *bir1Δ-ad* strains, we grouped the 102 strains relative to the presence or absence of one aneuploid chromosome and compared the time taken between successive population doublings. The growth rates of all the *bir1Δ-ad* strains calculated using optical density measurements allowed direct comparisons of adapted strains with and without extra copies of chromosomes 1, 3, 8, and 10. Since there were insufficient number of strains without a gain of chromosome 2 (6 of 102 *bir1Δ-ad* strains), it was not possible to make meaningful comparisons. The adapted strains that acquired an extra copy of chromosomes 3 or 8 displayed an enhanced growth rate, when compared to those that did not have the

respective aneuploid chromosomes. While chromosome 1 disomy was associated with a small insignificant increase in growth rate (P = 0.14), surprisingly the disomy of chromosome 10 did not correlate with better fitness. Although an extra copy of chromosome 10 was gained in more than half of the strains (Figs. 8D, E), this aneuploidy resulted in a decrease in fitness.

One of the two theories that could help explain this discrepancy is that the aneuploidy of chromosome 10 is neutral with respect to cellular fitness and during the clonal expansions roughly half of the strains would be expected to gain an extra copy of chromosome 10. Alternatively, the disomy of chromosome 10 could initially provide benefits to cellular fitness, which decreases with time. For testing the latter hypothesis, we used a previously established technique (Anders KA et al., 2009) to engineer individual chromosome disomy prior to the deletion of the *BIR1* gene. A strong galactose-inducible promoter placed proximal to the centromere of a chromosome of choice allows for a controlled non-disjunction of a specific chromosome. The disomy of a chromosome can subsequently be selected by a stochastic event involving an engineered genetic recombination ultimately resulting in restoration of a selectable marker on the extra copy of the chromosome (Fig. 10A). The *BIR1* gene is subsequently lost by counterselection of the *URA3* marker by growing the engineered strains in media containing the drug 5-Fluoroorotic acid (5-FOA) (Fig. 10A). When grown on 5-FOA plates for selection of *BIR1* deleted strains, those engineered strains that contained an extra copy of either chromosomes 2, 3, 8, and 10 showed improved growth relative to the euploid control (Fig. 10B).

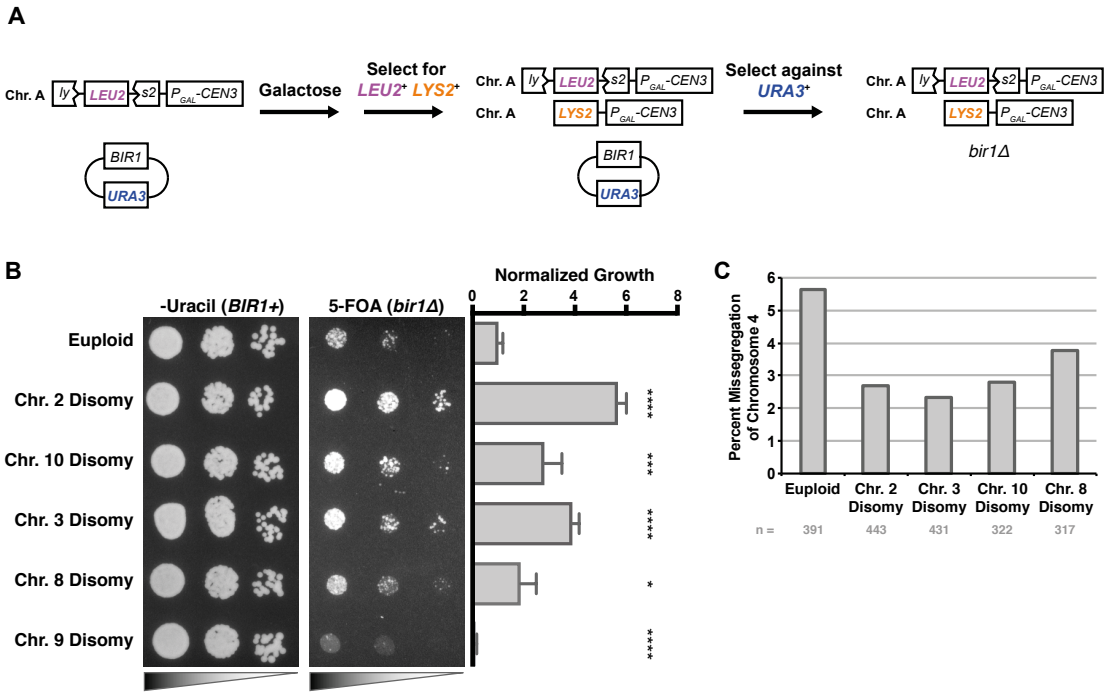

Figure 10: Gain of an extra copy of specific chromosomes gives an initial advantage to the *BIR1* deletion strains.
A) Graphical depiction of a galactose-inducible method to engineer gains of specific chromosomes prior to the deletion of *BIR1* (Refer to "Materials and Methods"). B) Dilution spotting (10-fold) of engineered disomic strains on minimal media plates with the drug 5-FOA (counter-selects the *URA3* gene) or minimal media lacking uracil (selects for *URA3*) plates. The plotted graph represents the quantification of the fitness of each strain after counter-selecting for *BIR1* with 5-FOA. Every value was normalized to the euploid strain. ∗p ≤ 0.05, ∗∗∗p ≤ 0.0001, ∗∗∗∗p ≤ 0.00001 (unpaired t-test).
C) Rates of missegregation for *bir1Δ-ad* strains measured by tracking *GFP*-labeled chromosome IV for *bir1Δ* strains generated from 5-FOA plates as in B. The number of chromosome segregation events counted (n) are indicated under the graph. See Figure 9A for representative examples of segregation vs missegregation events.
Taken from Ravichandran MC et al., 2018

Conversely, the disomy of chromosome 9, which was never observed across all the *bir1Δ-ad* strains, drastically impaired fitness when combined with the euploid *BIR1* deletion strain. As a control for the dilution assay, equal growth was observed for all five disomic strains on the non-selective (*BIR+*) plates. Further, the increase in fitness of the engineered disomic strains upon deletion of *BIR1* corresponded with a decrease in the missegregation rate (Fig. 10C). Together these results indicate that the aneuploidies benefit the growth rates upon *BIR1* deletion by partially suppressing the CIN phenotype associated with

the *bir1Δ* mutants. Hence, we conclude that each of the disomies of chromosome 2, 3, 8, and 10 are frequently gained by the *bir1Δ-ad* strains because they confer an initial benefit after the induction of CIN.

Among all the engineered disomic *bir1Δ* strains, chromosome 2 displayed a strong rescue of the fitness deficit associated with *BIR1* deletion. It was also the most common aneuploidy selected across the adapted *bir1Δ* strains, suggesting the presence of a gene or group of genes on chromosome 2 that strongly contributes and may be necessary to survive the deletion of *BIR1*. Notably, the gene *SLI15*, encoding a scaffolding subunit in the CPC, is present on chromosome 2 and was picked as a candidate gene on chromosome 2 to test if doubling its copy number rescues the *bir1Δ* phenotype. To determine this, we added an additional copy of *SLI15* at the *URA3* locus on chromosome 5 (Fig. 11A). Duplication of the *SLI15* gene leads to a similar level of growth as an extra copy of chromosome 2 (Fig. 11B). In contrast to the *bir1Δ-ad* strains, when strains with *SLI15* duplication and *BIR1* deletion were adapted for a long period of time (~200 generations), they showed a drastic decrease in the frequency of chromosome 2 disomy and superior growth rates (Figs. 11C, D). Copy number determination from sequencing 12 of the adapted *SLI15-duplicated bir1Δ* strains showed that albeit displaying a reduced frequency of chromosome 2 disomy, they still maintained the 4 other frequent chromosome

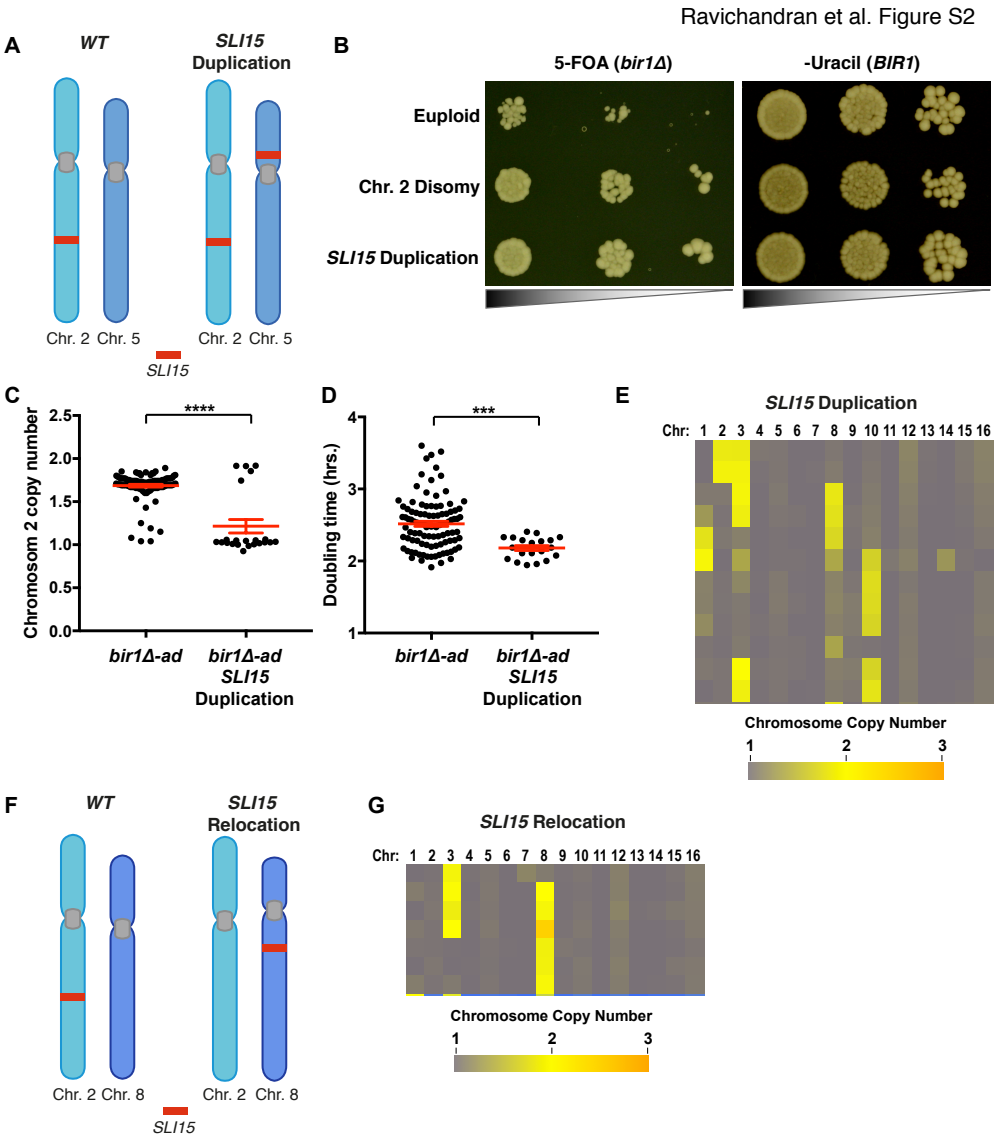

Figure 11: Extra copy of Chromosome 2 is beneficial for bir1Δ-ad strains by effectively doubling the SLI15 gene copy number. Associated with Figures 10 and 12.
A) An illustration of the *SLI15* gene duplication. A second copy of *SLI15* was placed on chromosome 5.
B) A dilution series (10-fold) of strains on medium that selects against the *URA3* gene (5-FOA plates) and medium that selects for *URA3* gene (-uracil plates). Selection on 5-FOA plates selects for cells that have spontaneously lost the minichromosome with the *URA3* gene, thus also eliminating the only functional copy of BIR1 present on the same minichromosome, ultimately generating a *bir1Δ* cells.
C) qPCR data depicting chromosome 2 copy numbers of the adapted *bir1Δ* strains and *SLI15* duplication + *bir1Δ-ad* strains before adaptation via clonal selection. Standard errors and mean values are shown in red.
D) Proliferation rate of the adapted *bir1Δ* strains and *SLI15* duplication + *bir1Δ-ad* strains before adaptation via clonal selection measured in rich media using optical density. Standard errors and mean values are shown in red.
E) Visualization of the karyotypes using heat-map for the *SLI15* duplication + *bir1Δ-ad* strains . Every strain is depicted as a row.
F) An illustration of the *SLI15* gene relocation, with the only copy of this gene relocated to chromosome 8.
G) Visualization of the karyotypes using heat-map for the *SLI15* duplication + *bir1Δ-ad* strains. Every strain is depicted as a row.
Taken from Ravichandran MC et al., 2018

disomies (chromosomes 1, 3, 8, and 10) previously observed in the original *bir1Δ-ad* strains (Fig. 11E).

This demonstrates that during the course of adaptation against the CIN induced by *BIR1* deletion, the *bir1Δ-ad* strains acquired disomies of chromosomes 1, 3, 8, and 10 independent of chromosome 2 disomy. Our attempts to create a strain with the only copy of *SLI15* on chromosome 5 were unsuccessful as all spores were not viable. As chromosome 5 disomy is associated with severe growth defects (Torres EM et al., 2007), this result further indicates the importance of *SLI15* duplication as an important initial step towards adaptation to *BIR1* deletion. To overcome this, we relocated *SLI15* to chromosome 8, a chromosome that we knew could be selected in extra copies. As expected all the spores with the only copy of *SLI15* on chromosome 8 were viable and none of them had a disomy of chromosome 2 (0 of 7 strains, Figs. 11F, G). This further supports the idea that the sole purpose of frequently selecting an extra copy of chromosome 2 in the *bir1Δ-ad* strains was to increase the expression of *SLI15*.

3. Chromosome copy number alterations in bir1Δ-ad strains share positive and negative correlations

Surprisingly, chromosome 10 disomy provided an initial growth advantage, yet among the *bir1Δ-ad* strains gaining an extra copy of chromosome 10 did not correlate with better fitness. However, until this point, we have only analyzed each chromosomal gain independently, while most of the *bir1Δ-ad* strains had

complex karyotypes with multiple aneuploid chromosomes (98 out of 102 *bir1Δ-ad* strains). Since most of the *bir1Δ-ad* strains had more than one chromosomal copy number alteration (or referred to as complex karyotypes), we determined if any correlations existed between the different chromosome copy number alterations (Fig. 8C). A heat map of the clustered karyotypes of all the *bir1Δ-ad* strains reveals a striking pattern between disomy of chromosomes 8 and 10. 76 percent (78 of 102) of the adapted *bir1Δ* strains have either an extra copy of chromosome 8 or 10, while only one strain had both ($P = 2.6 \times 10^{-9}$, Hypergeometric test) (Fig. 12A). On the other hand, a positive correlation is observed between chromosomes 8 and 3. Almost all strains (24 of 26) with an elevated copy number of chromosome 8 also have an elevated copy number of chromosome 3, while only 59% (45 of 76) of *bir1Δ-ad* strains missing the aneuploidy of chromosome 8 have the aneuploidy of chromosome 3 ($P < 0.001$, Hypergeometric test) (Fig. 12B). Furthermore, an exhaustive analysis computed all the pairwise correlations between every aneuploid chromosome across the *bir1Δ-ad* strains disclosed five correlations that were highly significant ($P < 0.001$) also including the two mentioned above (Fig. 12C). In conclusion, we found that across the highly aneuploid karyotypes of the *bir1Δ-ad* strains each aneuploidy does not act independently. This could help explain why some chromosomal gains such as chromosome 10 do not directly correlate with improved fitness (Fig. 8E) despite providing an initial fitness advantage to the *bir1Δ* strains (Fig. 10B).

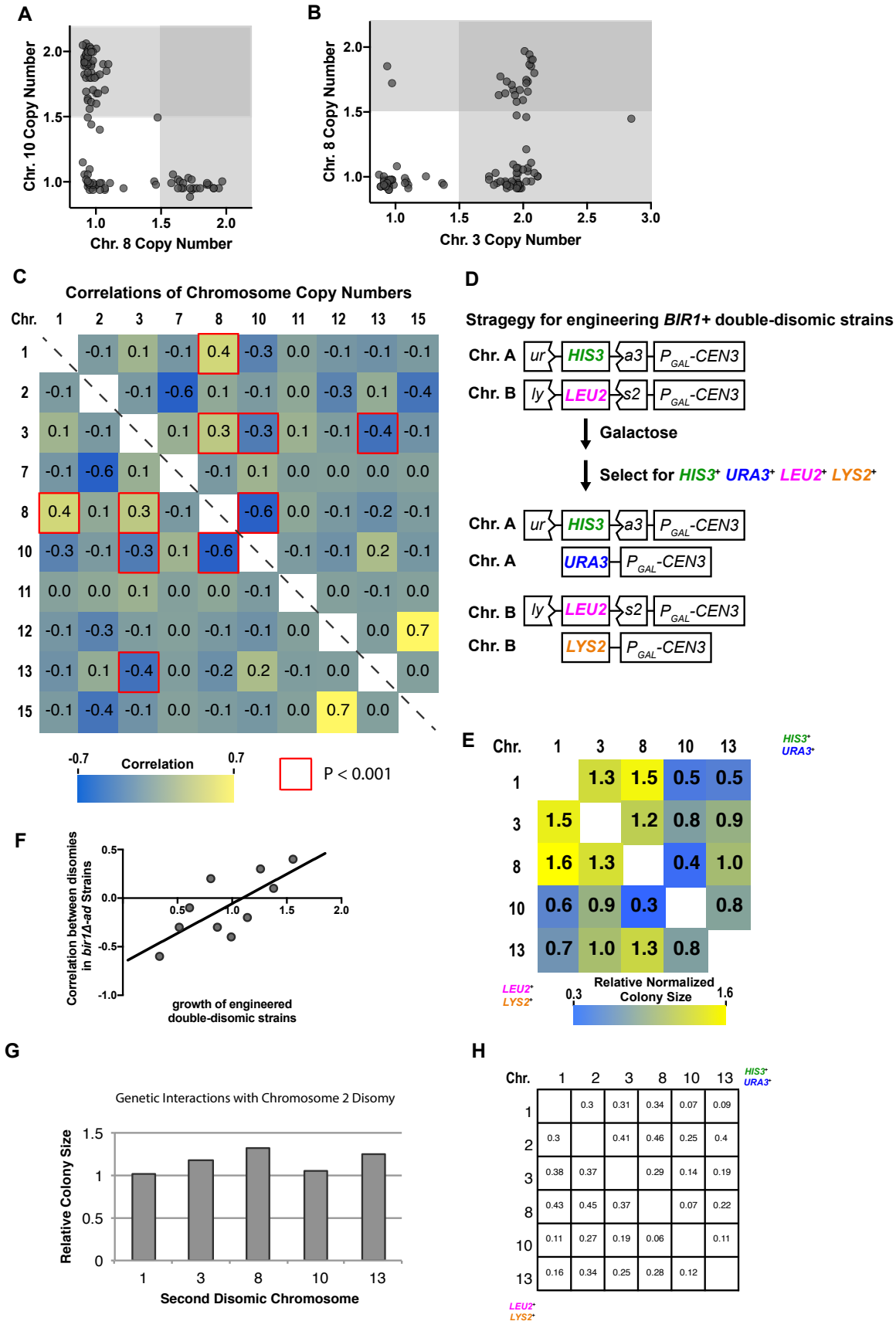
A
Chr. 10 Copy Number
Chr. 8 Copy Number
B
Chr. 8 Copy Number
Chr. 3 Copy Number
C
Correlations of Chromosome Copy Numbers
Chr. 1 2 3 7 8 10 11 12 13 15
1 -0.1 0.1 -0.1 0.4 -0.3 0.0 -0.1 -0.1 -0.1
2 -0.1 -0.1 -0.6 0.1 -0.1 0.0 -0.3 0.1 -0.4
3 0.1 -0.1 0.1 0.3 -0.3 0.1 -0.1 -0.4 -0.1
7 -0.1 -0.6 0.1 -0.1 0.1 0.0 0.0 0.0 0.0
8 0.4 0.1 0.3 -0.1 -0.6 0.0 -0.1 -0.2 -0.1
10 -0.3 -0.1 -0.3 0.1 -0.6 -0.1 -0.1 0.2 -0.1
11 0.0 0.0 0.1 0.0 0.0 -0.1 0.0 -0.1 0.0
12 -0.1 -0.3 -0.1 0.0 -0.1 -0.1 0.0 0.0 0.7
13 -0.1 0.1 -0.4 0.0 -0.2 0.2 -0.1 0.0 0.0
15 -0.1 -0.4 -0.1 0.0 -0.1 -0.1 0.0 0.7 0.0
-0.7 Correlation 0.7
P < 0.001
D
Stragegy for engineering BIR1+ double-disomic strains
Chr. A ur HIS3 a3 P GAL -CEN3
Chr. B ly LEU2 s2 P GAL -CEN3
Galactose
Select for HIS3+ URA3+ LEU2+ LYS2+
Chr. A ur HIS3 a3 P GAL -CEN3
Chr. A URA3 P GAL -CEN3
Chr. B ly LEU2 s2 P GAL -CEN3
Chr. B LYS2 P GAL -CEN3
E
Chr. 1 3 8 10 13
HIS3+ URA3+
1 1.3 1.5 0.5 0.5
3 1.5 1.2 0.8 0.9
8 1.6 1.3 0.4 1.0
10 0.6 0.9 0.3 0.8
13 0.7 1.0 1.3 0.8
LEU2+ LYS2+
Relative Normalized Colony Size
0.3 1.6
F
Correlation between disomies in bir1Δ-ad Strains
growth of engineered double-disomic strains
G
Genetic Interactions with Chromosome 2 Disomy
Relative Colony Size
Second Disomic Chromosome
H
Chr. 1 2 3 8 10 13
HIS3+ URA3+
1 0.3 0.31 0.34 0.07 0.09
2 0.3 0.41 0.46 0.25 0.4
3 0.38 0.37 0.29 0.14 0.19
8 0.43 0.45 0.37 0.07 0.22
10 0.11 0.27 0.19 0.06 0.11
13 0.16 0.34 0.25 0.28 0.12
LEU2+ LYS2+

Figure 12: Genetic interactions between whole chromosome disomies dictate patterns in complex aneuploidy.
A, B) Chromosome copy numbers of specific chromosomes represented as a scatter plot across all the 102 *bir1Δ-ad* strains demonstrating negative (A) and positive (B) correlations between distinct chromosome disomies. Copy number data was calculated as in Figure 8C. The grey regions that are darker contain strains which are aneuploid for both of the chromosomes.
C) Visualization of the karyotypes using heat-map for the correlations within chromosome copy numbers of all 102 haploid *bir1Δ-ad* strains. Only those correlations between aneuploid chromosomes are shown. Each unit of the matrix represents the correlation coefficient between the two chromosomes indicated in the row and column. Those correlations with $P < 0.001$ in the hypergeometric test have a red highlighted border.
D) Graphical depiction of a method to engineer strains (*BIR1+*) that harbor a gain of two chromosomes. Cells were transformed with PCR fragments containing *PGAL-CEN3 ura3::HIS3* on one of the chromosomes (say Chr A) and *PGAL-CEN3 lys2::LEU2* on the other chromosome (say Chr B). Using chromosome non-disjunction by inducing with galactose both chromosomes were specifically missegregated and selected with all four auxotrophic markers (*URA3, HIS3, LYS2,* and *LEU2*).
E) Relative colony sizes of the engineered double disomic strains on rich medium (YPAD) plates were normalized to all the values in their corresponding rows and columns. Raw data with colony sizes prior to normalization are shown in Panel H.
F) Comparison of the chromosome copy number correlation coefficients of the bir1Δ-ad strains (from C) and the relative cellular fitness of double disomic strains (from E). Relative values represent an average of both values in E (column:row and row:column for every chromosome pair). Pearson's correlation coefficient = 0.73. Two-tailed p-value = 0.016.
G) Relative colony sizes of strains that are engineered with a chromosome 2 disomy and a second chromosome that is correspondingly shown. Normalization was performed as in Panel E.
H) Median colony sizes in square millimeters of double disomic strains on YPAD plates. Normalized values are in Panel E.
Adapted from Ravichandran MC et al., 2018

4. Correlations between chromosomal copy number alterations are a result of genetic interactions among aneuploid chromosomes

The stark anti-correlation among disomies of chromosomes 8 and 10 could be explained by one of the two following scenarios. One, the disomies of chromosomes 8 and 10 may share a functional redundancy in providing an adaptive advantage to *BIR1* deletion, wherein gaining one of the aneuploidies results in the loss of positive selection for the second aneuploidy. Alternatively, when both the aneuploid chromosomes are concomitantly gained, a synthetic negative genetic interaction between them, independent of the *BIR1* deletion may result in a severe loss of cellular fitness. To test the latter, we modified the

previously mentioned technique to induce the disomy of specific chromosomes (Anders KA et al., 2009), such that two chromosomal disomies can be simultaneously engineered (Fig. 12D). After inducing missegregation by growing them in galactose containing medium, the disomy of both chromosomes were selected using four auxotrophic markers on plates lacking uracil, histidine, leucine, and lysine.

The strains engineered with the disomy of both chromosomes 8 and 10 displayed colony sizes, that were significantly smaller than expected (Fig. 13A). Moreover, pairwise combinations of each of the five chromosomes that displayed statistically significant negative or positive correlations between chromosome copy number alterations in *bir1Δ-ad* strains were engineered in wild-type yeast strains (Fig. 12E). The disomy of both chromosomes was verified by qPCR.

The colony size of the strains containing a pair of disomic chromosomes were measured and then normalized such that the growth differences in the individual aneuploidies are accounted for (Figs. 12E and 11I). An expected colony size was calculated for each pair and the colony sizes of the engineered double disomy strains ranged from 60% larger to 70% smaller than expected, indicative of strong positive and negative genetic interactions among aneuploid chromosomes. By comparing the relative growth of the chromosome pair that we tested and chromosome size, we found no significant correlation, demonstrating that these genetic interactions were not simply a consequence

of increasing amounts of excess DNA ($p = 0.48$, data not shown). We named these genetic interactions at the whole chromosome level as chromosome copy number interactions (CCNIs).

To evaluate the degree to which CCNIs among specific aneuploidies could help explain the patterns among the complex karyotypes of the *bir1Δ-ad* strains, we plotted the chromosome copy number correlations in the adapted strains (Fig. 12C) against the fitness data of the engineered double-disomic strains (Fig. 12E). There was a significant correlation between the fitness of the engineered pair of disomic chromosomes and the frequency of co-occurrence of that chromosomal pair in the *bir1Δ-ad* strains ($r = 0.73$, $p = 0.016$) (Fig. 12F). For example, the strains with disomy of both chromosomes 1 and 8 had the largest relative colony size across the engineered strains and accordingly displayed the highest significantly positive copy number correlation in the *bir1Δ-ad* strains. On the other hand, the aneuploidy pair that displayed the smallest relative colony size, chromosomes 8 and 10, had the highest significantly negative copy number correlation in the adapted strains (Figs. 12C, E, F, and 13A). Additionally when the selection markers were changed they showed similar results (Fig. 12E). Chromosome 2 displayed no negative genetic interactions with the other chromosomes which might have also contributed to its high frequency of occurrence in the *bir1Δ-ad* strains (Figs. 12G and 12H). This demonstrates that negative and positive genetic interactions among pairs of aneuploid chromosomes help explain the patterns observed across complex

karyotypes. Overall, the results indicate that CCNIs play a key role to govern the formative steps of complex aneuploid karyotypes.

Ravichandran et al. 2018 Figure S3

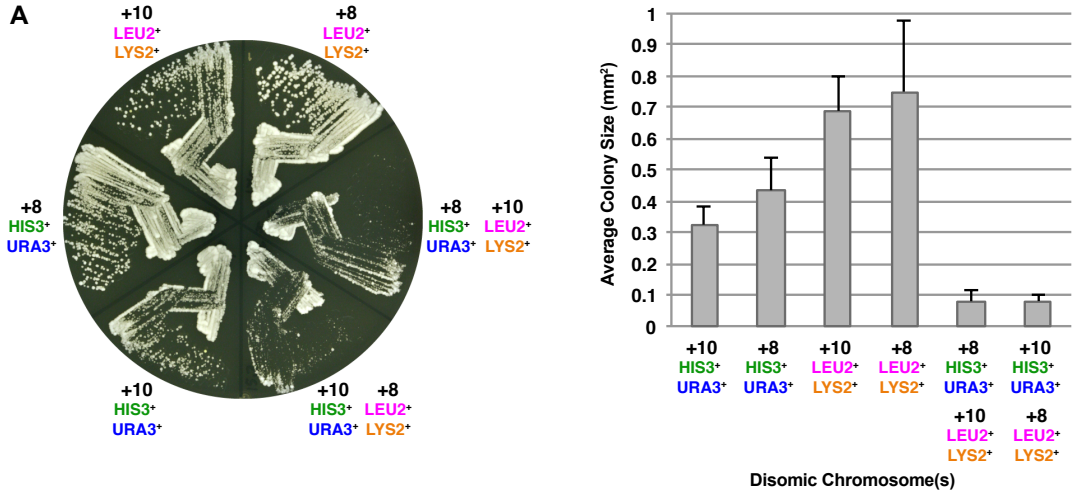

Figure 13: Strong negative genetic interaction between disomic chromosomes 8 and 10. Strains with engineered disomies of chromosome 8, 10 or both were struck out on rich media (YPAD) plates such that single colonies sizes could be measured. On the right, the graph represents the quantification of the colony sizes of the engineered strains (in square millimeters). Error bars were calculated using the standard deviations from three independent biological repeats. Taken from Ravichandran MC et al., 2018

Since chromosomes 8 and 10 can display positive CCNIs with other aneuploid chromosomes, the strong negative CCNI between chromosomes 8 and 10 seems to be specific to this pair of aneuploid chromosomes. This specificity of CCNIs between chromosomes 8 and 10 suggests that they could result from expression imbalances of individual genes on each aneuploid chromosome. For identifying the genes responsible for the negative CCNIs between chromosomes 8 and 10, we first used the increased basal mutation rate associated with aneuploidy to identify a mutant that could rescue the fitness defects of the engineered double disomic strain.

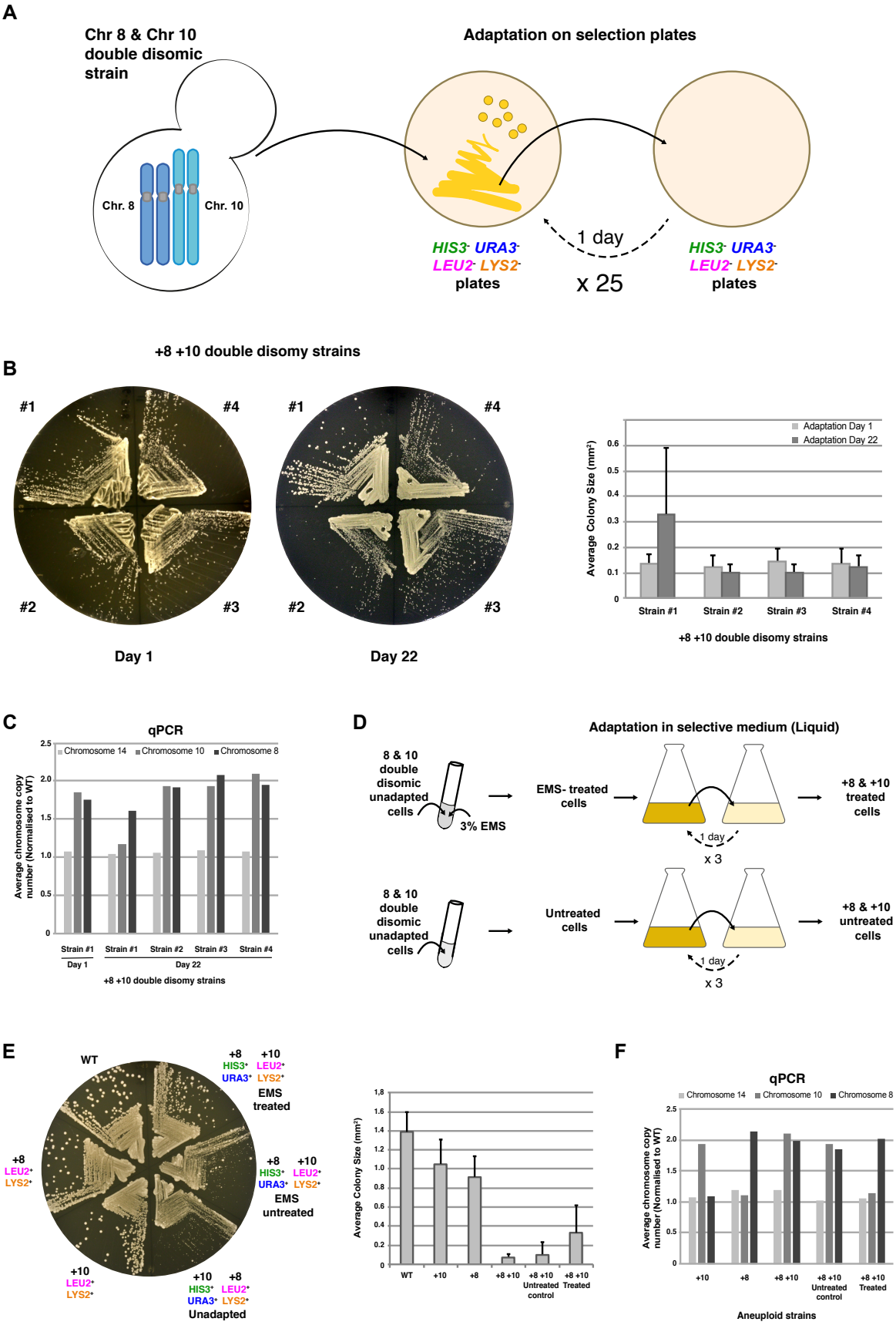
A
Chr 8 & Chr 10 double disomic strain
Chr. 8
Chr. 10
Adaptation on selection plates
HIS3- URA3-
LEU2- LYS2-
plates
1 day
x 25
HIS3- URA3-
LEU2- LYS2-
plates
B
+8 +10 double disomy strains
#1
#4
#2
#3
Day 1
Day 22
Adaptation Day 1
Adaptation Day 22
Average Colony Size (mm²)
Strain #1
Strain #2
Strain #3
Strain #4
+8 +10 double disomy strains
C
qPCR
Chromosome 14
Chromosome 10
Chromosome 8
Average chromosome copy number (Normalised to WT)
Day 1
Day 22
+8 +10 double disomy strains
D
Adaptation in selective medium (Liquid)
8 & 10 double disomic unadapted cells
3% EMS
EMS- treated cells
+8 & +10 treated cells
1 day
x 3
Untreated cells
+8 & +10 untreated cells
E
WT
+8 HIS3+ URA3+ +10 LEU2+ LYS2+
EMS treated
+8 LEU2+ LYS2+
+8 HIS3+ URA3+ +10 LEU2+ LYS2+
EMS untreated
+10 LEU2+ LYS2+
+10 HIS3+ URA3+ +8 LEU2+ LYS2+
Unadapted
Average Colony Size (mm²)
WT
+10
+8
+8 +10
+8 +10 Untreated control
+8 +10 Treated
F
qPCR
Chromosome 14
Chromosome 10
Chromosome 8
Average chromosome copy number (Normalised to WT)
+10
+8
+8 +10
+8 +10 Untreated control
+8 +10 Treated
Aneuploid strains

Figure 14: Experiments to identify the mechanistic basis behind negative genetic interaction.
A) Schematic of further adaptation experiment of the chromosome 8 and 10 double disomic strains.
B) Colony sizes of four independent chromosome 8 and 10 double disomic strains before (Day 1) and after (Day 22) the further adaptation. The graph on the right indicate the quantification of the colony sizes. Error bars reflect the standard deviation within each strain.
C) qPCR quantification of the four independent chromosome 8 and 10 double disomic strains before (Day 1) and after (Day 22) the further adaptation. Normalization was performed as mentioned in the Materials and Methods section.
D) A schematic of the EMS mutagenesis experiments to identify the basis behind the negative CCNIs between chromosome 8 and 10.
E) Colony sizes of WT, single disomes of chromosome 8 or 10, and double disomic strains before and after treatment and adaptation with 3% EMS. The graph on the right indicate the quantification of the colony sizes. Error bars reflect the standard deviation within each strain.
F) qPCR quantification of the chromosome 8 and 10 single or double disomic strains before (Day 1) and after the adaptation after EMS treatment. Normalization was performed as mentioned in the Materials and Methods section.

We adapted the engineered chromosome 8 and 10 double-disomic strain for 22 days by continuously culturing them on selective plates and simultaneously measured the colony sizes as a measure of cellular fitness (Fig. 14A). Although the strains showed an increase in colony size over time, the increases in fitness were unfortunately due to the spontaneous loss of one of the aneuploid chromosomes (Figs. 14B, C). Similar experiments using a potent mutagen, Ethyl methanesulfonate (EMS) failed to provide suppressor strains with both aneuploidies and an enhanced cellular fitness (Figs. 14D, E and F).

As an alternate approach to identify the genes responsible for the chromosome 8 and 10 negative CCNI, we first attempted to identify the chromosomal regions on chromosomes 8 and 10 that contribute to this genetic interaction. Towards this, we induced specific reciprocal translocations of chromosomal arms by utilizing a CRISPR method mentioned in a recent report that successfully engineered whole-chromosome fusions in budding yeast (Luo Z et al., 2018; Shao Y et al., 2018) (Fig. 15A). As a proof of principle we first used CRSPR-assisted reciprocal translocations of chromosomal arms to rescue the lethality

associated with chromosome 6 disomy. Since chromosome 6 disomy is lethal and rescued only in the presence of chromosome 13, we induced reciprocal translocation of chromosomal arms of 6 and 13 such that the parts of both chromosomes that share a strong genetic interaction are fused on a single chromosome (referred to as Chr 6L-13L). Since the 6L-13L fusion chromosome resulted in placing the tubulin genes *TUB2* and *TUB1* on the same chromosome

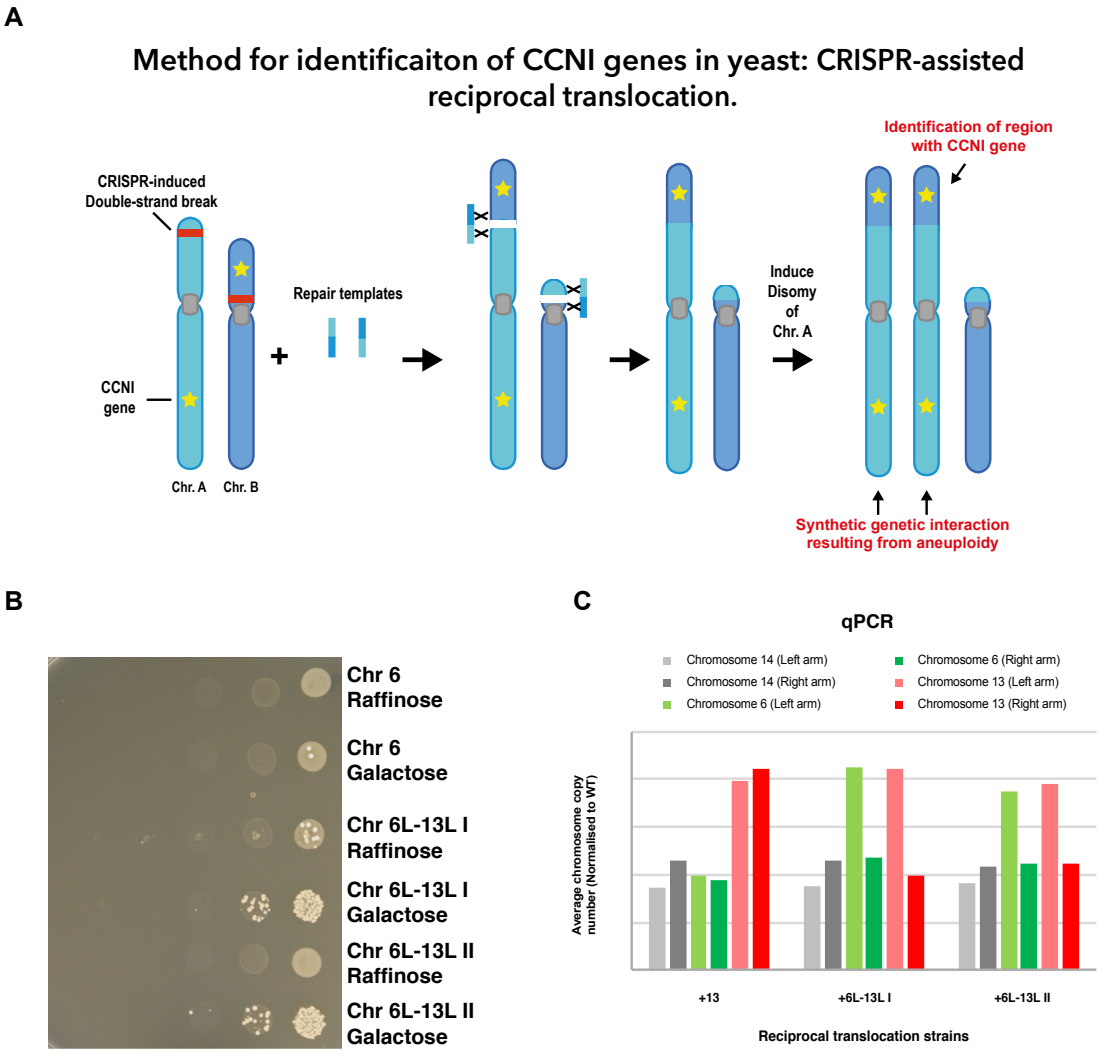

Figure 15: CRSPR-assisted reciprocal translocation strategy.
A) A schematic of the CRSPR-assisted strategy to create strains with reciprocal chromosome arm translocations which will help identify the basis behind the negative genetic interactions between aneuploidy of chromosome 8 and 10. The yellow star indicates The gene or genes that are responsible for the negative CCNIs.
B) Dilution spotting experiment to demonstrate the proof of concept experiment with chromosome 6 and 13.
C) qPCR quantification of the chromosome 8 and 10 single or double disomic strains before (Day 22) and after the adaptation. Normalization was performed as mentioned in the Materials and Methods section.

we were able to engineer strains with a disomy of Chr 6L-13L (Figs. 15B, C). The establishment of this technique is the first step to determine the genes responsible for the strong negative CCNI in future experiments.

5. Degree of aneuploidy is proportional to the degree of CIN induced

We next probed what effect varying the level of induced CIN has on the complexity of the resulting aneuploidy. To vary the degree of CIN induced, we generated mutants that perturb different parts of the error correction pathway (Fig. 16A). *NBL1*, *BUB1* and *SGO1* genes (referred to as *Borealin*, *BUB1* and *Shugoshin* in humans) were deleted and the strains were adapted through multiple rounds of clonal expansion (~400 generations) similar to the *bir1Δ-ad* strains. The doubling time measurements reveal that the *bir1Δ-ad* and *nbl1Δ-ad* strains have the strongest growth deficits, closely followed by the *bub1Δ-ad* strains, while the *sgo1Δ-ad* strains had a relatively weak phenotype (Fig. 16B). These growth rates followed the published measurements of chromosome missegregation rates for *BIR1* and *SGO1* mutant strains (Storchova Z et al., 2011; Campbell CS and Desai A, 2013). Similar to the adapted *BIR1* deletion strains, whole genome sequencing data of the *nbl1Δ-ad*, *bub1Δ-ad*, and *sgo1Δ-ad* strains were used to determine the chromosome copy numbers. The complex aneuploid karyotypes in the adapted strains of all four deletion mutants revealed very similar patterns. Aneuploidies of predominantly the same five chromosomes were observed across all four mutants (1, 2, 3, 8, and 10) (Figs. 16C, D). Barring one *sgo1Δ-ad* strain, the rest of the mutant strains also

displayed a strong negative correlation between disomies of chromosome 8 and 10 (Fig. 16C). While the general aneuploidy patterns across the complex karyotypes of the various adapted deletion strains remained the same, the degree of aneuploidy differed significantly among the deletion strains. The *nbl1Δ-ad* and *bir1Δ-ad* strains had the highest gains of aneuploidy, whereas *bub1Δ-ad* and *sgo1Δ-ad* strains accumulated comparatively lower levels of aneuploidy (Figs. 16E).

Ravichandran et al. Figure 4

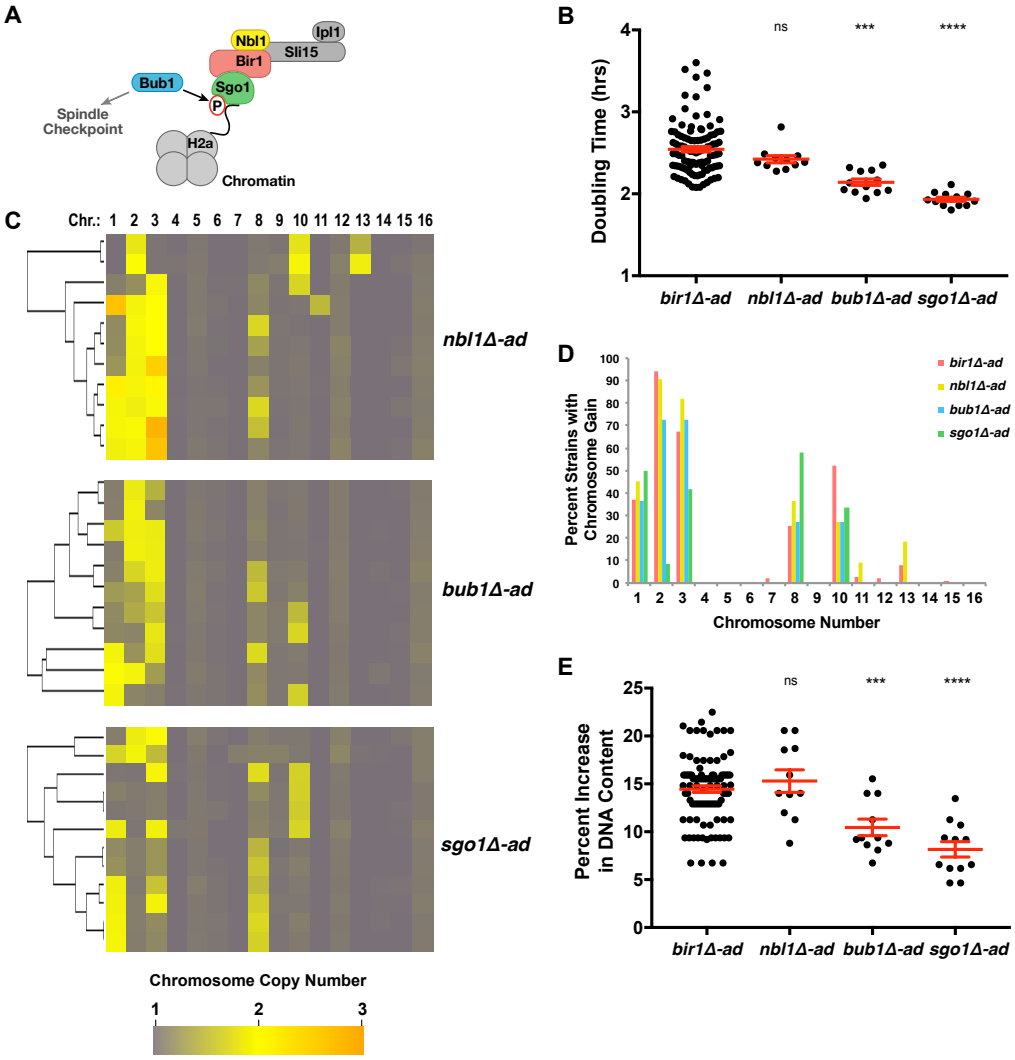

Figure 16: The severity of induced CIN correlates with the resultant degree of aneuploidy.
A) A schematic of the CPC, chromosomal passenger complex and its regulators of its chromatin localization.
B) Cellular fitness data depicting doubling times for each strain type indicated.
C) Visualization of the karyotypes using a clustered heat-map of the chromosome copy numbers of the four different mutant strains (*nbl1Δ-ad, bub1Δ-ad* and *sgo1Δ-ad* strains)
D) Graph displaying the proportion of strains that have gained a specific chromosome after binarization of the data shown previously in C and Figure 8C.
E) Changes in overall DNA content (as a percentage) as measured by considering the binarized chromosome copy number values, subsequently subtracting 1, and multiplying each by the genome fraction represented by that particular chromosome, and then taking a sun all of the chromosomes.
Standard errors and mean values the are shown in red. ***p ≤ 0.0001, ****p < 0.00001.
Taken from Ravichandran MC et al., 2018

The trend of the degree of aneuploidy accumulated by the mutant strains closely correlates to the published degree of CIN observed in these mutants. Together, the above results suggest that higher chromosome missegregation rates can increase the complexity of an aneuploid karyotype.

6. Correlations between chromosomal copy number alterations are affected by the ploidy of the cell

We subsequently wanted to learn if changes in ploidy could have an impact on the patterns in complex karyotypes that were previously observed in the bir1Δ-ad strains. Unlike the haploid genomes, there is a greater number of aneuploidy types in diploids that could potentially be exploited for adaptation. These aneuploidy states include a loss of a chromosome copy (Monosomy) or a 50% increase in chromosome copy number (Trisomy) and a gain of two extra copies of a chromosome (Tetrasomy). Theoretically this might allow more avenues of adaptation and fine-tune the paths taken to an optimal fitness state.

To test if multiple aneuploidy types can change the pattern in complex karyotypes, we generated 25 *bir1Δ* diploid yeast strains with both copies of the

BIR1 gene deleted and adapted them via clonal expansions. Subsequently, they were subjected to whole genome sequencing to determine the karyotype of each strain (Fig. 17A). Analogous to the haploid *bir1Δ-ad* strains, the diploid *bir1Δ/Δ-ad* strains frequently accumulated an extra copy of the same chromosomes 2, 3, 8, and 10 (Fig. 17B). Additionally, the *bir1Δ/Δ-ad* strains

Ravichandran et al. Figure 5

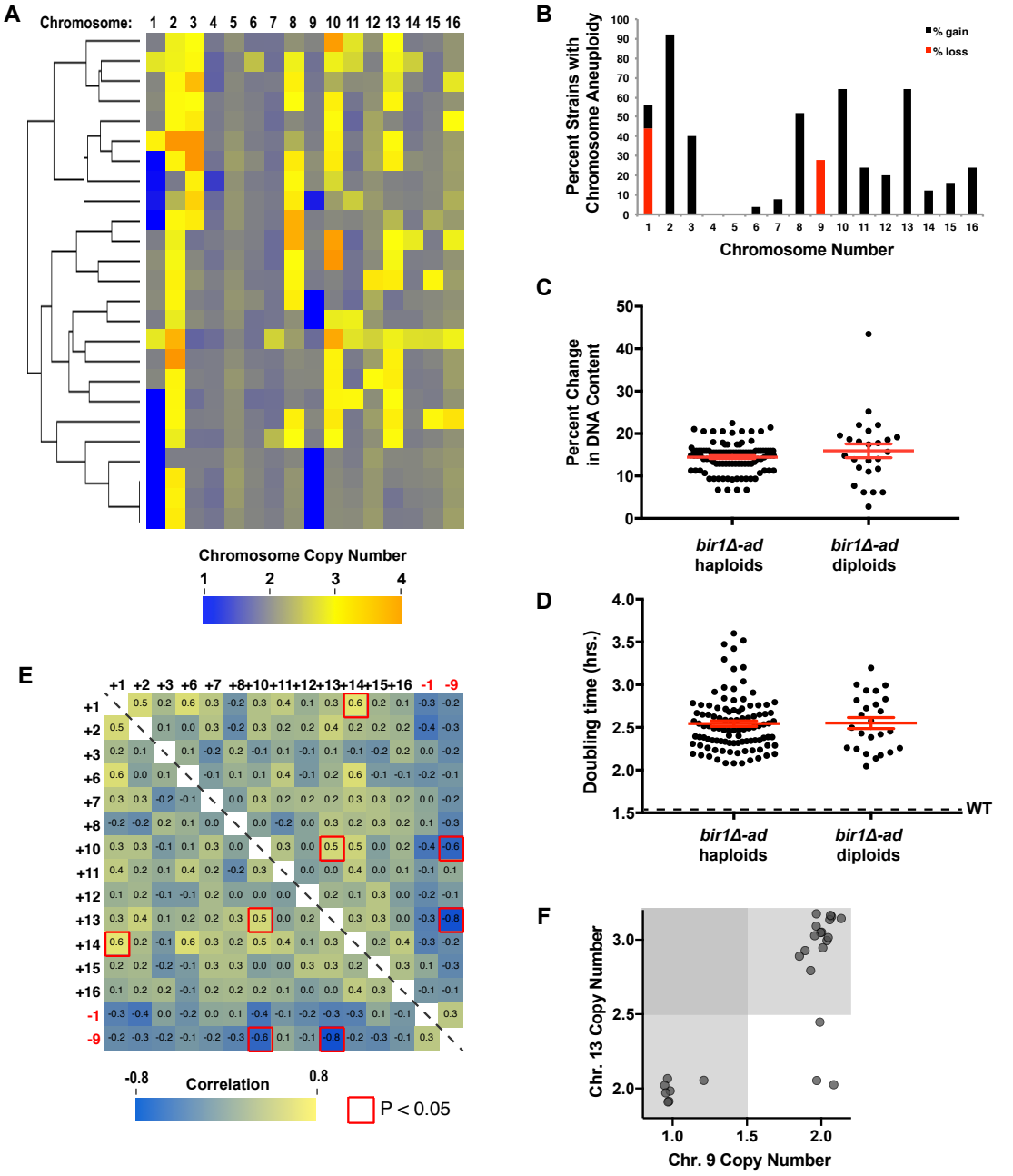

Figure 17: Chromosome copy number correlations are greatly affected by the ploidy.
A) Visualization of the karyotypes using a clustered heat-map of chromosome copy numbers for diploid *bir1Δ-ad* strains. All of the 25 diploid *bir1Δ-ad* strains are represented in a row.
B) Frequency of occurrence of each aneuploid chromosomes in the diploid *bir1Δ-ad* strains after binarization of the data shown in A.
C) Percentage change in DNA content that was calculated by taking the binarized copy number values of every chromosome, then subtracting the basal ploidy of 2, multiplying this value with the genome fraction represented by that particular chromosome, and then adding up the absolute values for every chromosome. The two groups were not significantly different. p = 0.16
D) Cellular fitness measured as doubling times for both the haploid and diploid *bir1Δ-ad* strains. The two groups were not significantly different. p = 0.91
E) Visualization of the karyotypes using a heat-map of the chromosome copy number correlations for all the 25 diploid *bir1Δ-ad* strains. Only those correlations between aneuploid chromosomes are shown. Each unit of the matrix represents the correlation coefficient between the two chromosomes indicated in the row and column. Those correlations with P < 0.05 in the hypergeometric test have a red highlighted border.
F) Graphical plot of particular chromosome copy numbers from the karyotypes of 25 diploid *bir1Δ-ad* strains representing a negative correlation among trisomy of chromosome 13 and monosomy of chromosome 9. Copy number data was calculated from read frequencies as before in E. The grey regions that are darker contain strains which are aneuploid for both of the chromosomes.
The standard error and mean values of each group are indicated in red with error bars.
Taken from Ravichandran MC et al., 2018

also gained an extra copy of chromosome 13 at much higher frequencies than in *bir1Δ-ad* strains (64% in diploids vs. 8% in haploids) (Figs. 17B and 8D).

Unlike the other chromosomal gains (2, 3, 8, and 10), chromosome 13 did not show any instances of tetrasomy (Fig. 17A). This suggests the cell displays a higher tolerance to a 50% increase in the copy number of chromosome 13, when compared to *bir1Δ-ad* strains with a 100% increase. Apart from chromosomal gains, losses of chromosomes 1 and 9 were observed at a high frequency (Chr 1 loss - 44% and Chr 9 loss - 28%, Fig. 17B). Across the *bir1Δ/Δ-ad* strains, copies of chromosome 1 were both gained and lost, suggesting that the chromosome aneuploidy is largely inconsequential and very likely does not contribute to the adaptation to *BIR1* deletion. Comparing haploids and diploids, the percent change in DNA content after normalization to the basal ploidy was very similar (Fig. 17C). This demonstrates that the

tolerated fraction of the cellular burden of aneuploidy scales with the ploidy of the cell. But despite having the ability to fine-tune the process of adaptation with multiple avenues, the diploids on average have similar growth rates to the haploids (Fig. 17D). Together, the above data clearly indicates that the initial ploidy of a cell is an important factor that affects the patterns in complex aneuploid karyotypes.

We next performed pairwise comparisons of the frequency of co-occurrence of specific aneuploidies in the *bir1Δ/Δ-ad* strains (Fig. 17E). Surprisingly the strongest negative chromosome copy number correlation seen in haploids between chromosomes 8 and 10 vanished in the diploid *bir1Δ/Δ-ad* strains. Alternatively, loss of chromosome 9 and the gain of chromosomes 10 or 13 shared the most significant negative correlations ($p = 0.003$ and 7×10^{-5}, respectively). About 92% of the strains (23 of 25) had either chromosome 9 loss or chromosome 13 gain but both aneuploidies were never observed simultaneously (Figs. 17E and 17F). Similar to chromosomes 8 and 10 in the haploid adapted strains, the strong negative correlation between chromosome

Ravichandran et al. 2018 Figure S3

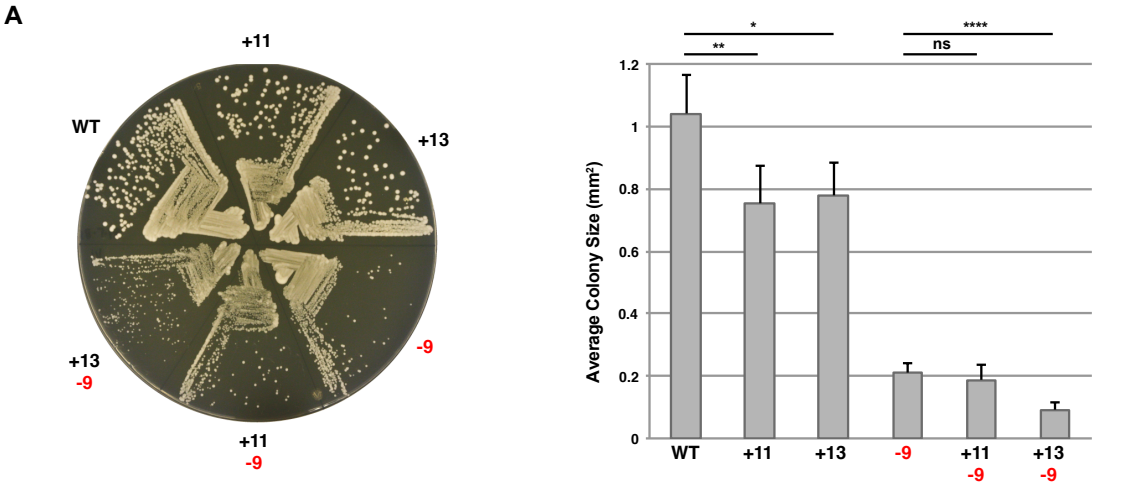

Figure 18: Strong negative genetic interaction between aneuploid chromosomes 9 and 13.
Strains with engineered monosomy of chromosome 9, trisomy of chromosome 10 or both were struck out on rich media (YPAD) plates such that single colonies sizes could be measured. On the right, the graph represents the quantification of the colony sizes of the engineered strains (in square millimeters). Error bars were calculated using the standard deviations from three independent biological repeats.
Taken from Ravichandran MC et al., 2018

9 monosomy and 13 trisomy is due to a negative CCNI. Strains engineered with monosomy of chromosome 9 and chromosome 13 trisomy had a 50% smaller colony size when compared to the monosomy of chromosome 9 alone ($p < 0.0001$) (Fig. 18A). Hence, CCNIs also govern the formation of complex aneuploid karyotypes in cells with a diploid basal ploidy. In conclusion, chromosome copy number correlations and interactions are observed across different ploidy states, although there are dramatic changes in the patterns.

7. Aneuploid cancer karyotypes also display chromosome copy number correlations

Aneuploid cancer karyotypes were collected from The Cancer Genome Atlas database to determine whether patterns similar to those in the *BIR1* deletion strains could also be seen among complex cancer karyotypes. By analyzing the competitive genome hybridization (CGH) data from the databases, we were able to build a matrix comparing the pairwise correlations between the frequently observed aneuploidies across fifteen different cancer types. The five cancers with the highest frequency of whole arm complex aneuploidy or whole chromosome aneuploidy were analyzed in greater detail (Figs. 19A and 20, Table 2). Strong chromosome copy number correlations were observed across

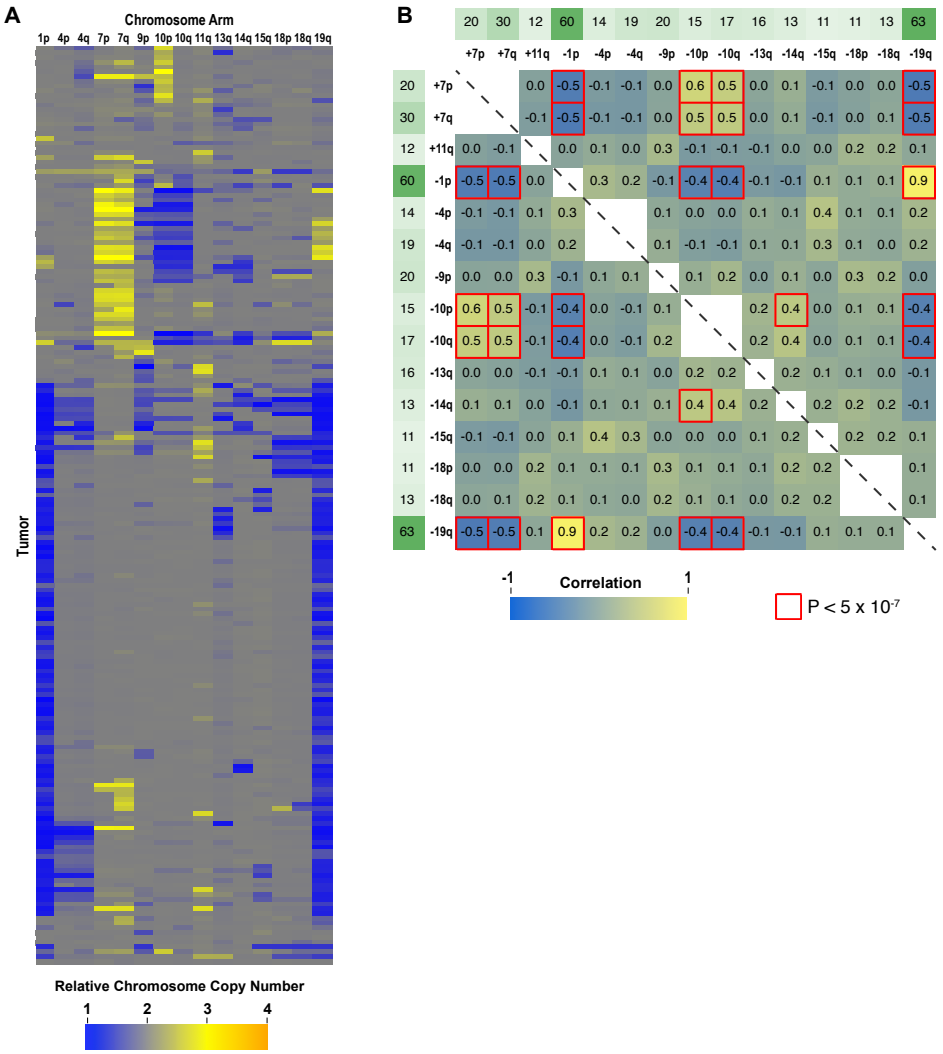

Figure 19: Identification of correlations among chromosome copy numbers in Brain Lower Grade Glioma (LGG) tumors.
A) Visualization of the karyotypes using a heat-map of the Brain Lower Grade Glioma tumor samples. The karyotype data was acquired from both the Cancer Genome Atlas (TCGA) database and the competitive genome hybridization (CGH) data. Every karyotype of the 193 Low Grad Glioma is represented as a row and the column indicates the chromosome copy number of each chromosomal arms. Only those chromosomal arms whose aneuploidy was present in more than 10% of the tumor samples are displayed.
B) Visualization of the karyotypes using a heat-map of the chromosomal arm copy number correlations. The frequency of occurrence (as a percentage) of every aberration is shown on top in green. Those correlations with P < 5 x 10-7 in the hypergeometric test have a red highlighted border. Figure 20 represents similar analysis of 4 other tumor types.
Taken from Ravichandran MC et al., 2018

all the five cancer types. Among them the patterns observed in Lower Grade Glioma (LGG) resembled the patterns in the *bir1Δ-ad* strains, comprising of both strong negative and positive copy number correlations (Figs. 19A, B). LGG

cancer type largely showed two main positive correlations, those with chromosome 7 gain and chromosome 10 loss and with losses of both chromosomal arms 1p and 19q (Fig. 19B). The latter is a consequence of a frequent translocation between chromosomes 1 and 19. Intriguingly, the LGG karyotypes that displayed this translocation of 1p and 19q did not co-occur with the gain of chromosome 7 or loss of chromosome 10 and hence, shared a strong negative chromosome copy number correlation (Fig. 19B). The other aneuploidies that occur at a high frequency like the loss of chromosome 18 did not show any correlation with the other chromosomal aneuploidies. This suggests that positive or negative chromosome copy number correlations are specific to certain aneuploidies. Overall we observe chromosome copy number correlations across various cancer karyotypes, which may reflect the presence of CCNIs between different aneuploidies within aneuploid cancer karyotypes.

8. The adapted strains converge on an optimal karyotype after an extended period of competitive adaptation

So far, we found that after an initial round of adaptation, the *BIR1* deletion strains acquired various complex aneuploid karyotypes and most of those karyotypes strongly correlated with enhanced cellular fitness. But it is surprising that the aneuploid karyotypes were heterogeneous and not all the strains acquired the most beneficial combination of aneuploid chromosomes. Perhaps one reason could be that the *bir1Δ-ad* strains were not given enough time to adapt in a competitive environment and the heterogeneous aneuploid karyotypes are a result of an intermediate state along the course of adaptation.

Possibly after further adaptation to *BIR1* deletion, the *bir1Δ-ad* strains may converge on an "ideal" aneuploid karyotype. On the other hand additional adaptation may instead provide the strains enough time to sample alternate pathways and obtain the advantageous traits independent of the aneuploidy. Ultimately, the further adapted strains could eliminate the disadvantages of the aneuploid karyotype by returning to the euploid state, as illustrated in a previous study (Yona AH et al., 2012).

Therefore we selected 16 haploid and 16 diploid *bir1Δ-ad* strains for further adaptation by growing them in rich liquid media for an additional ~200 generations (Fig. 21A). These further adapted haploid strains will be referred to as *bir1Δ-ad2* strains and as *bir1Δ/Δ-ad2* strains for the diploids. The CIN phenotype after additional adaptation in liquid media had not greatly changed, as the 16 *bir1Δ/Δ-ad2* strains displayed nearly no change in sensitivity to Benomyl when compared to their corresponding *bir1Δ/Δ-ad* counterparts (Fig. 22A). Copy number determination from the sequencing data revealed that the haploid *bir1Δ-ad2* strains had completely lost the aneuploidy of chromosomes 8 and 10 (Figs. 21B, C). Hence, the further adapted strains had more similar karyotypes, as measured by the decrease in the pooled standard deviation from 0.18 to 0.13 after liquid adaptation. In contrast, chromosome copy numbers of chromosomes 1 and 2 were unchanged. Four *bir1Δ-ad2* haploid strains that started with a disomy of chromosome 10 and a single copy of chromosome 3 lost the aneuploidy of chromosome 10 and gained an extra copy of chromosome 3. This suggests that among the haploids, the karyotype converges on an "optimal" *bir1Δ* karyotype, which includes just the aneuploidy

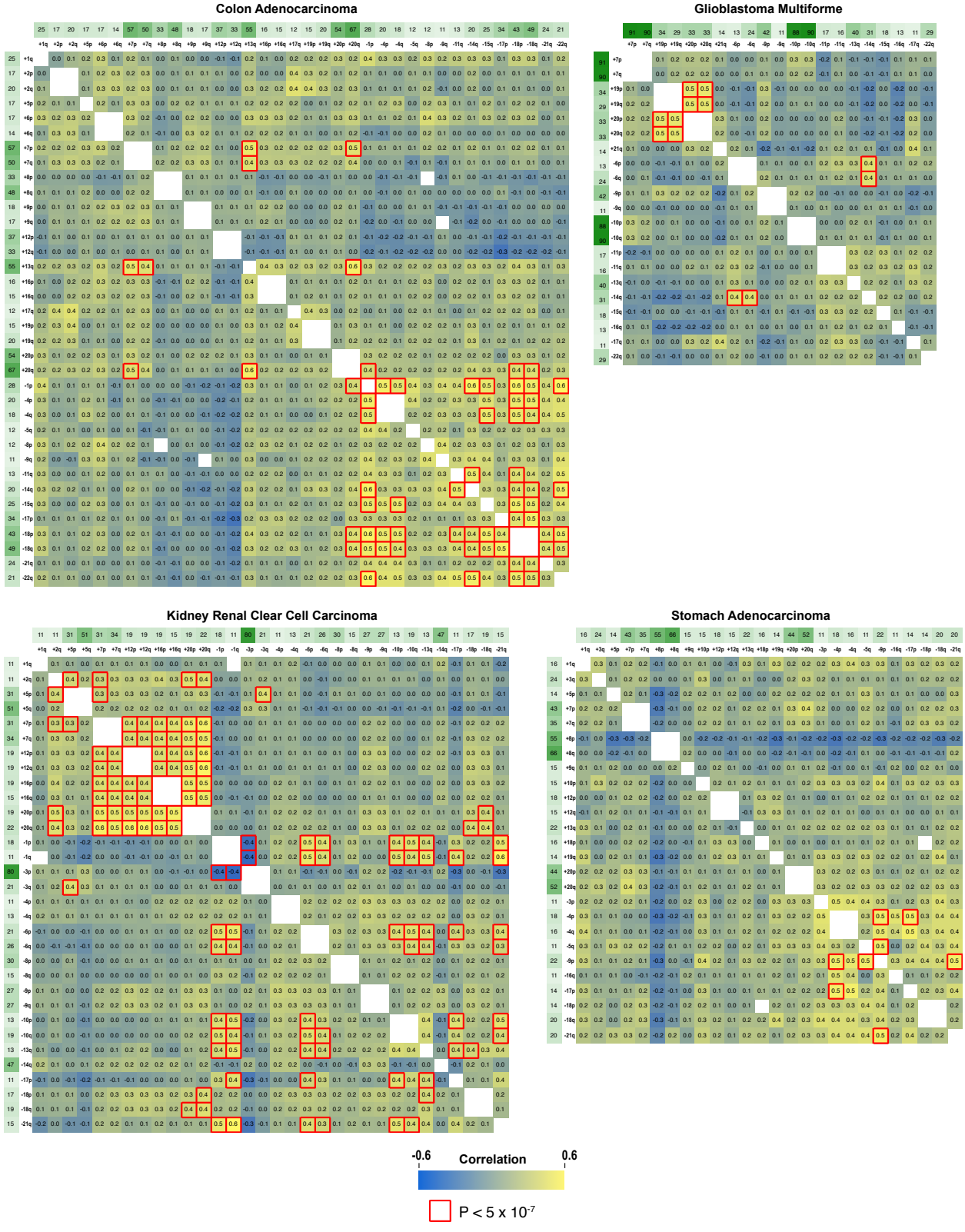

Figure 20: Correlations across chromosome arm aneuploidies in four different cancer types. Pairwise correlation coefficients of chromosome arm aneuploidies are visualized as a heat map for 138 Colon Adenocarcinoma, 253 Kidney Renal Clear Cell Carcinoma, 160 Glioblastoma Multiforme, and 119 Stomach Adenocarcinoma tumors. The frequency of occurrence (as a percentage) of every aberration is shown in green. Those correlations with P < 5 x 10-7 in the hypergeometric test have a red highlighted border.
Taken from Ravichandran MC et al., 2018

of chromosomes 2 and 3, while chromosome 10 disomy is eliminated due to a negative CCNI between the disomy of chromosomes 3 and 10 (Figs. 12C, E). Intriguingly, among the *bir1Δ/Δ-ad2* diploid strains the pooled standard deviation decreased from 0.36 to 0.17, which indicates that after liquid adaptation they developed much more homogenous complex karyotypes. Nearly all the diploids had trisomies of chromosomes 2, 3, 10, and 13 (Figs. 21D, E). Strikingly, chromosome 9 monosomy that was present in three of the *bir1Δ/Δ-ad* strains, lost the aneuploidy by regaining a copy of chromosome 9 but also gained an extra copy of chromosome 13. This exchange between the

Ravichandran et al. Figure 7

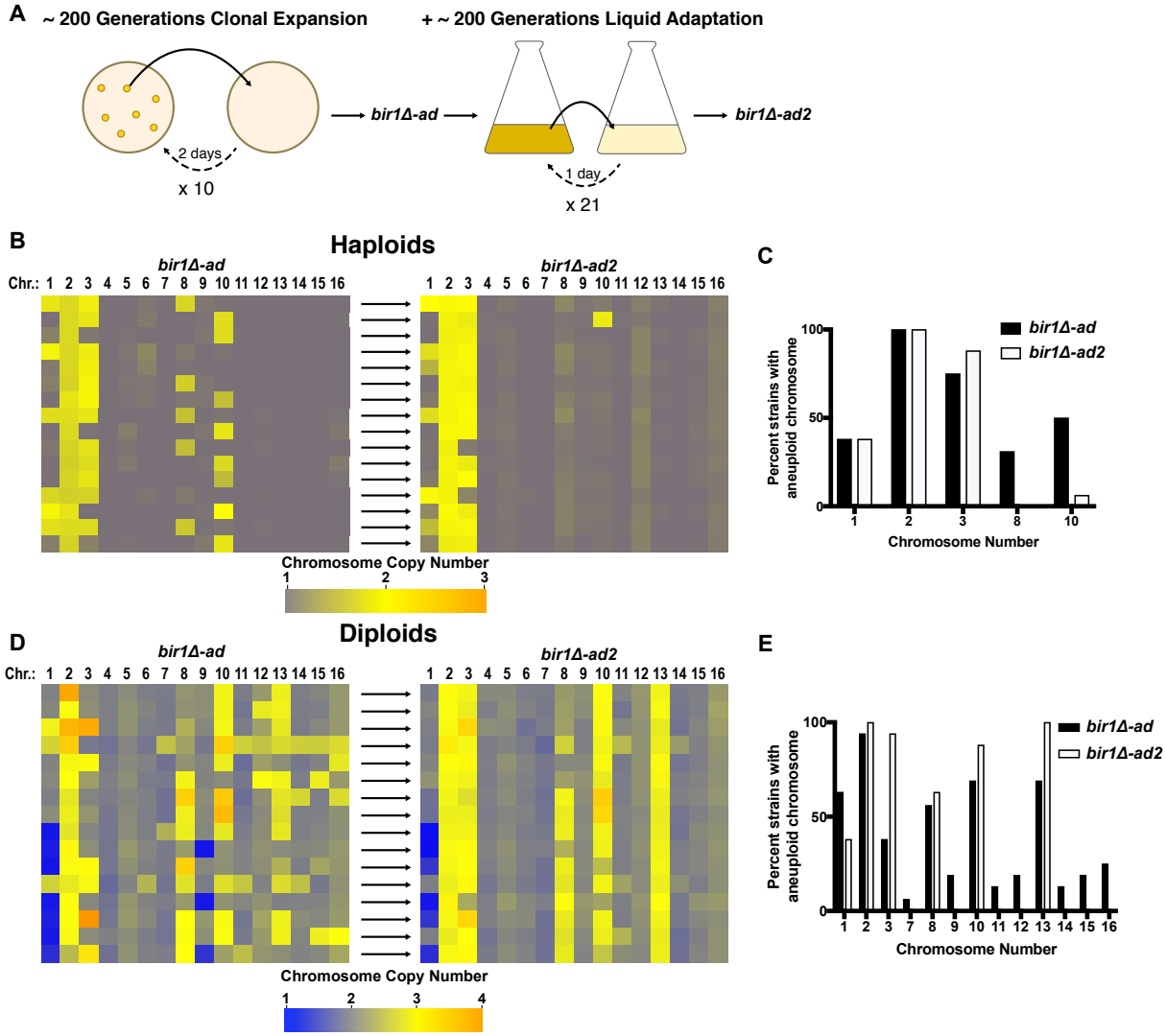

Figure 21: Convergence on "ideal" karyotypes after additional adaptation of the BIR1 deletion strains.
A) Pictorial representation of the clonal expansion (adaptation process on solid) (see Figure 8A) followed by further adaptation in liquid medium. On the solid medium the *BIR1* deletion strains were struck out such that single colonies were allowed to grow for 2 days at 30°C. After ten rounds of clonal expansion on solid medium, a few of *bir1Δ-ad* strains, selected such that they represent a diverse set of karyotypes, and these strains were grown further for an additional 21 days (~200 generations) in liquid medium. Liquid cultures were diluted each day for 3 weeks, which generated the further adapted haploid/diploid strains (*bir1Δ-ad2* strains).
B) Visualization of the karyotypes using a heat-map of chromosome copy number values for the haploid *bir1Δ* strains prior to (see Figure 8C) and after further adaption in liquid medium. The bir1Δ-ad strains before adaptation are shown on the left and directly correspond to the further adapted bir1Δ-ad2 strains on the right.
C) Frequency of occurrence of each aneuploid chromosome amongst the haploid *bir1Δ-ad* and *bir1Δ-ad2* strains after binarization of the data in B.
D) Visualization of the karyotypes using a heat-map of chromosome copy number values for the diploid *bir1Δ* strains prior to (similar to Figure 17A) and after further adaption in liquid medium. The *bir1Δ-ad* strains before adaptation are shown on the left and directly correspond to the further adapted *bir1Δ-ad2* strains on the right.
E) Frequency of occurrence of each aneuploid chromosome amongst the diploid *bir1Δ-ad* and *bir1Δ-ad2* strains after binarization of the data in D.
Taken from Ravichandran MC et al., 2018

aneuploidy of chromosomes 9 and 13 occurred inside a week of each other and happened in the first two weeks of additional adaptation (Fig. 22B). In conclusion certain types of aneuploidy, which provide an early fitness advantage like chromosome 10 disomy in the haploid strains or the chromosome 9 monosomy in diploid strains, will eventually be replaced by other incompatible aneuploidies that comparatively provide a better

growth advantage (chromosome 3 gain in haploid strains and chromosome 13 gain in diploid strains). Collectively, these results indicate that although there are multiple, sometimes conflicting routes to obtain the optimal karyotype, aneuploid cell populations with high levels of CIN will ultimately converge on a common complex aneuploid karyotype.

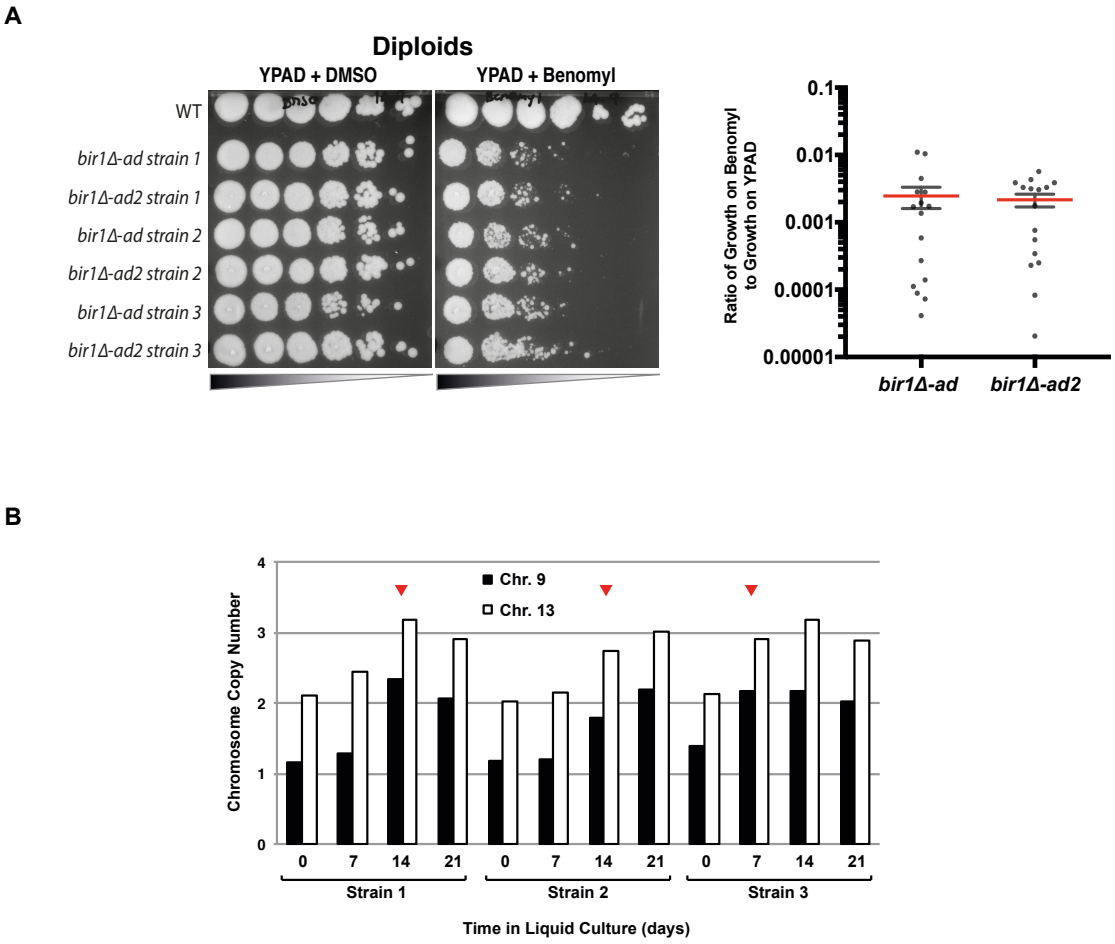

Figure 22: Benomyl sensitivity and chromosome copy numbers changes over time of the diploid bir1Δ-ad2 strains.
A) Benomyl sensitivity test as a secondary measure of missegregation rates of the *bir1Δ-ad*2 diploids. Moderate (10 µg/ml) amount of the microtubule-depolymerizing drug Benomyl were added to the media in which the *bir1Δ-ad*2 diploids strains were grown for two days. Dilution spotting (10-fold) were performed with wildtype, and multiple *bir1Δ-ad*2 diploids on DMSO control (YPAD + DMSO) plates and plates supplemented with Benomyl.
B) qPCR quantification of the chromosome 9 and 13 copy number changes over the course of the liquid adaptation. Cultures taken at after every week were subjected to qPCR to visualize the stepwise changes of aneuploidies of chromosome 9 and 13 that share a negative CCNI.
Taken from Ravichandran MC et al., 2018

Chapter 3: Discussion

In our study, we established a method to study the formation of complex karyotypes in the context of extremely high rates of chromosome missegregation (CIN). We induced CIN using genomic lesions in the Bir1, a subunit of CPC which is an error correction machinery functioning at the kinetochore-microtubule interface. Along with increasing the frequency of aneuploidy, we found that high CIN also creates selective pressure to optimize cellular fitness via aneuploidy. We successfully generated complex aneuploid karyotypes, which led to the identification of strong correlations and anticorrelations within specific pairs of aneuploid chromosomes. We then hypothesized that such patterns might arise as a consequence of genetic interactions amongst specific pairs of aneuploid chromosomes. To test this hypothesis, we engineered strains that were simultaneously aneuploid for two chromosomes. Cellular fitness measurements of all engineered strains indicated that genetic interactions (or chromosome copy number interactions (CCNIs)) were indeed responsible for the correlative relationships observed within the complex karyotypes of the adapted strains. Further, the fitness consequences of such CCNIs correlated well with the patterns observed among the complex karyotypes of the CIN adapted strains. Given enough time to adapt, there is an increase in homogeneity across the adapted strains as they converge on a common karyotype. The complex karyotypes were refined to an optimal state by the elimination of chromosome pairs with negative CCNIs and the enrichment of those that share positive CCNIs in an attempt to maximize cellular fitness.

From all the observations above, we derived a model that describes the different paths explored by the yeast in order to obtain a final, ideal aneuploid state, which minimizes the fitness deficits from the BIR1 deletion (Fig. 23). These paths to an adapted state were derived based on i) relating the growth rates of the different aneuploid karyotypes (Figs. 8E and 10B), ii) changes in the karyotypes after liquid adaptation (Figs. 21B-E), iii) the identified CCNIs between specific pairs of aneuploid chromosomes (Figs. 12E, 13A, and C).

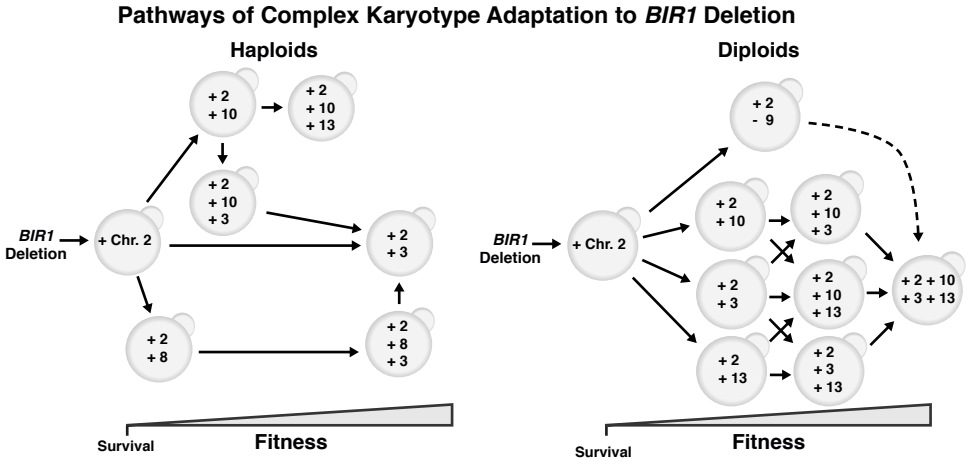

Figure 23: An empirical model of paths taken by BIR1 deletion strains to acquire an optimal karyotype.
An empirical model portraying the paths of adaptation to deletion of *BIR1* based on synthesizing data from Figures 8, 10, 12, 17, and 21. The adaptation begins with the gain of an extra copy of chromosome 2, which seems to be beneficial for initial survival. Following the gain of chromosome 2, multiple different routes can be taken by both diploid and haploid yeast during complex karyotype formation. Note that certain aneuploid chromosomes (like the monosomy of chromosome 9 in diploids and disomy of chromosome 10 in haploids) offer an early growth advantage during adaptation but since such aneuploidies share a negative CCNIs with more beneficial aneuploid chromosomes the cells must lose such aneuploidies to reach an "optimal" complex karyotype.
Taken from Ravichandran MC et al., 2018

Although the paths leading to the adapted state and the ideal karyotype are different for the haploid and diploid strains, they have several traits in common. Both the ploidies show step-wise changes in aneuploidy and corresponding alterations in fitness. All the paths begin with the gain of an extra copy of chromosome 2, which is initially essential for survival. Subsequently, the strains could acquire a variety of aneuploidies, each with their selective advantage. A

proportion of the strains would likely proceed down a direct route resulting in quickly acquiring the optimal karyotype such as the disomy of chromosome 3 in haploid strains. Instead, very often, the cultures may take a detour by gaining an aneuploidy that is beneficial early on, but, paradoxically, due to negative CCNIs, it acts as a barrier to acquire the final, optimal complement of aneuploid chromosomes. Examples depicting this are aneuploidies like the gain of chromosome 10 in haploids and the loss of a copy of chromosome 9 in diploids. Although these aneuploidies are initially advantageous, due to negative CCNIs with more beneficial aneuploidies, such initially advantageous aneuploidies are eventually replaced with aneuploidies that are more useful like disomy of chromosome 3 in haploids and trisomy of chromosome 13 in diploids. Together, our observations shed light on a versatile mechanism of adaptation via aneuploidy, with multiple chromosomal aneuploidies providing a competitive edge under similar selective conditions. However, despite these divergent paths of adaptation, cell populations with high chromosomal instability, settle on an ideal karyotype through the acquisition of specific beneficial aneuploid chromosomes over time.

Synergistic genetic interactions between specific chromosome pairs have been reported before, depicted by the disomy of chromosome 6 in haploid strains being tolerated only with a simultaneous gain of chromosome 13 (Torres EM et al., 2007; Anders KR et al., 2009). The basis behind this positive interaction is the imbalanced expression of the tubulin gene *TUB2* present on chromosomes 6, encoding the beta subunit of the tubulin complex. When chromosome 13 is

also present in an extra copy, the orphaned beta subunit of the tubulin complex is bound by the increased production of the alpha subunit of the tubulin complex encoded by the TUB1 gene on chromosome 13. In our study, we demonstrate that such whole chromosome genetic interactions of both positive and negative nature are potentially prevalent and have a strong influence on the formation of complex aneuploid karyotypes. The basis behind the CCNIs we observed remain unknown, and whether they are a result of genetic interaction between a pair of genes as seen with chromosomes 6 and 13 also remains elusive. Alternatively, CCNIs could also result from the cumulative effects of several interactions among multiple genes, as previously reported for aneuploidy-associated growth defects (Bonney ME et al., 2015). However, the specificity of CCNIs between different aneuploid chromosomes suggests that these interactions are likely due to the copy number alterations of a few specific genes.

Another open question that stems from our work is whether adapting cell populations eventually find ways to maintain the beneficial aspects of aneuploidy while lowering the negative fitness consequences of genetic interactions between aneuploid chromosomes. Whether or not an aneuploid chromosome is advantageous hangs on the balance of negative and positive selective forces (Fig. 24). The positive selective pressure for an aneuploid chromosome mainly arises from the increased expression of a gene or group of genes that enhance growth in a specific context (Rancati G et al., 2008; Ryu H-Y et al., 2016; Hughes TR et al., 2000).

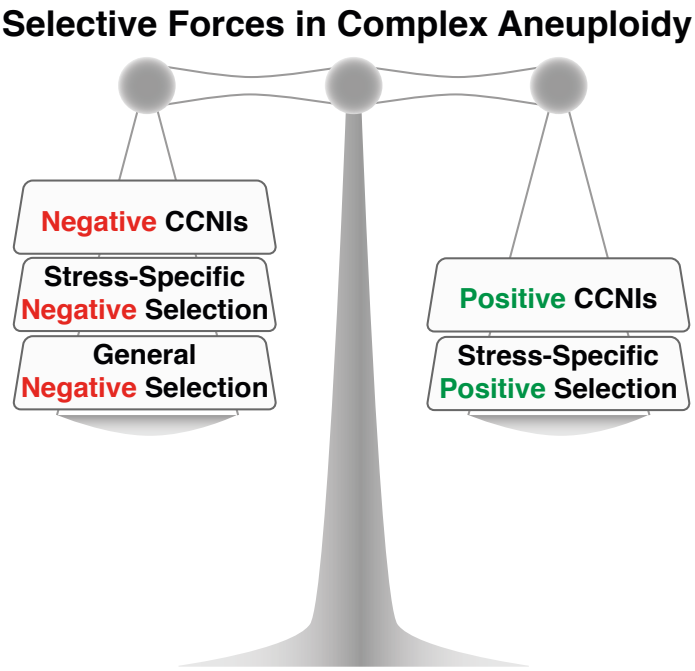

Figure 24: Selective forces that influence the formation of complex karyotypes.
A cartoon of the balance of selective forces that ultimately determine whether certain aneuploid chromosomes are advantageous and help shape the complex karyotypes.
Taken from Ravichandran MC et al., 2018

On the other hand, the negative selective pressure can either come from general stresses that arise from the negative consequences of the aneuploidy-associated proteome imbalance or stress-specific negative selection that arises from the context of the stressful environment (Bonney ME et al., 2015; Chen G et al., 2015). However, nothing is known about how these selective forces act on complex karyotypes. Here, in our study, we propose that in the context of complex karyotype evolution, an additional set of forces due to particular genetic interactions between aneuploid chromosomes either positively or negatively influence the balance of the selective forces on aneuploid chromosomes (Fig. 24). Furthermore, the basal ploidy of a cell heavily contributes to such chromosome copy number interactions and result in different aneuploidy patterns across the adapted haploid and diploid strains. On comparison, the haploids and diploids, on average, acquire a proportional

degree of aneuploidy as a consequence of CIN. These findings are in agreement with previous observations that the gain of an extra chromosome copy results in a much weaker phenotype in diploids when compared to haploids (Beach RR et al., 2017). Furthermore, tetraploid yeast strains are relatively more likely to adapt against a stressful environment via aneuploidy (Selmecki A et al., 2015). Moreover, with every increment in the ploidy state, there is a proportional increase in the number of aneuploid states that could be sampled by cells with persistent CIN. Such minute changes can influence the path of adaptation and the final optimized karyotype. For example, in our study, the haploids displayed a low frequency of chromosome 13 disomy. Nevertheless, with double the ploidy in diploids, despite the same source of CIN, the adapted diploid strains experienced positive selective force on the trisomy of chromosome 13. Since the diploid ploidy state permitted a 50% increase in the copy number of chromosome 13, relative to the haploids, new paths of adaptation could help explore an alternate final karyotype. Overall, these results highlight how subtle changes in the selective forces that act either for or against an aneuploid chromosome can have a massive impact on how a cell population samples the adaptive potential of the aneuploidy.

Overall our study highlights how complex karyotypes are formed under the selective pressures exerted by persistent CIN. Although aneuploidy can be a versatile tool to adapt against stress, specific aneuploidies are incompatible with each other and hence, cannot coexist together in the optimized state. For example, in our study, gaining aneuploidies of either chromosome 8 or 10 was

beneficial for cellular fitness. However, these two forms of aneuploidy were very rarely found together in the same strain after adaptation. Such an anticorrelation was driven by a negative CCNI between these two chromosomes. Another such negative CCNI in diploid yeast strains was observed between the chromosome 9 monosomy and the chromosome 13 trisomy, resulting in their mutual exclusivity across the adapted complex karyotypes. The identification of such CCNIs within a small subset of complex aneuploid karyotypes indicates that CCNIs may be very common. Currently, it is unclear if these CCNIs commonly exist across all chromosomes in budding yeast, hence, a systematic study to engineer every combination of aneuploid chromosomes in both haploids and diploids would comprehensively identify all CCNIs. Subsequently, if CCNIs are ubiquitous such strain collections may help explain other open questions, such as the influence of cellular context on these CCNIs.

Complex karyotypes were generated in our study from a combination of CIN and selective pressure as cells adapted against the detrimental effect of high CIN. However, the karyotypic patterns observed were limited by defects of the biorientation machinery as the only source of CIN. However, such an analysis can be easily expanded to complex aneuploidy patterns that arise from various other sources of CIN, for example, genetic lesions of the spindle pole body, kinetochore mutants, etc. Such experiments will increase our understanding of how different complex aneuploid karyotypes are formed under different sources of CIN. Further, challenging our adapted *bir1Δ* strains with multiple

environmental stresses (such as high pH, high salt, and nutrient deprivation) may shed light on the formative steps during stress-specific complex karyotype evolution. Moreover, the magnitude of external stresses can be varied to follow the corresponding changes in the complex karyotypes. These experiments could differentiate between the individual effects of CIN and magnitude of selective pressures on the formation of complex karyotypes.

Additionally, the engineered strains may help identify if CCNIs are due to general or specific genetic interactions. General genetic interactions arise from cumulative effects of various aneuploidy associated stresses like proteotoxic stress, that affects all aneuploid chromosomes. These effects are likely due to the imbalance of several genes that cause severe proliferative defects (Torres EM et al., 2010) or the burden of degrading the overexpressed proteins (Geiler-Samerotte KA et al., 2011). Further, proliferative defects induced by aneuploidy show a negative linear correlation with the number of imbalanced genes. Hence, general genetic interactions within complex karyotypes must also linearly correlate with imbalances in gene dosage. Deviations from such negative linear correlations may be indicative of specific CCNIs likely due to the expression imbalances of a few genes on the aneuploid chromosomes.

To identify the genes that are responsible for positive CCNIs, we successfully demonstrated a CRSPR-assisted reciprocal translocation approach that generated fusion chromosomes. These fusion chromosomes effectively brought the genetically interacting genes (*TUB2* and *TUB1*) on the same

chromosome (6L-13L fusion chromosome). By inducing the aneuploidy of this fusion chromosome, we were able to show that the lethality associated with increased dosage of the *TUB2* gene was rescued with a simultaneous increase of the *TUB1* gene. Similar experiments utilizing this technique may reveal the pair or group of genes responsible for the negative CCNI between chromosomes 8 and 10. Similarly, such a technique could be used to systematically screen for the genetic basis behind all observed CCNIs between aneuploid chromosomes in the yeast genome.

CIN rates measured by multiple reports in cancer cell lines by quantifying the degree of lagging chromosomes describe a strong correlation between higher instances of aneuploidy and the high rates of CIN (Duesberg P et al., 1998; Nicholson JM and Cimini D, 2013). Because studies that have stably engineered aneuploid strains often observed CIN, the correlation between aneuploidy and CIN is sometimes viewed as CIN being downstream of aneuploidy (Sheltzer JM et al., 2011; Passerini V et al., 2016; Zhu J et al., 2012). In our report we showcase that the inverse relationship between aneuploidy and CIN also exists. Yeast strains with genomic lesions that induce a higher rate of CIN often acquire a proportional amount of aneuploidy after adaptation. This correlation, where the degree of aneuploidy is a consequence of the degree of induced CIN might also help clarify why we observed highly complex aneuploid karyotypes while another study that induced lower levels of CIN, generated aneuploid karyotypes of lower complexity (Chen G et al., 2012).

Analysis of various cancer karyotypes from the TCGA database, resulted in the identification of strong correlations within commonly observed somatic copy number alterations (SCNAs). Positive correlations between whole chromosome aneuploidies have been previously reported in a pan cancer analysis (Ozery-Flato M et al., 2011). However, by restricting our analysis to aneuploidy of chromosomal arms and certain cancer types, the frequencies of the SCNAs were high enough to spot strong negative correlations along with several strong positive correlations among the aneuploid chromosomal arms. This agrees with studies that have utilized tumor biopsies from several patients diagnosed with renal carcinoma where similar positive and negative correlations were observed among driver SCNAs (Turajlic S et al., 2018). The high frequency of such correlations are indicative of genetic interactions among aneuploidies and these correlations could be a starting point to discover strong CCNIs in human cells. Further, our observations that multiple paths through the aneuploidy landscape can result in an optimized adaptive karyotype, provide the first glance into the formative steps of complex karyotypes in cancer and help unravel why the complex aneuploid karyotypes of some tumors develop high intratumoral heterogeneity.

Identification of genetic interaction between aneuploid chromosomes in cancers can also lead to new therapeutic interventions. All negative genetic interactions among complex cancer karyotypes can be targeted to specifically inhibit the growth of cancer cells. For example, if negative CCNIs between a gain of chromosome A and loss of chromosome B are prevalent in certain

cancers we can easily target cancers with gains of chromosome A by using drugs that inhibit the genetically interacting gene located on chromosome B. Much like how common mutational signatures have been exploited for therapeutic interventions, synthetically lethal interactions between aneuploid chromosomes can also be exploited to thwart cancer progression. Overall our study describes the multifaceted selective forces on complex aneuploid karyotypes in eukaryotic cells and further investigation will help address several open questions regarding complex karyotypes that likely influence karyotype evolution in cancers.

Chapter 4: Materials & Methods

Stains and growth conditions:

Every plasmid and yeast strain utilized in this study is mentioned in Table 1. The strains were either cultured in yeast extract peptone medium containing 40 *µ*g/ml adenine-HCl (YPAD) or minimal media, both were supplemented with 2% Dextrose. In specific experiments the YPA medium contained 1% Raffinose (YPAR) and 1% Galactose (YPAGR) as the primary sources of sugar. Drugs such as 5-Fluoroorotic Acid (5-FOA, Chempur 220141-70-8) and Benomyl (Sigma-Aldrich 381586) were added to the medium at concentrations of 1 mg/ml and 10 *µ*g/ml respectively. The strains were grown at an incubated temperature of 30°C. Gene deletions and many such genetic manipulations were performed similar to commonly used techniques as described in Longtine MS et al., 1998. To generate haploid gene deletion strains of the CIN genes we primarily used tetrad dissection. Deletion of both copies of the *BIR1* gene in diploids were generated in two different ways. One method involved mating of two heterozygous *BIR1*/*bir1Δ* diploids, which was achieved by deleting either the MATalpha or MATa locus to allow diploid strains to mate. Subsequently, the tetraploid strains were sporulated and tetrad dissection was performed to get diploids with a homozygous deletion of the *BIR1* gene. The other method involved using a minichromosome carrying the *BIR1* and *URA3* genes and a subsequent deletion of both copies of *BIR1* from the yeast genome. This diploid strain (*bir1Δ* /*bir1Δ*) had a functional copy of *BIR1* on the minichromosome and hence, did not display the lethal phenotype associated with *BIR1* deletion. The minichromosome was subsequently selected against by growing the *bir1Δ*/*bir1Δ* diploids on plates containing 5-FOA, thus selecting for cells with a homozygous *BIR1* deletion.

Aneuploid cells with one extra copy of a chromosome (n+1 strains) were engineered using a conditional centromere as shown previously in Anders KA et al., 2009. Briefly, a galactose inducible promoter placed upstream of the centromere prevents the formation of a functional kinetochore, causing a non-disjunction event that specifically leads to missegregation of a chromosome of choice. Endogenous centromeres were targeted and replaced using homologous recombination at sites both downstream and upstream of the centromere. A repressible centromere P_{GAL1}-*CEN3* with either *URA3* or *LYS2* replaced the endogenous centromere. The *URA3* or *LYS2* genes were subsequently disrupted with a plasmid linearized with either Stu2 or EcoRV restriction enzyme, that contains the *HIS3* or *LEU2* genes along with pieces of *URA3* or *LYS2* such that self-recombination at a low rate (1×10^{-4}) would result in the previous undisrupted functional *URA3* or *LYS2*. Subsequently, haploids with P_{GAL1}-*CEN3 lys2*::*LEU2* and/or P_{GAL1}-CEN3 *ura3*::*HIS3* constructs were cultured to log phase in YPAR medium and subsequently transferred to YPAGR medium for 3 hours. The cells were then plated onto complete synthetic media plates lacking either lysine and leucine (-LYS -LEU) or uracil and histidine (-URA -HIS). All aneuploid strains generated by this method were verified by qPCR. This method of generating aneuploid strains through non-disjunction of a specific chromosome was easily adapted for engineering either a simultaneous gain of two different chromosomes or a gain and loss of two chromosomes. The former was generated in haploids containing P_{GAL1}-*CEN3 lys2*::*LEU2* and P_{GAL1}-*CEN3 ura3*::*HIS3* in separate chromosomes. While the latter was performed in diploid strains containing P_{GAL1}-*CEN3 lys2*::*LEU2* and P_{GAL1}-*CEN3 URA3* in separate chromosomes to be gained and lost respectively. The gain-loss strains were induced in YPAGR as above but were finally plated of 5-FOA plates to select initially for the chromosomal loss. Single colonies were then picked and

plated on -LYS-LEU medium for the selection of the chromosome gain. Both aneuploidies were respectively tested and verified by qPCR.

Adaptation via clonal expansion:

The *BIR1* deleted haploid or diploid strains were grown up on YPAD plates such that single colonies were clearly visible and be picked for the next round of clonal expansion. The haploids were generated by tetrad dissection of the heterozygous diploids. On the fourth day of growth small colonies (*bir1Δ*) emerged in tetrads with two large colonies (*BIR1+*). They were grown on YPAD plates and 6 colonies from each initial *bir1Δ* spore was selected for the subsequent 10 rounds of clonal expansion. Each round of clonal expansion involved streaking one large colony on a fresh plate, every two days. At the end of 10 clonal expansions all 102 strains derived from 19 different spores were kept frozen at -80°C in a solution of 25% glycerol. Each experiment was conducted thereafter using the frozen stocks. Genome sequencing and Hygromycin resistance confirmed the *bir1Δ* genotype in the adapted strains.

Doubling time measurements:

Cultures were grown overnight and subsequently diluted in YPAD to an optical density (OD_{600}) of 0.01. Measurements of OD were taken using a spectrophotometer after 3, 4, 5.5, 7, and 8.5 hours of growth. The doubling times were calculated using the slope of the logarithmic curves in Microsoft Excel.

Colony size measurements:

Strains were struck out and grown for 40 hours ,such that single colonies were distinguishable from each other. Images of the plates were taken using an SPimager

(S&P Robotics Inc.) that was fitted with a Canon Rebel XS1 dSLR camera. The images were subsequently analyzed using ImageJ. In ImageJ, the images were thresholded and the colony sizes were acquired using the "Analyze Particles" function with specific parameters (Particle size: 0.03 - 3 mm^2; Circularity: 0.90 - 1). The average of the median for each strain was used for normalization.

Flow cytometry:

Cultures were grown to log phase (OD at 600nm ~ 1.0), pelleted and then resuspended in a 50mM Sodium Citrate solution. The cells were then treated overnight at 37°C with enzymes RNaseA (250 μg/mL, Sigma-Aldrich R6513) and Proteinase K (1 mg/mL, Sigma-Aldrich P2308). Lastly, the strains were resuspended in a solution of 50 mM Sodium Citrate containing the DNA dye SYTOX green (1 μM, ThermoFischer 10768273). After an incubation of one hour at room temperature the cells were diluted in 1:4 of 50 mM Sodium Citrate solution and finally run on a BD FACSCallibur flow cytometer. A 15mW 488 nm laser was used and using the BD FACSDiva 8.0.1 software the maximum count peaks of the measured fluorescence intensities were calculated.

Next generation sequencing and analysis:

Cultures were grown overnight to saturation and DNA was isolated using the Promega Wizard® Genomic DNA Purification Kit. The DNA samples were then fragmented using the Bioruptor® Pico Sonicator for 2 – 3 cycles (30 seconds on/off) to a target size of approximately 500 bp. Fragment length was verified by running the fragmented DNA samples on a 0.8% agarose gel. The fragments were subsequently utilized for DNA library generation using the NEBNext® Ultra™ II DNA Library Prep Kit for

Illumina® (New England Biosciences). The size selection and purification were carried out using the AMPure® XP Beads. About 12 to 16 strains were mixed in equimolar ratios to create a multiplex with NEBNext® Multiplex Oligos (96-index Primers) that contain unique barcodes to distinguish between samples. The multiplexes were submitted to the Vienna BioCenter Next Generation Sequencing facility (VBCF) for next generation sequencing on a Illumina HiSeq 2500 System which was run at the 50 base pair paired-end setting. Datasets were demultiplexed and then yeast genome alignment with our datasets were performed using bowtie2 (version 2.2.9; http://bowtie-bio.sourceforge.net/bowtie2). The files generated by bowtie2 were converted to bed files using bedtools (v2.14, http://bedtools.readthedocs.io) and samtools (v1.3.1; http://samtools.sourceforge.net). The final bed files were subjected to custom scripts in Python2 for copy number determination from the read densities. For the normalization of the differences that originated from the chromosome size, a region 15 kb big close to the telomere was used. The mutations were identified in the *bir1Δ-ad* strains by supplying the output file from bowtie2 to the mpileup function in samtools. The datasets were subsequently filtered by considering both the read depth and the quality scores generated by the mpileup function. The resulting bcf files were converted to variant call format files (.vcf) by using bcftools (version1.3.1). Next, VCFtools (version0.1.13) were utilized to compare the mutations found in the *bir1Δ-ad* strains to the diploid parent strain (CCY149, see Table 1). Finally, the unique mutations with the strain identity, the type of mutation (coding/non-coding), and the precise coordinates (in bp) was filtered into a list by using a custom Python2 script. A list of all the CIN genes was generated by using a custom Python2 script that searched the Saccharomyces Genome Database (SGD) for genes that were associated with 6 Gene Ontology (GO) terms: chromosome segregation: premature and chromosome

segregation: decreased; chromosome/plasmid maintenance: decreased rate; colony sectoring: increased; chromosome segregation: abnormal; chromosome/plasmid maintenance: abnormal. The enrichment tests for the GO terms were conducted using the Panther database website (http://pantherdb.org/) with appropriate parameters (model organism - "S. cerevisiae"; "GO biological process complete"; "statistical overrepresentation test").

Microscopy:

Each strain was grown to saturation overnight and then diluted 100-fold. The dilutions were grown to mid log phase (approximately 5 hours). Mid-log phase cells were then pelleted, washed, and resuspended in 1XPBS (100mM Phosphate buffer, pH 7.4). The cells were then diluted and pipetted onto 1% agarose pads containing complete synthetic medium. The pads were airdried for few minutes, covered with a coverslip and sealed with VALAP (a 1:1:1 mixture of petroleum jelly [Vaseline], lanolin, and paraffin [Thermo Fisher Scientific] by weight). The Olympus cellSens microscope (Olympus Corporation) system with the cellVivo system for controlled temperature of 30°C was used for time-lapse imaging of the cells. Imaging was performed with a 60x objective lense (1.42 NA, oil immersion, Olympus Plan Apochromat objective) and an sCMOS camera (Hamamatsu ORCA-Flash4.0 V2). The microscope was fully operated by the Olympus cellSens v1.18 software and took 11 Z-sections, each with a step size of 0.7 μm. Time-lapse imaging was done by taking images every 15 minutes for a total duration of 4 hours. The hyperstacks were stored in the original Olympus file format and were opened in ImageJ using the BioFormats plugin. All images shown with one panel were taken on the same day and contrast adjusted to the same extent. Missegregation rates were measured by tracking the foci over

several cycles of chromosome segregation that were formed by chromosome 4 labelled by lacI-GFP. An event of missegregation was scored when both the dots ended up in either the daughter or mother cell after complete nuclear division (judged by the background nuclear fluorescence). The missegregation rate was represented as a percentage that was calculated by dividing the total number of missegregation event by the total number of observed nuclear divisions.

Quantitative-PCR (qPCR):

Small proportion of cells from selection plates were boiled in 0.02 N NaOH at 100°C in a thermocyler for 10 minutes. The boiled samples were then spun down in a benchtop centrifuge to separate cellular debris and the lysate was used for the qPCR reaction mixture. Each 20 μL reaction mixture consisted of 10 μL of Luna qPCR Master Mix (New England Biolabs), 1 μM of each primer and 1 μL of lysate. Primers were designed in non-coding regions of each chromosomal arm. The reaction mixture was setup for qPCR in 96-well plates (Eppendorf, twin.tec real-time PCR 96-well plate) and run using a Mastercycler® RealPlex^2 (Eppendorf). Cycling program included initial denaturation at 95°C for 5 minutes and then 40 cycle repeats of denaturation (at 95°C) for 15 seconds and extension (at 60°C) for 1 minute. Melting curves depicting the dissociation of the product were carried out to verify the absence of secondary products during amplification. The Eppendorf RealPlex^2 software automatically determined the C_t values using the default thresholding. Every reaction was run in duplicate along with the corresponding parental controls or wild-type. A modified "$\Delta\Delta C_t$ procedure" (Livak KJ and Schmittgen TD, 2001) was used to determine the chromosome copy numbers. Briefly, the C_t values from the duplicate reactions were averaged and this average was used to obtain the ΔC_t. The negative of this was then

raised to the power of 2 to calculate the fold change. The fold change of the test strains were divided to that of a parental or wild-type strain to obtain the relative chromosome copy numbers.

Data from Cancer genome databases and its analysis:

Data files pertaining to Copy number variation (CNV) were accessed from the Genomic data commons (GDC) portal (https://portal.gdc.cancer.gov) and downloaded on October 19th, 2017. Using a custom Python2 script we calculated the relative copy numbers of each chromosomal arm across the human genome. Chromosome arms that displayed large insertions or deletions in tumor samples were excluded (those where the mean and median copy numbers varied greater than 0.2) from analysis. Only karyotypes with complex aneuploidy (more than two copy number aberrations) were a part of the statistical analyses.

CRSPR-assisted chromosomal arm translocations:

Translocations between chromosomes were induced by a CRISPR method similar to one that was recently used to engineer whole-chromosome fusions in budding yeast (Luo Z et al., 2018; Shao Y et al., 2018). Strains that contained P_{GAL1}-*CEN3 ura3*::*HIS3* instead of CEN 6 were grown to saturation. These cultures were diluted the next day and were grown for 5 hours to bring them to log phase growth. They were transformed with a plasmid containing *pCUP1-1-Cas9 URA3*, appropriate guide RNAs (targeting gene free regions on the left arm of chromosome 6 and chromosome 13), and donor fragments that contained 50 bp homology of the left arm of chromosome 6, a selectable marker (Hygromycin or Kanamycin) and 50 bp homology of the left arm of chromosome 13. The donor fragments were generated by PCR using appropriate

primers. These fragments were utilized as a template for homology directed repair after Cas9 cleavage on chromosome 6. The cells were plated first on selectable plates lacking uracil and subsequently replica plated on solid medium containing Hygromycin (HYG) and Kanamycin (KAN). This selection specifically permitted the growth of strains that have successfully translocated the chromosomal arms which formed chimeric chromosomes 6L-13L (containing *pCUP1-1-Cas9 URA3* and HYG) and 6R-13R (containing KAN). The strains were then checked by PCR using primers centered around the cut site and their identity was verified by Sanger sequencing. These strains were subsequently induced using YPAGR medium to induce missegregation of the chimeric 6L-13L chromosome and selected on -URA -HIS plates from the disomic chromosome. The absence of chromosome 6 lethality was readily observed after dilution spotting during the selection of the disomic chimeric chromosome.

Liquid adaptation:

Overnight cultures were grown to saturation and diluted to an optical density (at 600nm) of 0.1. Next, the cultures diluted again in 96-well plates (Nunc 96 Deepwell Plates Volume 2ml) by a 1000 fold into 200 μL of YPAD and to allow exchange of oxygen it was covered by Breathe-Easier strip (Sigma 2763624). These deepwell plates were fixed using custom made holders onto an incubator shaker (New Brunswick Innova 4000 Benchtop Incubator Shaker) to grow the cultures for 24 hours at 30°C with 300 revolutions per minute. Each day for 3 weeks after 24 hours of growth the cultures were diluted in fresh media (1:1000) and the above procedure was repeated.

Statistics:

Graphpad (Prism 7.0) software was utilized to perform t-tests on all our datasets and the hypergeometric tests were performed in Python2 by using the hypergeom.pmf" function in the scipy.stats module. Either the "pearsonr" function within the scipy.stats module of Python2 or the "correl" formula in Microsoft Excel was used to calculate the Pearson's correlation coefficients.

Tables

Table 1. Plasmids and Yeast Strains used in this study.

Strain	Genotype	Source	Background	Figure(s)
CCY747	*MATα, leu2,3-112, lys2Δ, ura3-1, his3-11:pCUP1-GFP12-lacI12:HIS3, trp1-1:256lacO:TRP1*	a	W303	8B
CCY149	*MATa/MATα, ura3-1/ura3-1, LEU2/leu2,3-112, LYS2/lys2Δ, ADE2/ade2-1, can1-100, bar1Δ, his3-11:pCUP1-GFP12-lacI12:HIS3/his3-11:pCUP1-GFP12-lacI12:HIS3 trp1-1:256lacO:TRP1/ trp1-1:256lacO:TRP1, BIR1/bir1Δ::hphNT1*	a	W303	8
bir1Δ-ad haploids	*All 102 strains were derived from tetrad dissection of CCY149*	c	W303	8B, 8C, 8D, 8E, 12A, 12B, 12C, 12F, 9
bir1Δ-ad2 haploids	*All haploid strains were derived from bir1Δ-ad haploids*	c	W303	21B, 21C
BY4741	*MATa, his3Δ1, leu2Δ0, ura3Δ0, met15Δ0*	b	S288c	-
BY4742	*MATα, his3Δ1, leu2Δ0, ura3Δ0*	b	S288c	-
CCY1865	*MATa, his3Δ1, leu2Δ0, ura3Δ0*	c	S288c	-
CCY1905	*MATa, leu2,3-112, lys2Δ, ura3-1, his3-11:pCUP1-GFP12-lacI12:HIS3, trp1-1:256lacO:TRP1, bir1Δ::hphNT1, pCC598:URA3*	c	W303	-
CCY1976	*CCY1905 + cen2::p-$_{GAL1}$-CEN3:LYS2/cen2::p-$_{GAL1}$-CEN3:lys2::pCC644:LEU2*	c	W303	10B
CCY1947	*CCY1905 + cen10::p-$_{GAL1}$-CEN3:LYS2/cen10::p-$_{GAL1}$-CEN3:lys2::pCC644:LEU2*	c	W303	10B
CCY2161	*CCY1905 + cen3::p-$_{GAL1}$-CEN3:LYS2/cen3::p-$_{GAL1}$-CEN3:lys2::pCC644:LEU2*	c	W303	10B
CCY1943	*CCY1905 + cen8::p-$_{GAL1}$-CEN3:LYS2/cen8::p-$_{GAL1}$-CEN3:lys2::pCC644:LEU2*	c	W303	10B
CCY2284	*CCY1905 + cen9::p-$_{GAL1}$-CEN3:LYS2/cen9::p-$_{GAL1}$-CEN3:lys2::pCC644:LEU2*	c	W303	10B
CCY1924	*CCY1865 + cen8::p-$_{GAL1}$-CEN3:URA3/cen8::p-$_{GAL1}$-CEN3:ura3::pCC644:HIS3*	c	S288c	13A
CCY1927	*CCY1865 + cen10::p-$_{GAL1}$-CEN3:URA3/cen10::p-$_{GAL1}$-CEN3:ura3::pCC644:HIS3*	c	S288c	13A

CCY2122	*CCY1865 + cen10::p-$_{GAL1}$-CEN3:LYS2/cen10::p-$_{GAL1}$-CEN3:lys2::pCC644:LEU2*	c	S288c	13A
CCY2125	*BY4742 + cen8::p-$_{GAL1}$-CEN3:LYS2/cen8::p-$_{GAL1}$-CEN3:lys2::pCC644:LEU2*	c	S288c	13A
CCY2073	*BY4742 + cen3::p-$_{GAL1}$-CEN3:URA3/cen3::p-$_{GAL1}$-CEN3:ura3::pCC644:HIS3, cen8::p-$_{GAL1}$-CEN3:LYS2/cen8::p-$_{GAL1}$-CEN3:lys2::pCC644:LEU2*	c	S288c	12E, 12F
CCY2074	*BY4742 + cen2::p-$_{GAL1}$-CEN3:URA3/cen2::p-$_{GAL1}$-CEN3:ura3::pCC644:HIS3, cen8::p-$_{GAL1}$-CEN3:LYS2/cen8::p-$_{GAL1}$-CEN3:lys2::pCC644:LEU2*	c	S288c	12G
CCY2075	*BY4742 + cen3::p-$_{GAL1}$-CEN3:URA3/cen3::p-$_{GAL1}$-CEN3:ura3::pCC644:HIS3, cen10::p-$_{GAL1}$-CEN3:LYS2/cen10::p-$_{GAL1}$-CEN3:lys2::pCC644:LEU2*	c	S288c	12E, 12F
CCY2076	*BY4742 + cen10::p-$_{GAL1}$-CEN3:URA3/cen10::p-$_{GAL1}$-CEN3:ura3::pCC644:HIS3, cen8::p-$_{GAL1}$-CEN3:LYS2/cen8::p-$_{GAL1}$-CEN3:lys2::pCC644:LEU2*	c	S288c	12E, 12F
CCY2077	*BY4742 + cen2::p-$_{GAL1}$-CEN3:URA3/cen2::p-$_{GAL1}$-CEN3:ura3::pCC644:HIS3, cen10::p-$_{GAL1}$-CEN3:LYS2/cen10::p-$_{GAL1}$-CEN3:lys2::pCC644:LEU2*	c	S288c	12G
CCY2078	*BY4742 + cen8::p-$_{GAL1}$-CEN3:URA3/cen8::p-$_{GAL1}$-CEN3:ura3::pCC644:HIS3, cen10::p-$_{GAL1}$-CEN3:LYS2/cen10::p-$_{GAL1}$-CEN3:lys2::pCC644:LEU2*	c	S288c	12E, 12F
CCY2260	*BY4741 + cen1::p-$_{GAL1}$-CEN3:URA3/cen1::p-$_{GAL1}$-CEN3:ura3::pCC644:HIS3, cen8::p-$_{GAL1}$-CEN3:LYS2/cen8::p-$_{GAL1}$-CEN3:lys2::pCC644:LEU2*	c	S288c	12E, 12F
CCY2261	*BY4741 + cen1::p-$_{GAL1}$-CEN3:URA3/cen1::p-$_{GAL1}$-CEN3:ura3::pCC644:HIS3, cen10::p-$_{GAL1}$-CEN3:LYS2/cen10::p-$_{GAL1}$-CEN3:lys2::pCC644:LEU2*	c	S288c	12E, 12F
CCY2264	*BY4741 + cen3::p-$_{GAL1}$-CEN3:URA3/cen3::p-$_{GAL1}$-CEN3:ura3::pCC644:HIS3, cen8::p-$_{GAL1}$-CEN3:LYS2/cen8::p-$_{GAL1}$-CEN3:lys2::pCC644:LEU2*	c	S288c	12E, 12F
CCY2266	*BY4742 + cen13::p-$_{GAL1}$-CEN3:URA3/cen13::p-$_{GAL1}$-CEN3:ura3::pCC644:HIS3, cen10::p-$_{GAL1}$-CEN3:LYS2/cen10::p-$_{GAL1}$-CEN3:lys2::pCC644:LEU2*	c	S288c	12E, 12F
CCY2364	*BY4742 + cen13::p-$_{GAL1}$-CEN3:URA3/cen13::p-$_{GAL1}$-CEN3:ura3::pCC644:HIS3, cen3::p-$_{GAL1}$-CEN3:LYS2/cen3::p-$_{GAL1}$-CEN3:lys2::pCC644:LEU2*	c	S288c	12E, 12F
CCY2366	*BY4741 + cen2::p-$_{GAL1}$-CEN3:URA3/cen2::p-$_{GAL1}$-CEN3:ura3::pCC644:HIS3, cen3::p-$_{GAL1}$-*	c	S288c	12G

	CEN3:LYS2/cen3::p-$_{GAL1}$-CEN3:lys2::pCC644:LEU2			
CCY2368	*BY4742 + cen8::p-$_{GAL1}$-CEN3:URA3/cen8::p-$_{GAL1}$-CEN3:ura3::pCC644:HIS3, cen3::p-$_{GAL1}$-CEN3:LYS2/cen3::p-$_{GAL1}$-CEN3:lys2::pCC644:LEU2*	c	S288c	12E, 12F
CCY2369	*BY4741 + cen10::p-$_{GAL1}$-CEN3:URA3/cen10::p-$_{GAL1}$-CEN3:ura3::pCC644:HIS3, cen3::p-$_{GAL1}$-CEN3:LYS2/cen3::p-$_{GAL1}$-CEN3:lys2::pCC644:LEU2*	c	S288c	12E, 12F
CCY2370	*BY4742 + cen13::p-$_{GAL1}$-CEN3:URA3/cen13::p-$_{GAL1}$-CEN3:ura3::pCC644:HIS3, cen3::p-$_{GAL1}$-CEN3:LYS2/cen3::p-$_{GAL1}$-CEN3:lys2::pCC644:LEU2*	c	S288c	12E, 12F
CCY2372	*BY4741 + cen2::p-$_{GAL1}$-CEN3:URA3/cen2::p-$_{GAL1}$-CEN3:ura3::pCC644:HIS3, cen1::p-$_{GAL1}$-CEN3:LYS2/cen1::p-$_{GAL1}$-CEN3:lys2::pCC644:LEU2*	c	S288c	12G
CCY2374	*BY4741 + cen3::p-$_{GAL1}$-CEN3:URA3/cen3::p-$_{GAL1}$-CEN3:ura3::pCC644:HIS3, cen1::p-$_{GAL1}$-CEN3:LYS2/cen1::p-$_{GAL1}$-CEN3:lys2::pCC644:LEU2*	c	S288c	12E, 12F
CCY2376	*BY4741 + cen8::p-$_{GAL1}$-CEN3:URA3/cen8::p-$_{GAL1}$-CEN3:ura3::pCC644:HIS3, cen1::p-$_{GAL1}$-CEN3:LYS2/cen1::p-$_{GAL1}$-CEN3:lys2::pCC644:LEU2*	c	S288c	12E, 12F
CCY2378	*BY4742 + cen10::p-$_{GAL1}$-CEN3:URA3/cen10::p-$_{GAL1}$-CEN3:ura3::pCC644:HIS3, cen1::p-$_{GAL1}$-CEN3:LYS2/cen1::p-$_{GAL1}$-CEN3:lys2::pCC644:LEU2*	c	S288c	12E, 12F
CCY2379	*BY4742 + cen13::p-$_{GAL1}$-CEN3:URA3/cen13::p-$_{GAL1}$-CEN3:ura3::pCC644:HIS3, cen1::p-$_{GAL1}$-CEN3:LYS2/cen1::p-$_{GAL1}$-CEN3:lys2::pCC644:LEU2*	c	S288c	12E, 12F
CCY1480	*MATa/MATα, ura3-1/ura3-1, LEU2/leu2,3-112, LYS2/lys2Δ, ADE2/ade2-1, can1-100, bar1Δ, his3-11:pCUP1-GFP12-lacI12:HIS3/his3-11:pCUP1-GFP12-lacI12:HIS3 trp1-1:256lacO:TRP1/ trp1-1:256lacO:TRP1, NBL1/nbl1Δ::hphNT1*	c	W303	-
nbl1Δ-ad haploids	*All nbl1Δ-ad strains were derived from tetrad dissection of CCY1480*	c	W303	16B, 16C, 16D, 16E
CCY1482	*MATa/MATα, ura3-1/ura3-1, LEU2/leu2,3-112, LYS2/lys2Δ, ADE2/ade2-1, can1-100, bar1Δ, his3-11:pCUP1-GFP12-lacI12:HIS3/his3-11:pCUP1-GFP12-lacI12:HIS3 trp1-1:256lacO:TRP1/ trp1-1:256lacO:TRP1, SGO1/sgo1Δ::hphNT1*	c	W303	-

sgo1Δ-ad haploids	*All sgo1Δ-ad strains were derived from tetrad dissection of CCY1482*	c	W303	16B, 16C, 16D, 16E
CCY1484	*MATa/MATα, ura3-1/ura3-1, LEU2/leu2,3-112, LYS2/lys2Δ, ADE2/ade2-1, can1-100, bar1Δ, his3-11:pCUP1-GFP12-lacI12:HIS3/his3-11:pCUP1-GFP12-lacI12:HIS3 trp1-1:256lacO:TRP1/ trp1-1:256lacO:TRP1, BUB1/bub1Δ::hphNT1*	c	W303	-
bub1Δ-ad haploids	*All bub1Δ-ad strains were derived from tetrad dissection of CCY1484*	c	W303	16B, 16C, 16D, 16E
CCY1739	*tetradploid, MATa/MATaΔ::natNT2/Matα/MatαΔ::kanMX 4, ura3-1, lys2Δ, LEU2/leu2,3-112, his3-11:pCUP1-GFP12-lacI12:HIS3 trp1-1:256lacO:TRP1 ADE2/ade2-1, can1-100, bar1Δ, BIR1/BIR1/bir1Δ::hphNT1/bir1Δ::hphNT1*	c	W303	-
CCY1743	*MATa/MATα, ura3-1/ura3-1, lys2Δ/lys2Δ, LEU2/leu2,3-112, his3-11:pCUP1-GFP12-lacI12:HIS3, trp1-1:256lacO:TRP1, ADE2/ade2-1, can1-100, bar1Δ, bir1Δ::hphNT1/bir1Δ::natNT2, pCC599::URA3*	c	W303	-
CCY1744	*MATa/MATα, ura3-1/ura3-1, lys2Δ/lys2Δ, LEU2/leu2,3-112, his3-11:pCUP1-GFP12-lacI12:HIS3, trp1-1:256lacO:TRP1, ADE2/ade2-1, can1-100, bar1Δ, bir1Δ::hphNT1/bir1Δ::kanMX4, pCC599::URA3*	c	W303	-
bir1Δ-ad diploids	*All 25 strains were derived from tetrad dissection of strains with the genotype of CCY1739, or from counter-selection of URA3 plasmid of CCY1743, CCY1744*	c	W303	17
bir1Δ-ad2 diploids	*All bir1Δ-ad2 diploid strains were derived from bir1Δ-ad diploids*	c	W303	21D, 21E
CCY1295	*CCY149 + SLI15/Sli15Δ:natNT2*	c	W303	-
CCY1320	*CCY1295 + ura3-1:pCC411:URA3*	c	W303	-
bir1Δ-ad SLI15 Duplication	*All bir1Δ-ad SLI15 Duplication strains were derived from spores of CCY1320*	c	W303	11C, 11D, 11E
CCY2761	*CCY1295 + cup1-1:pCC607:URA3*	c	W303	-
bir1Δ-ad SLI15 Relocation	*All bir1Δ-ad SLI15 Relocation strains were derived from spores of CCY2761*	c	W303	11G
CCY2115	*CCY1905 + trp1-1:pCC272:TRP1*	c	W303	11B
Plasmid	**Description**	**Source**		

pRS306	*pBluescript URA3*	d		
pCC272	*SLI15 + 1kb upstream in pRS304*	c		
pCC283	*BIR1 + 1kb upstream in pRS306*	a		
pKA52	*HIS3 integration plasmid with part of URA3 inserted at the MCS. Can insert HIS3 into a URA3 locus. Used for making disomic strains.*	e		
pGALCEN-JC3-13	*For replacing centromeres with CEN3 under the GAL-10 promoter (URA3)*	e		
pCC658	*For replacing centromeres with CEN3 under the GAL-10 promoter (LYS2)*	c		
pCC644	*LEU2 integration vector with bases 3043-3538 of LYS2 for Disruption of the LYS2 gene. Used for making disomic strains.*	c		
pCC598	*BIR1 + 1kb upstream in pRS306*	c		
pCC411	*SLI15 + 1kb upstream in pRS306*	c		
pCC607	*pCC411 + sequence from Cup1-1 gene for integrating Sli15 plus promoter into that location of chromosome 8*	c		

Key **Source**

a Campbell and Desai, Nature 497: 118–121 (2013)
b Brachmann CB et al., Yeast. (1998)
c This study
d Sinorski and Hieter Genetics 122: 19-27 (1989)
e Anders et. al., BMC Genetics (2009)

Table 2. Filtering of cancer karyotypes based on type of aneuploidy. Related to Figure 19.

Cancer type	Number of samples	Samples with only whole chromosome/ arm aneuploidy	Number with complex whole chromosome/arm aneuploidy	Percent with complex whole chromosome/ arm aneuploidy
Breast Invasive Carcinoma	1096	214	177	16
Glioblastoma Multiforme	593	170	161	27
Ovarian Serous Cystadenocarcinoma	573	13	11	2
Lung Adenocarcinoma	518	114	97	19
Uterine Corpus Endometrial Carcinoma	547	323	137	25
Kidney Renal Clear Cell Carcinoma	532	273	253	48
Head and Neck Squamous Cell Carcinoma	531	120	98	18
Brain Lower Grade Glioma	514	225	193	38
Thyroid Carcinoma	505	468	42	8
Lung Squamous Cell Carcinoma	504	59	49	10
Prostate Adenocarcinoma	498	198	75	15
Skin Cutaneous Melanoma	470	91	78	17
Colon Adenocarcinoma	458	198	138	30
Stomach Adenocarcinoma	443	159	119	27
Bladder Urothelial Carcinoma	412	65	47	11

Table 3. List of genes mutated in the *bir1Δ-ad* strains.

Systematic	Standard	Mutant	Residue	CIN gene
tS(UGA)I	SUP17	missense	A18G	no
tV(AAC)G2	None	missense	E15*	no
YAL051W	OAF1	missense	V939I	no
YAR028W	None	missense	D32N	no
YCR017C	CWH43	missense	E250G	no
YCR021C	HSP30	missense	R11C	no
YCR033W	SNT1	missense	F870I	yes
YDL101C	DUN1	missense	A307V	yes
YDL137W	ARF2	missense	S147C	no
YDL145C	COP1	missense	I307S	no
YDL156W	CMR1	missense	L27F	yes
YDL171C	GLT1	missense	D1583V	no
YDL190C	UFD2	missense	Q88E	no
YDL243C	AAD4	indel	70	no
YDR104C	SPO71	missense	D814N	no
YDR142C	PEX7	missense	L253I	no
YDR159W	SAC3	missense	I1097L	no
YDR180W	SCC2	missense	N63Y	yes
YDR189W	SLY1	missense	D151N	yes
YDR190C	RVB1	missense	T322K	no
YDR238C	SEC26	missense	F555L	no
YDR302W	GPI11	missense	R29L	no
YDR304C	CPR5	missense	V188L	no
YDR321W	ASP1	missense	R55I	no
YDR325W	YCG1	missense	G677R	yes
YDR333C	RQC1	indel	565	no
YDR335W	MSN5	missense	H426Y	no
YDR387C	CIN10	missense	S311T	yes
YDR389W	SAC7	missense	L511F	no
YDR422C	SIP1	missense	E357D	no
YDR440W	DOT1	missense	H142N	no
YDR451C	YHP1	missense	A273T	no
YDR492W	IZH1	missense	E35K	no
YDR523C	SPS1	missense	F248S	no
YDR527W	RBA50	missense	G22V	no
YEL060C	PRB1	missense	G304R	no
YER002W	NOP16	missense	D122V	no
YER008C	SEC3	missense	Q495R	no
YER027C	GAL83	missense	P78S	no
YER043C	SAH1	missense	R241C	no
YER053C	PIC2	missense	N49Y	no
YER066W	RRT13	missense	G93S	no
YER095W	RAD51	missense	G40V	y
YER109C	FLO8	missense	A529T	no
YER116C	SLX8	missense	P150S	yes
YER154W	OXA1	missense	D239H	no

YER155C	BEM2	missense	H2114Q	no
YER167W	BCK2	missense	S414P	no
YER172C	BRR2	missense	K351N	no
YER172C	BRR2	missense	N352Y	no
YER173W	RAD24	missense	T622A	yes
YER176W	ECM32	indel	781	no
YFL002C	SPB4	missense	R207S	no
YFL013C	IES1	missense	D309V	no
YFL013C	IES1	missense	Y572*	no
YFL021W	GAT1	missense	H182Y	no
YFL024C	EPL1	indel	Q790	no
YFL024C	EPL1	indel	Q790	no
YFR015C	GSY1	missense	A639T	no
YFR029W	PTR3	missense	D19E	no
YFR040W	SAP155	missense	D780H	no
YGL017W	ATE1	missense	A274S	no
YGL203C	KEX1	missense	P43S	no
YGL206C	CHC1	missense	P1463Q	no
YGL207W	SPT16	missense	W54R	yes
YGL207W	SPT16	missense	T713A	yes
YGR054W	None	missense	P242Q	no
YGR070W	ROM1	missense	V248A	no
YGR080W	TWF1	missense	E51D	no
YGR090W	UTP22	missense	S819L	no
YGR130C	None	indel	190	no
YGR142W	BTN2	indel	310	no
YGR208W	SER2	missense	A271T	no
YGR241C	YAP1802	indel	514	no
YGR253C	PUP2	missense	D71N	yes
YGR257C	MTM1	indel	344	no
YGR271C-A	EFG1	missense	L118F	no
YGR271W	SLH1	missense	N924K	no
YHL008C	None	indel	449	no
YHL034C	SBP1	missense	V44I	no
YHL041W	None	missense	S101F	no
YHR030C	SLT2	missense	L159F	no
YHR042W	NCP1	missense	L315M	no
YHR046C	INM1	missense	G112V	no
YHR072W	ERG7	missense	S612F	no
YHR078W	None	missense	C408Y	no
YHR106W	TRR2	missense	C165F	no
YHR117W	TOM71	missense	T293A	no
YHR138C	None	missense	V27A	no
YIL010W	DOT5	missense	S14F	yes
YIL042C	PKP1	missense	R97K	no
YIL073C	SPO22	missense	Q38*	no
YIL078W	THS1	missense	P174S	no
YIL090W	ICE2	missense	C364R	yes
YIL166C	SOA1	indel	394	no

YIL169C	CSS1	indel	942	no
YIR016W	None	missense	D252H	no
YJL005W	CYR1	missense	H1984L	no
YJL080C	SCP160	missense	R152G	no
YJL158C	CIS3	missense	S191N	no
YJR062C	NTA1	missense	S424G	no
YJR109C	CPA2	missense	A1049P	no
YKL021C	MAK11	missense	C252R	no
YKL040C	NFU1	missense	M213I	no
YKL078W	DHR2	missense	G161A	no
YKL080W	VMA5	missense	L130S	no
YKL182W	FAS1	missense	A632T	no
YKL183W	LOT5	missense	D54V	no
YKL191W	DPH2	missense	N386K	no
YKL215C	OXP1	missense	T310A	no
YKR021W	ALY1	missense	L621M	no
YKR039W	GAP1	missense	A527T	no
YKR054C	DYN1	missense	N2915I	no
YKR095W	MLP1	missense	Q1040P	no
YLL061W	MMP1	missense	H550N	no
YLR020C	YEH2	missense	Q479L	no
YLR024C	UBR2	missense	S1400C	no
YLR024C	UBR2	nonsense	S1483	no
YLR045C	STU2	missense	P146S	no
YLR067C	PET309	missense	G350D	no
YLR096W	KIN2	indel	730	no
YLR145W	RMP1	missense	C132Y	no
YLR196W	PWP1	missense	E129D	yes
YLR332W	MID2	missense	I359L	no
YLR369W	SSQ1	missense	K303R	no
YLR383W	SMC6	missense	M270V	yes
YLR410W	VIP1	missense	K262T	yes
YLR417W	VPS36	missense	A412G	no
YLR422W	DCK1	missense	S370L	no
YLR454W	FMP27	missense	M1621I	no
YML072C	TCB3	missense	D168E	no
YML097C	VPS9	missense	C260Y	no
YML100W	TSL1	missense	M121I	no
YMR026C	PEX12	missense	T241M	no
YMR092C	AIP1	missense	Y515H	no
YMR129W	POM152	missense	G1069S	no
YMR154C	RIM13	missense	A93G	no
YMR178W	None	missense	S234T	no
YMR207C	HFA1	missense	G110D	yes
YMR246W	FAA4	missense	F356C	yes
YMR317W	None	indel	270	yes
YMR317W	None	indel	270	yes
YNL054W	VAC7	missense	P143S	no
YNL077W	APJ1	missense	P107Q	no

YNL078W	NIS1	indel	4	no
YNL082W	PMS1	missense	T92M	no
YNL178W	RPS3	missense	A80T	no
YNL258C	DSL1	missense	K615N	no
YNL261W	ORC5	missense	D323G	yes
YNL287W	SEC21	missense	S405Y	no
YNR016C	ACC1	missense	A1019V	yes
YNR030W	ALG12	missense	N477K	no
YNR059W	MNT4	missense	W285*	no
YOL039W	RPP2A	missense	G74A	no
YOL075C	None	missense	C506F	no
YOL081W	IRA2	missense	A1845S	yes
YOL110W	SHR5	missense	R113P	no
YOR076C	SKI7	missense	D430V	no
YOR101W	RAS1	missense	R109T	no
YOR107W	RGS2	missense	H71Q	no
YOR151C	RPB2	missense	G888C	yes
YOR168W	GLN4	missense	F61Y	yes
YOR195W	SLK19	missense	N291S	yes
YOR204W	DED1	missense	H93Q	no
YOR241W	MET7	missense	E306D	no
YOR275C	RIM20	missense	E269*	no
YOR291W	YPK9	missense	E1231V	no
YOR301W	RAX1	missense	Q179H	no
YOR335C	ALA1	missense	K611M	no
YOR354C	MSC6	missense	T562R	no
YPL045W	VPS16	missense	V617I	no
YPL056C	LCL1	missense	V55L	no
YPL086C	ELP3	missense	L512F	no
YPL100W	ATG21	missense	K32N	no
YPL106C	SSE1	missense	L278F	yes
YPL116W	HOS3	missense	Q578P	no
YPL184C	MRN1	missense	E91Q	no
YPL249C	GYP5	missense	M472I	no
YPL264C	None	missense	M273I	no
YPL272C	PBI1	missense	G25R	no
YPR014C	None	missense	V39G	no
YPR029C	APL4	missense	H64N	no
YPR043W	RPL43A	missense	C12S	no
YPR095C	SYT1	missense	Y1058N	no
YPR097W	None	missense	V368L	no
YPR116W	RRG8	missense	S86*	no
YPR120C	CLB5	missense	D43N	yes
YPR138C	MEP3	missense	A26P	no
YPR173C	VPS4	missense	E126Q	no
YPR192W	AQY1	missense	F62S	no

References

- Abe Y, Sako K, Takagaki K, et al. HP1-assisted AURORA B kinase activity prevents chromosome segregation errors. Dev Cell. 2016;36:487–497.
- Adikusuma F, Williams N, Grutzner F, Hughes J, Thomas P. Targeted deletion of an entire chromosome using CRISPR/Cas9. Molecular Therapy. 2017;25:1736–1738.
- Ainsztein AM, Kandels-Lewis SE, Mackay AM, et al. INCENP centromere and spindle targeting: identification of essential conserved motifs and involvement of heterochromatin protein HP1. J Cell Biol. 1998;143:1763–1774.
- Alver RC, Chadha GS, and Blow JJ (2014). The contribution of dormant origins to genome stability: from cell biology to human genetics. DNA Repair (Amst.) 19, 182–189.
- Anders KR, Kudrna JR, Keller KE, Kinghorn B, Miller EM, Pauw D, Peck AT, Shellooe CE, and Strong IJT (2009). A strategy for constructing aneuploid yeast strains by transient nondisjunction of a target chromosome. BMC Genetics 10, 36–36.
- Ariyoshi K, Miura T, Kasai K, Fujishima Y, Oshimura M, Yoshida MA. Induction of genomic instability and activation of autophagy in artificial human aneuploid cells. Mutat Res Mol Mech Mutagen. (2016) 790:19–30.
- Aziz NM, Guedj F, Pennings JLA, et al. Lifespan analysis of brain development, gene expression and behavioral phenotypes in the Ts1Cje, Ts65Dn and Dp(16)1/Yey mouse models of Down syndrome. Dis Model Mech 2018.
- Papp B, Pál C, Hurst LD. Dosage sensitivity and the evolution of gene families in yeast. Nature. 2003;424: 194–197.
- Babu JR, Jeganathan KB, Baker DJ, Wu X, Kang-Decker N, van Deursen JM. Rael is an essential mitotic checkpoint regulator that cooperates with Bub3 to prevent chromosome missegregation. J Cell Biol. 2003;160:341-53.
- Baek K-H, Zaslavsky A, Lynch RC, Britt C, Okada Y, et al. 2009. Down's syndrome suppression of tumour growth and the role of the calcineurin inhibitor DSCR1. Nature 459(7250):1126–30
- Baker D.J., Jeganathan K.B., Cameron J.D., Thompson M., Juneja S., Kopecka A., Kumar R., Jenkins R.B., de Groen P.C., Roche P., van Deursen J.M. 2004. BubR1 insufficiency causes early onset of aging-associated phenotypes and infertility in mice. Nat. Genet. 36:744–749
- Bakhoum S.F., Thompson S.L., Manning A.L., Compton D.A. Genome stability is ensured by temporal control of kinetochore-microtubule dynamics. Nat. Cell Biol. 2009;11:27–35.
- Balaburski, G.M., Hontz, R.D., and Murphy, M.E. (2010). p53 and ARF: unex- pected players in autophagy. Trends Cell Biol. 20, 363–369.
- Barber TD, McManus K, Yuen KWY, Reis M, Parmigiani G, et al. 2008. Chromatid cohesion defects may underlie chromosome instability in human colorectal cancers. PNAS 105(9):3443–48

- Bastola, P., Oien, D. B., Cooley, M. & Chien, J. Emerging cancer therapeutic targets in protein homeostasis. AAPS J. 20, 94 (2018).
- Bazrgar, M., Gourabi, H., Valojerdi, M. R., Yazdi, P. E. & Baharvand, H. Self-correction of chromosomal abnormalities in human preimplantation embryos and embryonic stem cells. Stem Cells Dev. 22, 2449–2456 (2013).
- Beach RR, Ricci-Tam C, Brennan CM, Moomau CA, Hsu PH, Hua B, Silberman RE, Springer M, and Amon A (2017). Aneuploidy Causes Non-genetic Individuality. Cell 189, 229–242.
- Beijersbergen, R.L. et al. Synthetic lethality in cancer therapeutics Ann. Rev. Cancer Biol., 1 (2017), pp. 141-161
- Ben-David U., Arad G., Weissbein U., Mandefro B., Maimon A., Golan-Lev T., Narwani K., Clark A.T., Andrews P.W., Benvenisty N. Aneuploidy induces profound changes in gene expression, proliferation and tumorigenicity of human pluripotent stem cells. Nat. Commun. 2014;5:4825.
- Beroukhim R, Mermel CH, Porter D, Wei G, Raychaudhuri S, et al. 2010. The landscape of somatic copy- number alteration across human cancers. Nature 463(7283):899–905.Birkbak NJ, Eklund AC, Li Q, McClelland SE, Endesfelder D, Tan P, Tan IB, Richardson AL, Szallasi Z, and Swanton C (2011). Paradoxical relationship between chromosomal instability and survival outcome in cancer. Cancer Res 71, 3447–3452.
- Blakeslee AF, Belling J, Farnham ME, Bergner AD. A haploid mutant in the jimson weed, “Datura stramonium” Science. 1922;16:646–7.
- Blakeslee AF. The globe, a simple trisomic mutant in Datura. Proc Natl Acad Sci USA. 1921;7:148–52.
- Blank, H.M., Sheltzer, J.M., Meehl, C.M., and Amon, A. (2015). Mitotic entry in the presence of DNA damage is a widespread property of aneuploidy in yeast. Mol. Biol. Cell 26, 1440–1451.
- Bolton H., Graham S. J., Van der Aa N., Kumar P., Theunis K., Fernandez Gallardo E., Voet T., Zernicka-Goetz M., Mouse model of chromosome mosaicism reveals lineage-specific depletion of aneuploid cells and normal developmental potential. Nat. Commun. 7, 11165 (2016).
- Bonney, M. E., Moriya, H. & Amon, A. Aneuploid proliferation defects in yeast are not driven by copy number changes of a few dosage-sensitive genes. Genes Dev. 29, 898–903 (2015).
- Boveri T. 1914. Zur Frage der Entstehung maligner Tumoren. Jena, Ger.: Gustav Fischer Verlag
- Brewer CM, Holloway SH, Stone DH, Carothers AD, and FitzPatrick DR (2002). Survival in trisomy 13 and trisomy 18 cases ascertained from population based registers. Journal of medical genetics 39, e54.
- Bridges CB (1921). Genetical and Cytological Proof of Non-disjunction of the Fourth Chromosome of Drosophila Melanogaster. Proceedings of the National Academy of Sciences of the United States of America 7, 186–192.
- Bridges CB, 1921. Proof of non-disjunction for the fourth chromosome of Drosophila melanogaster. Science 53 308.
- Brown S. Miscarriage and Its Associations. Semin Reprod Med. 2008;26:391-400.

- Burckstummer T, Banning C, Hainzl P, Schobesberger R, Kerzendorfer C, Pauler FM, et al. A reversible gene trap collection empowers haploid genetics in human cells. Nat Methods. 2013;10:965–71.
- Bryant HE, Schultz N, Thomas HD, Parker KM, Flower D, et al. 2005. Specific killing of BRCA2-deficient tumours with inhibitors of poly(ADP-ribose) polymerase. Nature 434:913–17
- Buccitelli, C. et al. Pan-cancer analysis distinguishes transcriptional changes of aneuploidy from proliferation. Genome Res. 27, 501–511 (2017).
- Burrell RA, McClelland SE, Endesfelder D, Groth P, Weller M-C, et al. 2013. Replication stress links structural and numerical cancer chromosomal instability. Nature 494(7438):492–96
- Byrd JC, Mrózek K, Dodge RK, Carroll AJ, Edwards CG, et al., 2002. Pretreatment cytogenenic abnormalities are predictive of induction success, cumulative incidence of relapse, and overall survival in adult patients with de novo acute myeloid leukemia: results from Cancer and Leukemia Group B (CALGB 8461). Blood 100(13):4325–36
- Callier, P.; Faivre, L.; Cusin, V.; Marle, N.; Thauvin-Robinet, C.; Sandre, D.; Rousseau, T.; Sagot, P.; Lacombe, E.; Faber, V. & Mugneret, F. (2005). Microcephaly is not mandatory for the diagnosis of mosaic variegated aneuploidy syndrome. American Journal of Medical Genetics, Part A, Vol. 137, No. 2, pp. 204-207, ISSN 1552-4833
- Carfi A, Antocicco M, Brandi V, Cipriani C, Fiore F, Mascia D, Settanni S, Vetrano DL, Bernabei R, and Onder G (2014). Characteristics of adults with down syndrome: prevalence of age-related conditions. Frontiers in medicine 1, 51.
- Carmena, M., Wheelock, M., Funabiki, H., and Earnshaw, W. C. (2012). The chromosomal passenger complex (CPC): from easy rider to the godfather of mitosis. Nat. Rev. Mol. Cell. Biol. 13, 789–803.
- Carter SL, Cibulskis K, Helman E, McKenna A, Shen H, et al. 2012. Absolute quantification of somatic DNA alterations in human cancer. Nat. Biotechnol. 30(5):413–21
- Chan, Y. W., Fugger, K. & West, S. C. Unresolved recombination intermediates lead to ultra-fine anaphase bridges, chromosome breaks and aberrations. Nat. Cell Biol. 20, 92–103 (2018).
- Chen B, Retzlaff M, Roos T, Frydman J. (2011). Cellular strategies of protein quality control. Cold Spring Harb Perspect Biol , a004374.
- Chen G., Bradford W.D., Seidel C.W., Li R. Hsp90 stress potentiates rapid cellular adaptation through induction of aneuploidy. Nature. 2012;482:246–250. doi: 10.1038/nature10795.
- Chen G., Mulla W.A., Kucharavy A., Tsai H.-J., Rubinstein B., Conkright J., McCroskey S., Bradford W.D., Weems L., Haug J.S., et al. Targeting the adaptability of heterogeneous aneuploids. Cell. 2015;160:771–784.
- Chen Y, Chen S, Li K, Zhang Y, Huang X, Li T, Wu S, Wang Y, Carey L.B, Qian W. Overdosage of Balanced Protein Complexes Reduces Proliferation Rate in Aneuploid Cells. Cell Syst. 2019; p129-142
- Chunduri N.K., Storchová Z. The diverse consequences of aneuploidy. Nat. Cell Biol. 2019;21:54–62.

- Cimini D, Wan X, Hirel CB, Salmon ED. Aurora kinase promotes turnover of kinetochore microtubules to reduce chromosome segregation errors. Curr Biol. 2006;16(17):1711–1718.
- Comai L. The advantages and disadvantages of being polyploid. Nat Rev Genet. 2005;6(11):836–846.
- Costanzo M, Kuzmin E, van Leeuwen J, Mair B, Moffat J, Boone C, Andrews B. Global genetic networks and the genotype-to-phenotype relationship. Cell. 2019;177:85–100.
- Coste, A., Selmecki, A., Forche, A., Diogo, D., Bougnoux, M.-E., d' Enfert, C., Berman, J., and Sanglard, D. (2007). Genotypic evolution of azole resistance mechanisms in sequential Candida albicans isolates. Eukaryot. Cell 6, 1889–1904.
- Crasta K, Ganem NJ, Dagher R, Lantermann AB, Ivanova EV, et al. 2012. DNA breaks and chromosome pulverization from errors in mitosis. Nature 482:53–58
- Dai, C. & Sampson, S. B. HSF1: guardian of proteostasis in cancer. Trends Cell Biol. 26, 17–28 (2016).
- Davoli T, Xu AW, Mengwasser KE, Sack LM, Yoon JC, et al. 2013. Cumulative haploinsufficiency and triplosensitivity drive aneuploidy patterns and shape the cancer genome. Cell 155(4):948–62
- Davoli, T., Uno, H., Wooten, E. C. & Elledge, S. J. Tumor aneuploidy correlates with markers of immune evasion and with reduced response to immunotherapy. Science 355, eaaf8399 (2017).
- de Graaf G, Buckley F, and Skotko BG (2015). Estimates of the live births, natural losses, and elective terminations with Down syndrome in the United States. American journal of medical genetics Part A 167a, 756–767.
- Delhanty, J. D. et al. Detection of aneuploidy and chromosomal mosaicism in human embryos during preimplantation sex determination by fluorescent in situ hybridisation, (FISH). Hum. Mol. Genet. 2, 1183–1185 (1993). 49.
- Dephoure N, Zhou C, Villen J, Beausoleil SA, Bakalarski CE, Elledge SJ, et al. A quantitative atlas of mitotic phosphorylation. Proc Natl Acad Sci U S A. 2008;105:10762–7.
- Deutschbauer AM, et al. Mechanisms of haploinsufficiency revealed by genome-wide profiling in yeast. Genetics. 2005;169:1915–1925.
- Dobson CM 2003. Protein folding and misfolding. Nature 426: 884–890
- Donnelly, N., Passerini, V., Durrbaum, M., Stingele, S. & Storchova, Z. HSF1 deficiency and impaired HSP90-dependent protein folding are hallmarks of aneuploid human cells. EMBO J. 33, 2374–2387 (2014).
- Dorsett D (2011) Cohesin: genomic insights into controlling gene transcription and development. Curr Opin Genet Dev 21: 199–206
- Duesberg P, Rausch C, Rasnick D, Hehlmann R. Genetic Instability of Cancer Cells is Proportional to their Degree of Aneuploidy. Proc Natl Acad Sci USA. 1998;95:13692–13697.
- Duijf, P. H., Schultz, N. & Benezra, R. Cancer cells preferentially lose small chromosomes. Int. J. Cancer 132, 2316–2326 (2013).
- Duncan AW, Taylor MH, Hickey RD, et al. The ploidy conveyor of mature hepatocytes as a source of genetic variation. Nature 2010;467:707–10.

- Dunham, M.J., Badrane, H., Ferea, T., Adams, J., Brown, P.O., Rosenzweig, F., and Botstein, D. (2002). Characteristic genome rearrangements in experimental evolution of Saccharomyces cerevisiae. Proc. Natl. Acad. Sci. U. S. A. 99, 16144–16149.Durrbaum, M., Kuznetsova, A.Y., Passerini, V., Stingele, S., Stoehr, G., and Storchova, Z. (2014). Unique features of the transcriptional response to model aneuploidy in human cells. BMC Genomics 15, 139.
- Edwards, J.H., Harnden, D.G., Cameron, A.H., Crosse, V.M., and Wolff, O.H. (1960). A new trisomic syndrome. Lancet 1, 787–790.
- Ertych N, Stolz A, Stenzinger A, Weichert W, Kaulfuß S, et al. 2014. Increased microtubule assembly rates influence chromosomal instability in colorectal cancer cells. Nat. Cell Biol. 16(8):779–91
- Farmer H, McCabe N, Lord CJ, Tutt AN, Johnson DA, et al. 2005. Targeting the DNA repair defect in BRCA mutant cells as a therapeutic strategy. Nature 434:917–21
- Fedier A, Schlamminger M, Schwarz VA, Haller U, Howell SB, Fink D. 2003. Loss of atm sensitises p53-deficient cells to topoisomerase poisons and antimetabolites. Ann. Oncol. 14:938–45
- Fisher, R.A. (1918). The correlation between relatives on the supposition of Mendelian inheritance. Proc R Soc Endinburgh 52, 399–433.
- Foijer, F. et al. Chromosome instability induced by Mps1 and p53 mutation generates aggressive lymphomas exhibiting aneuploidy-induced stress. Proc. Natl Acad. Sci. USA 111, 13427–13432 (2014).
- Fournier, R.E., and F.H. Ruddle. 1977. Microcell-mediated transfer of murine chromosomes into mouse, Chinese hamster, and human somatic cells. PNAS. 74:319–323.
- Futcher B, Carbon J. Toxic effects of excess cloned centromeres. Mol Cell Biol. 1986;6:2213-22.
- Gaillard H, Garcia-Muse T, Aguilera A. Replication stress and cancer. Nat. Rev. Cancer. 2015;15:276–289
- Ganem NJ, Godinho SA, Pellman D. A mechanism linking extra centrosomes to chromosomal instability. Nature. 2009;460:278–282.
- García-Castillo H., Vásquez-Velásquez A.I., Rivera H., Barros-Núñez P. 2008. Clinical and genetic heterogeneity in patients with mosaic variegated aneuploidy: delineation of clinical subtypes. Am. J. Med. Genet. A. 146A:1687–1695 10.1002/ajmg.a.32315
- Garraway LA, Lander ES. Lessons from the cancer genome. Cell. 2013;153(1):17–37.
- Gasch, A.P., Spellman, P.T., Kao, C.M., Carmel-Harel, O., Eisen, M.B., Storz, G., Botstein, D., and Brown, P.O. (2000). Genomic expression programs in the response of yeast cells to environmental changes. Mol. Biol. Cell 11, 4241–4257.
- Geiler-Samerotte K.A, Dion M.F, Budnik B.A, Wang S.M, Hartl D.L, Drummond D.A. Misfolded proteins impose a dosage-dependent fitness cost and trigger a cytosolic unfolded protein response in yeast. Proc. Natl. Acad. Sci. USA. 2011; 108: 680-685

- Giaever, G. et al. Functional profiling of the Saccharomyces cerevisiae genome. Nature 418, 387–391 (2002).
- Godek, K. M. et al. Chromosomal instability affects the tumorigenicity of glioblastoma tumor-initiating cells. Cancer Discov. 6, 532–545 (2016).
- Goldberg AL. Protein degradation and protection against misfolded or damaged proteins. Nature. 2003; 426:895–899.
- Gregan J, Polakova S, Zhang L, Tolić-Nørrelykke IM, Cimini D. Merotelic kinetochore attachment: causes and effects. Trends Cell Biol. 2011;21:374–381.
- Gresham, D., Desai, M.M., Tucker, C.M., Jenq, H.T., Pai, D.A., Ward, A., DeSevo, C.G., Botstein, D., and Dunham, M.J. (2008). The repertoire and dynamics of evolutionary adaptations to controlled nutrient-limited environments in yeast. PLoS Genet. 4, e1000303.
- Gropp A. Proceedings: hypoplasia and malformation in trisomy syndromes of the mouse foetus. Mutat Res. 1975;29:216.
- Halevy, T., Biancotti, J. C., Yanuka, O., Golan-Lev, T. & Benvenisty, N. Molecular characterization of Down syndrome embryonic stem cells reveals a role for RUNX1 in neural differentiation. Stem Cell Rep. 7, 777–786 (2016).
- Hanks S., Coleman K., Reid S., Plaja A., Firth H., Fitzpatrick D., Kidd A., Méhes K., Nash R., Robin N., et al. 2004. Constitutional aneuploidy and cancer predisposition caused by biallelic mutations in BUB1B. Nat. Genet. 36:1159–1161
- Hanks S, Rahman N, Snape K. Mosaic variegated aneuploidy syndrome. Orphanet. May 2012.
- Hanna, J. et al. Deubiquitinating enzyme Ubp6 functions noncatalytically to delay proteasomal degradation. Cell 127, 99–111 (2006).
- Hardy, P. A. & Zacharias, H. Reappraisal of the Hansemann–Boveri hypothesis on the origin of tumors. Cell Biol. Int. 29, 983–992 (2005).
- Hartl FU, Bracher A, Hayer-Hartl M. 2011. Molecular chaperones in protein folding and proteostasis. Nature 475: 324–332.
- Haruki N, Saito H, Harano T, Nomoto S, Takahashi T, et al. 2001. Molecular analysis of the mitotic check-point genes BUB1, BUBR1and BUB3 in human lung cancers. Cancer Lett. 162(2):201–5
- Hasle H, Clemmensen IH, Mikkelsen M. 2000. Risks of leukaemia and solid tumours in individuals with Down's syndrome. Lancet 355(9199):165–69
- Hassold T, Abruzzo M, Adkins K, Griffin D, Merrill M, Millie E, et al. Human aneuploidy: Incidence, origin, and etiology. Environ Mol Mutagen. 1996;28:167-75.
- Hegemann B, Hutchins JR, Hudecz O, Novatchkova M, Rameseder J, Sykora MM, Liu S, Mazanek M, Lénárt P, Hériché JK, Poser I, Kraut N, Hyman AA, Yaffe MB, Mechtler K, Peters JM. Systematic phosphorylation analysis of human mitotic protein complexes. Sci Signal. 2011 Nov 8;4(198):rs12.
- Hieronymus H, et al. (2014) Copy number alteration burden predicts prostate cancer relapse. Proc Natl Acad Sci USA 111:11139–11144.

- Hieronymus H, et al. (2018) Tumor copy number alteration burden is a pan-cancer prognostic factor associated with recurrence and death. eLife 7:e37294.
- Hodgkin J, Horvitz HR, Brenner S. Nondisjunction Mutants of the Nematode Caenorhabditis Elegans. Genetics. 1979;91:67-94.
- Hodgkin J. X chromosome dosage and gene expression in Caenorhabditis elegans: Two unusual dumpy genes. MGG Mol Gen Genet. 1983;192:452-8.
- Honda, R., Korner, R., and Nigg, E. A. (2003). Exploring the functional interactions between Aurora B, INCENP, and survivin in mitosis. Mol. Biol. Cell 14, 3325–3341.
- Hose J., Yong C.M., Sardi M., Wang Z., Newton M.A., Gasch A.P. Dosage compensation can buffer copy-number variation in wild yeast. eLife. 2015;4:e05462.
- Huettel, B., Kreil, D. P., Matzke, M. & Matzke, A. J. Effects of aneuploidy on genome structure, expression, and interphase organization in Arabidopsis thaliana. PLoS Genet. 4, e1000226 (2008).
- Hughes T.R., Roberts C.J., Dai H., Jones A.R., Meyer M.R., Slade D., Burchard J., Dow S., Ward T.R., Kidd M.J., et al. Widespread aneuploidy revealed by DNA microarray expression profiling. Nat. Genet. 2000;25:333–337.
- Hwang, S., Gustafsson, H.T., O'Sullivan, C., Bisceglia, G., Huang, X., Klose, C., Schevchenko, A., Dickson, R.C., Cavaliere, P., Dephoure, N., et al. (2017). Serine-dependent sphingolipid synthesis is a metabolic liability of aneuploid cells. Cell Rep. 21, 3807–3818.
- Jahn T. R., Radford S. E. (2005). The Yin and Yang of protein folding. FEBS J. 272, 5962–5970.
- Janssen A, van der Burg M, Szuhai K, Kops GJPL, Medema RH. 2011. Chromosome segregation errors as a cause of DNA damage and structural chromosome aberrations. Science 333(6051):1895–98
- Janssen, A., Kops, G. J. & Medema, R. H. Elevating the frequency of chromosome mis-segregation as a strategy to kill tumor cells. Proc. Natl Acad. Sci. USA 106, 19108–19113 (2009).
- Jeganathan K, Malureanu L, Baker DJ, Abraham SC, van Deursen JM. 2007. Bub1 mediates cell death in response to chromosome missegregation and acts to suppress spontaneous tumorigenesis. J. Cell Biol. 179(2):255–67
- Jeyaprakash, A. A., Klein, U. R., Lindner, D., Ebert, J., Nigg, E. A., and Conti, E. (2007). Structure of a Survivin-Borealin-INCENP core complex reveals how chromosomal passengers travel together. Cell 131, 271–285.
- Jiang J, Jing Y, Cost GJ, Chiang J-C, Kolpa HJ, Cotton AM, et al. Translating dosage compensation to trisomy 21. Nature. 2013;500:296-300.
- Kaitna, S., Mendoza, M., Jantsch-Plunger, V., and Glotzer, M. (2000). Incenp and an Aurora-like kinase form a complex essential for chromosome segregation and efficient completion of cytokinesis. Curr. Biol. 10, 1172–1181.

- Katz W, Weinstein B, Solomon F. Regulation of tubulin levels and microtubule assembly in Saccharomyces cerevisiae: consequences of altered tubulin gene copy number. Mol Cell Biol. 1990;10:5286-94.
- Knouse, K. A., Davoli, T., Elledge, S. J. & Amon, A. Aneuploidy in cancer: Seq-ing answers to old questions. Annu. Rev. Cancer Biol. 1, 335–354 (2017).
- Knouse, K. A., Wu, J., Whittaker, C. A. & Amon, A. Single cell sequencing reveals low levels of aneuploidy across mammalian tissues. Proc. Natl Acad. Sci. USA 111, 13409–13414 (2014).
- Kops GJPL, Foltz DR, Cleveland DW. Lethality to human cancer cells through massive chromosome loss by inhibition of the mitotic checkpoint. Proc Natl Acad Sci U S A. 2004;101:8699-704.
- Korbel J. O., Tirosh-Wagner T., Urban A. E., Chen X. N., Kasowski M., Dai L., Grubert F., Erdman C., Gao M. C., Lange K., et al. (2009). The genetic architecture of Down syndrome phenotypes revealed by high-resolution analysis of human segmental trisomies. Proc. Natl. Acad. Sci. USA 106, 12031–12036
- Krushinskii LV, Dyban AP, Baranov VS, Poletaeva II, Romanova LG. Behavior of mice with robertsonian translocations of chromosomes. Genetika. 1986;22:434–41.
- L. H. Hartwell, Dutcher, S. K., Wood, J. S., and Garvik, B. (1982). The fidelity of mitotic chromosome reproduction in S. cerevisiae. Recent Adv. Yeast Mol. Biol. 1, 28–38.
- Lana-Elola E, Watson-Scales SD, Fisher EM, Tybulewicz VL. Down syndrome: searching for the genetic culprits. Dis Model Mech. 2011;4(5):586–95.
- Lane AA, Chapuy B, Lin CY, Tivey T, Li H, et al. 2014. Triplication of a 21q22 region contributes to B cell transformation through HMGN1 overexpression and loss of histone H3 Lys27 trimethylation. Nat. Genet. 46(6):618–23
- Levine M.S., Bakker B., Boeckx B., Moyett J., Lu J., Vitre B. et al. (2017) Centrosome amplification is sufficient to promote spontaneous tumorigenesis in mammals. Dev. Cell 40, 313–322.e5
- Li G-W, Burkhardt D, Gross C, Weissman JS. 2014. Quantifying absolute protein synthesis rates reveals principles underlying allocation of cellular resources. Cell 157: 624–635
- Li J. (1927). Development in drosophila melanogaster. Genetics 12, 1–58.
- Li M, Fang X, Baker DJ, Guo L, Gao X, Wei Z, et al. The ATM-p53 pathway suppresses aneuploidy-induced tumorigenesis. Proc Natl Acad Sci USA. 2010;107:14188-93.
- Li M, Fang X, Wei Z, York JP, Zhang P. 2009. Loss of spindle assembly checkpoint–mediated inhibition of Cdc20 promotes tumorigenesis in mice. J. Cell Biol. 185(6):983–94
- Lindsley DL, Sandler L, Baker BS, Carpenter ATC, Denell RE, Hall JC, et al. Segmental aneuploidy and the genetic gross structure of the drosophila genome. Genetics. 1972;71:157-84.
- Liu, G., M.Y.J. Yong, M. Yurieva, K.G. Srinivasan, J. Liu, J.S.Y. Lim, M. Poidinger, G.D. Wright, F. Zolezzi, H. Choi, N. Pavelka, and G. Rancati.

2015. Gene Essentiality Is a Quantitative Property Linked to Cellular Evolvability. Cell.
- Liu, X. et al. Trisomy eight in ES cells is a common potential problem in gene targeting and interferes with germ line transmission. Dev. Dyn. 209, 85–91 (1997).
- Livak KJ, Schmittgen TD. Analysis of relative gene expression data using real-time quantitative PCR and the 2– ΔΔCT method. methods. 2001;25(4):402–8.
- Lockstone, H. E. et al. Gene expression profiling in the adult Down syndrome brain. Genomics 90, 647–660 (2007).
- Longtine MS, et al. Additional modules for versatile and economical PCR-based gene deletion and modification in Saccharomyces cerevisiae. Yeast. 1998;14:953–961.
- Lorke DE. Developmental characteristics of trisomy 19 mice. Acta Anat (Basel) 1994;150(3):159–69.
- Luo Z, Wang L, Wang Y, Zhang W, Guo Y, Shen Y, et al. Identifying and characterizing SCRaMbLEd synthetic yeast using ReSCuES. Nat Commun. 2018
- Mani R., St Onge R. P., Hartman J. L. 4th, Giaever G., Roth F. P., Defining genetic interaction. Proc. Natl. Acad. Sci. U.S.A. 105, 3461–3466 (2008).
- Mao, R. et al. Primary and secondary transcriptional effects in the developing human Down syndrome brain and heart. Genome Biol. 6, R107 (2005).
- Mazouzi, A., Velimezi, G., and Loizou, J.I. (2014). DNA replication stress: causes, resolution and disease. Exp. Cell Res. 329, 85–93.
- McCabe N, Turner NC, Lord CJ, Kluzek K, Bialkowska A, et al. 2006. Deficiency in the repair of DNA damage by homologous recombination and sensitivity to poly(ADP-ribose) polymerase inhibition. Cancer Res. 66:8109–15
- McClintock B. A Cytological and Genetical Study of Triploid Maize. Genetics. 1929; 14:180-222.
- McGranahan, N. et al. Allele-specific HLA loss and immune escape in lung cancer evolution. Cell 171, 1259–1271 (2017).
- Meena, J. K. et al. Telomerase abrogates aneuploidy-induced telomere replication stress, senescence and cell depletion. EMBO J. 34, 1371–1384 (2015).
- Michel, L. S. et al. MAD2 haplo-insufficiency causes premature anaphase and chromosome instability in mammalian cells. Nature 409, 355–359 (2001).
- Musacchio A, Salmon ED. The spindle-assembly checkpoint in space and time. Nat Rev Mol Cell Biol. 2007;8:379–393.Nagaoka, S.I., Hassold, T.J., and Hunt, P.A. (2012). Human aneuploidy: mechanisms and new insights into an age-old problem. Nat. Rev. Genet. 13, 493–504.
- Nakatogawa, H., Suzuki, K., Kamada, Y. and Ohsumi, Y. (2009). Dynamics and diversity in autophagy mechanisms: lessons from yeast. Nat. Rev. Mol. Cell Biol. 10, 458-467

- Nasmyth K., Haering C. H. (2009). Cohesin: its roles and mechanisms. Annu. Rev. Genet. 43 525–558.
- Nicholson, J. M. et al. Chromosome mis-segregation and cytokinesis failure in trisomic human cells. eLife 4, e05068 (2015).
- Nicholson, J.M., and D. Cimini. 2013. Cancer karyotypes: survival of the fittest. Front Oncol. 3:148.
- Niggli FK, Powell JE, Parkes SE, Ward K, Raafat F, et al. 1994. DNA ploidy and proliferative activity (S-phase) in childhood soft-tissue sarcomas: their value as prognostic indicators. Br. J. Cancer 69(6):1106–10
- Niwa O, Tange Y, Kurabayashi A. Growth arrest and chromosome instability in aneuploid yeast. Yeast. 2006;23:937-50.
- Niwa O, Yanagida M. Triploid meiosis and aneuploidy in Schizosaccharomyces pombe: an unstable aneuploid disomic for chromosome III. Curr Genet. 1985;9:463-70.
- O'Duibhir, E., Lijnzaad, P., Benschop, J.J., Lenstra, T.L., van Leenen, D., Groot Koerkamp, M.J., Margaritis, T., Brok, M.O., Kemmeren, P., and Holstege, F.C. (2014). Cell cycle population effects in perturbation studies. Mol. Syst. Biol. 10, 732.
- Ohashi, A. et al. Aneuploidy generates proteotoxic stress and DNA damage concurrently with p53-mediated post-mitotic apoptosis in SAC-impaired cells. Nat. Commun. 6, 7668 (2015).
- Ohyama S, Yonemura Y, Miyazaki I. 1990. Prognostic value of S-phase fraction and DNA ploidy studied with in vivo administration of bromodeoxyuridine on human gastric cancers. Cancer 65(1):116–21
- Oromendia, A. B., Dodgson, S. E. & Amon, A. Aneuploidy causes proteotoxic stress in yeast. Genes Dev. 26, 2696–2708 (2012).
- Ozery-Flato M., Linhart C., Trakhtenbrot L., Izraeli S., Shamir R. Large-scale analysis of chromosomal aberrations in cancer karyotypes reveals two distinct paths to aneuploidy. Genome Biol. 2011;12:R61.
- Pagliarini R, Shao W, Sellers WR. 2015. Oncogene addiction: pathways of therapeutic response, resistance, and road maps toward a cure. EMBO Rep. 16:280–96
- Pai GS, Jr RCL, Borgaonkar DS. Handbook of Chromosomal Syndromes. 1st ed. Wiley-Liss; 2002.
- Passerini, V., Ozeri-Galai, E., de Pagter, M.S., Donnelly, N., Schmalbrock, S., Kloosterman, W.P., Kerem, B., and Storchova, Z. (2016). The presence of extra chromosomes leads to genomic instability. Nat. Commun. 7, 10754.Patau, K., Smith, D.W., Therman, E., Inhorn, S.L., and Wagner, H.P. (1960). Multiple congenital anomaly caused by an extra autosome. Lancet 1, 790–793
- Pavelka, N. et al. Aneuploidy confers quantitative proteome changes and phenotypic variation in budding yeast. Nature 468, 321–325 (2010).
- Penny, G. D., Kay, G. F., Sheardown, S. A., Rastan, S. & Brockdorff, N. Requirement for Xist in X chromosome inactivation. Nature 379, 131–137 (1996).
- Prahallad A, Bernards R. 2015. Opportunities and challenges provided by crosstalk between signalling pathways in cancer. Oncogene 35:1073–79

- R. A. Veitia, Exploring the etiology of haploinsufficiency. BioEssays 24, 175–184 (2002).
- Rancati, G., N. Pavelka, B. Fleharty, A. Noll, R. Trimble, K. Walton, A. Perera, K. Staehling- Hampton, C.W. Seidel, and R. Li. 2008. Aneuploidy underlies rapid adaptive evolution of yeast cells deprived of a conserved cytokinesis motor. Cell. 135:879–893.
- Rao F, Caflisch A. The protein folding network. Journal of Molecular Biology. 2004;342:299.
- Rasmussen SA, Wong LY, Yang Q, May KM, Friedman JM. 2003. Population-based analyses of mortality in trisomy 13 and trisomy 18. Pediatrics 111:777–84
- Read AP, Strachan T (1999). "Chapter 18: Cancer Genetics". Human molecular genetics 2. New York: Wiley.
- Rehen, S. K. et al. Chromosomal variation in neurons of the developing and adult mammalian nervous system. Proc. Natl Acad. Sci. USA 98, 13361–13366 (2001).
- Rehen, S. K. et al. Constitutional aneuploidy in the normal human brain. J. Neurosci. 25, 2176–2180 (2005).
- Reinhardt HC, Aslanian AS, Lees JA, Yaffe MB. 2007. p53-deficient cells rely on ATM- and ATR-mediated checkpoint signaling through the p38MAPK/MK2 pathway for survival after DNA damage. Cancer Cell 11:175–89
- Richter K, Haslbeck M, Buchner J. The Heat Shock Response: Life on the Verge of Death. Mol Cell. 2010;40(2):253–266.
- Roizen N. J., Patterson D. Down's syndrome. The Lancet. 2003;361(9365):1281–1289.
- Romero P, Wagg J, Green ML, Kaiser D, Krummenacker M, Karp PD. Computational prediction of human metabolic pathways from the complete human genome. Genome Biol. 2005;6:R2.
- Roper RJ, and Reeves RH (2006). Understanding the basis for Down syndrome phenotypes. PLoS genetics 2, e50.
- Rosenstraus, M.J., and Chasin, L.A. (1978). Separation of linked markers in Chinese hamster cell hybrids: mitotic recombination is not involved. Genetics 90, 735–760.
- Rosenthal R, McGranahan N, Herrero J, Swanton C. Deciphering Genetic Intratumor Heterogeneity and Its Impact on Cancer Evolution. Annual Review of Cancer Biology. 2017;1(1):223–240.
- Runge KW, Zakian VA. Introduction of extra telomeric DNA sequences into Saccharomyces cerevisiae results in telomere elongation. Mol Cell Biol. 1989;9:1488-97.
- Rutledge, S. D. et al. Selective advantage of trisomic human cells cultured in non-standard conditions. Sci. Rep. 6, 22828 (2016).
- Ryu, H.-Y., N.R. Wilson, S. Mehta, S.S. Hwang, and M. Hochstrasser. 2016. Loss of the SUMO protease Ulp2 triggers a specific multichromosome aneuploidy. Genes Dev. 30:1881–1894.

- Sandall S, Severin F, McLeod IX, Yates JR, Oegema K, Hyman A, Desai A. 2006. A Bir1-Sli15 complex connects centromeres to microtubules and is required to sense kinetochore tension. Cell 127: 1179–1191.
- Sansregret, L. & Swanton, C. The role of aneuploidy in cancer evolution. Cold Spring Harb. Perspect. Med. 7, a028373 (2017).
- Santaguida, S. et al. Chromosome mis-segregation generates cell-cycle-arrested cells with complex karyotypes that are eliminated by the immune system. Dev. Cell 41, 638–651 (2017).
- Santaguida, S., Vasile, E., White, E., and Amon, A. (2015). Aneuploidy-induced cellular stresses limit autophagic degradation. Genes Dev. 29, 2010–2021.
- Segal, D. J. & McCoy, E. E. Studies on Down's syndrome in tissue culture. I. Growth rates and protein contents of fibroblast cultures. J. Cell Physiol. 83, 85–90 (1974).
- Selmecki, A., Forche, A. & Berman, J. Aneuploidy and isochromosome formation in drug-resistant Candida albicans. Science 313, 367–370 (2006).
- Selmecki, A., Forche, A. & Berman, J. Genomic plasticity of the human fungal pathogen Candida albicans. Eukaryot. Cell 9, 991–1008 (2010).
- Selmecki, A., Gerami-Nejad, M., Paulson, C., Forche, A., and Berman, J. (2008). An isochromosome confers drug resistance in vivo by amplification of two genes, ERG11 and TAC1. Mol. Microbiol. 68, 624–641.
- Sharma, K. et al. Quantitative proteomics reveals that Hsp90 inhibition preferentially targets kinases and the DNA damage response.Mol. Cell. Proteomics 11, M111.014654 (2012).
- Shao Y., Lu N., Wu Z., Cai C., Wang S., Zhang L.-L., et al. (2018). Creating a functional single-chromosome yeast. Nature 560, 331–335.
- Sheltzer JM, Amon A. (2012) The aneuploidy paradox: costs and benefits of an incorrect karyotype. Trends Genet. 2011;27:446–453.
- Sheltzer, J. M. et al. Single-chromosome gains commonly function as tumor suppressors. Cancer Cell 31, 240–255 (2017).
- Sheltzer, J. M. et al., A transcriptional and metabolic signature of primary aneuploidy is present in chromosomally unstable cancer cells and informs clinical prognosis. Cancer Res. 73, 6401–6412 (2013).
- Sheltzer, J.M., Torres, E.M., Dunham, M.J., and Amon, A. (2012). Transcriptional consequences of aneuploidy. Proc. Natl. Acad. Sci. USA 109, 12644–12649.
- Sidera, K. & Patsavoudi, E. HSP90 inhibitors: current development and potential in cancer therapy. Recent Pat. Anticancer Drug Discov. 9, 1–20 (2014).
- Siegel JJ, Amon A. New insights into the troubles of aneuploidy. Annu Rev Cell Dev Biol. 2012;28:189–214.
- Sigurdson DC, Herman RK, Horton CA, Kari CK, Pratt SE. An X-autosome fusion chromosome of Caenorhabditis elegans. MGG Mol Gen Genet. 1986;202:212-8.
- Silkworth WT, Nardi IK, Scholl LM, Cimini D. 2009. Multipolar spindle pole coalescence is a major source of kinetochore mis-attachment and chromosome mis-segregation in cancer cells. PLOS ONE 4(8):e6564

- Simonetti G., Bruno S., Padella A., Tenti E., Martinelli G. (2019). Aneuploidy: cancer strength or vulnerability? Int. J. Cancer 144, 8–25.
- Smith, J.C., and J.M. Sheltzer. 2018. Systematic identification of mutations and copy number alterations associated with cancer patient prognosis. elife. 7:248.
- Snape K., Hanks S., Ruark E., Barros-Núñez P., Elliott A., Murray A., Lane A.H., Shannon N., Callier P., Chitayat D., et al. 2011. Mutations in CEP57 cause mosaic variegated aneuploidy syndrome. Nat. Genet. 43:527–529
- Solimini NL, Xu Q, Mermel CH, Liang AC, Schlabach MR, et al. 2012. Recurrent hemizygous deletions in cancers may optimize proliferative potential. Science 337(6090):104–9
- Solomon DA et al (2011) Mutational inactivation of STAG2 causes aneuploidy in human cancer. Science 333: 1039–1043.
- Sopko R, Huang D, Preston N, Chua G, Papp B, Kafadar K, Snyder M, Oliver SG, Cyert M, Hughes TR, et al. 2006. Mapping pathways and phenotypes by systematic gene overexpression. Mol Cell 21: 319–330.
- Sotillo, R. et al. Mad2 overexpression promotes aneuploidy and tumorigenesis in mice. Cancer Cell 11, 9–23 (2007).
- Soto, M., Raaijmakers, J.A., Bakker, B., Spierings, D.C.J., Lansdorp, P.M., Foijer, F., and Medema, R.H. (2017). p53 prohibits propagation of chromosome segregation errors that produce structural aneuploidies. Cell Rep. 19, 2423–2431.
- Spurgers, K. B. et al. Identification of cell cycle regulatory genes as principal targets of p53-mediated transcriptional repression. J. Biol. Chem. 281, 25134–25142 (2006).
- Stefani, M. & Dobson, C. M. Protein aggregation and aggregate toxicity: new insights into protein folding, misfolding diseases and biological evolution. J. Mol. Med. (Berl.) 81, 678–699 (2003).
- Stephens P. J., Greenman C. D., Fu B., et al. Massive genomic rearrangement acquired in a single catastrophic event during cancer development. Cell. 2011;144(1):27–40.
- Stingele, S. et al. Global analysis of genome, transcriptome and proteome reveals the response to aneuploidy in human cells. Mol. Syst. Biol. 8,608 (2012).
- Stopsack KH, Whittaker CA, Gerke TA, Loda M, Kantoff PW, Mucci LA, Amon A. Aneuploidy drives lethal progression in prostate cancer. Proc Natl Acad Sci U S A. 2019 Jun 4;116(23):11390-11395
- Sussan TE, Yang A, Li F, Ostrowski MC, Reeves RH. 2008. Trisomy represses ApcMin-mediated tumours in mouse models of Down's syndrome. Nature 451(7174):73–75
- Taggart JC, Li G-W. 2018. Production of protein-complex compo- nents is stoichiometric and lacks general feedback regulation in eukaryotes. Cell Syst 7: 580–589.e4.
- Tang, Y. C., Williams, B. R., Siegel, J. J. & Amon, A. Identification of aneuploidy-selective antiproliferation compounds. Cell 144, 499–512 (2011).

- Tang, Y.C., Yuwen, H., Wang, K., Bruno, P.M., Bullock, K., Deik, A., Santaguida, S., Trakala, M., Pfau, S.J., Zhong, N., et al. (2017). Aneuploid cell sur- vival relies upon sphingolipid homeostasis. Cancer Res. 77, 5272–5286.
- Tanno Y, H. Susumu, M. Kawamura, H. Sugimura, T. Honda, Y. Watanabe The inner centromere–shugoshin network prevents chromosomal instability. Science, 349 (2015), pp. 1237–1240
- Tartaglia, N. R., Howell, S., Sutherland, A., Wilson, R. & Wilson, L. A review of trisomy X (47,XXX). Orphanet J. Rare Dis. 5, 8 (2010).
- Taylor, A. M. et al. Genomic and functional approaches to understanding cancer aneuploidy. Cancer Cell 33, 676–689 (2018).
- Thomas, R., Marks, D. H., Chin, Y. & Benezra, R. Whole chromosome loss and associated breakage- fusion-bridge cycles transform mouse tetraploid cells. EMBO J. 37, 201–218 (2018).
- Thompson S.L., Compton D.A. Examining the link between chromosomal instability and aneuploidy in human cells. J. Cell Biol. 2008;180:665–672.
- Thompson SL, Compton DA. Proliferation of aneuploid human cells is limited by a p53-dependent mechanism. J Cell Biol. 2010;188:369-81.
- Thorburn, R. R. et al. Aneuploid yeast strains exhibit defects in cell growth and passage through START. Mol. Biol. Cell 24, 1274–1289 (2013).
- Thorburn, R.R., Gonzalez, C., Brar, G.A., Christen, S., Carlile, T.M., Ingolia, N.T., Sauer, U., Weissman, J.S., and Amon, A. (2013). Aneuploid yeast strains exhibit defects in cell growth and passage through START. Mol. Biol. Cell 24, 1274–1289.
- Tighe A, Johnson VL, Albertella M, Taylor SS. 2001. Aneuploid colon cancer cells have a robust spindle checkpoint. EMBO Rep. 2(7):609–14
- Torres EM, Williams BR, Amon A. 2008. Aneuploidy: cells losing their balance. Genetics 179:737–746.
- Torres, E. M. et al. Effects of aneuploidy on cellular physiology and cell division in haploid yeast. Science 317, 916–924 (2007).
- Turajlic S, Xu H, Litchfield K, Rowan A, Horswell S, Chambers T, O'Brien T, Lopez JI, Watkins TB, Nicol D, Stares M, Challacombe B, Hazell S, et al, and TRACERx Renal Consortium. Deterministic Evolutionary Trajectories Influence Primary Tumor Growth: TRACERx Renal. Cell. 2018; 173:595 610.e11.
- Tyedmers J, Mogk A, Bukau B 2010a. Cellular strategies for controlling protein aggregation. Nat Rev Mol Cell Biol 11: 777–788
- Upender, M. B. et al. Chromosome transfer induced aneuploidy results in complex dysregulation of the cellular transcriptome in immortalized and cancer cells. Cancer Res. 64, 6941–6949 (2004).
- van der Lelij, P. et al. Synthetic lethality between the cohesin subunits STAG1 and STAG2 in diverse cancer contexts. Elife 6, (2017).
- van Echten-Arends, J. et al. Chromosomal mosaicism in human preimplantation embryos: a systematic review. Hum. Reprod. Update 17, 620–627 (2011).
- Venkitaraman AR. 2002. Cancer susceptibility and the functions of BRCA1 and BRCA2. Cell 108:171–82

- Vesely, M. D., Kershaw, M. H., Schreiber, R. D. & Smyth, M. J. Natural innate and adaptive immunity to cancer. Annu. Rev. Immunol. 29, 235–271 (2011).
- Wang Q, Fan S, Eastman A, Worland PJ, Sausville EA, O'Connor PM. 1996. UCN-01: a potent abrogator of G2 checkpoint function in cancer cells with disrupted p53. J. Natl. Cancer Inst. 88:956–65
- Weaver BAA, Cleveland DW. Does aneuploidy cause cancer? Curr Opin Cell Biol. 2006;18(6):658–67.
- Weaver, B. A., Silk, A. D., Montagna, C., Verdier-Pinard, P. & Cleveland, D. W. Aneuploidy acts both oncogenically and as a tumor suppressor. Cancer Cell 11, 25–36 (2007).
- Weinstein IB. 2002. Addiction to oncogenes—the Achilles heal of cancer. Science 297:63–64
- Wenger CR, Beardslee S, Owens MA, Pounds G, Oldaker T, et al. 1993. DNA ploidy, S-phase, and steroid receptors in more than 127,000 breast cancer patients. Breast Cancer Res. Treat. 28(1):9–20
- White, E. (2016). Autophagy and p53. Cold Spring Harb. Perspect. Med. 6, a026120.
- Williams, B. R. et al. Aneuploidy affects proliferation and spontaneous immortalization in mammalian cells. Science 322, 703–709 (2008).
- Winzeler, E. A. et al. Functional characterization of the S. cerevisiae genome by gene deletion and parallel analysis. Science 285, 901–906 (1999).
- Wójcik C, DeMartino GN. 2003. Intracellular localization of proteasomes. Int J Biochem Cell Biol 35:579–589
- Xiao J, Zhang, T., Xu, D., Wang, H., Cai, Y., Jin, T., Liu, M., Jin, M., Wu, K., and Yuan, J. (2015). FBXL20-mediated Vps34 ubiquitination as a p53 controlled checkpoint in regulating autophagy and receptor degradation. Genes Dev. 29, 184–196.
- Yang Q, Rasmussen SA, Friedman JM. 2002. Mortality associated with Down's syndrome in the USA from 1983 to 1997: a population-based study. Lancet 359(9311):1019–25
- Yona AH et al. Chromosomal duplication is a transient evolutionary solution to stress. Proc. Natl Acad. Sci. USA 109, 21010–21015 (2012).
- Yurov Y. B. et al. Aneuploidy and confined chromosomal mosaicism in the developing human brain. PLoS ONE 2, e558 (2007).
- Zack TI et al. Pan-cancer patterns of somatic copy number alteration. Nat. Genet. 45, 1134–1140 (2013).
- Zhang C-Z, Spektor A, Cornils H, Francis JM, Jackson EK, et al. 2015. Chromothripsis from DNA damage in micronuclei. Nature 522(7555):179–84
- Zhang, M. et al. Aneuploid embryonic stem cells exhibit impaired differentiation and increased neoplastic potential. EMBO J. 35, 2285–2300 (2016).
- Zhao X, Gao S, Wu Z, Kajigaya S, Feng X, Liu Q, Townsley DM, Cooper J, Chen J, Keyvanfar K, et al. (2017). Single-cell RNA-seq reveals a distinct transcriptome signature of aneuploid hematopoietic cells. Blood.

- Zhu J., Pavelka N., Bradford W.D., Rancati G., Li R. Karyotypic determinants of chromosome instability in aneuploid budding yeast. PLoS Genet. 2012;8:e1002719.
- Zuo E, Huo X, Yao X, Hu X, Sun Y, Yin J, He B, Wang X, Shi L, Ping J, Wei Y, Ying W, Wei W, Liu W, Tang C, Li Y, Hu J, Yang H. CRISPR/Cas9-mediated targeted chromosome elimination. Genome Biology. 2017;18:224.

Publications supplement

Ravichandran MC, Fink S, Clarke MN, Hofer FC, Campbell CS. 2018. Genetic interactions between specific chromosome copy number alterations dictate complex aneuploidy patterns. Gene Dev2018;32:1485–1498.